

AMERICAN UNIVERSITY OF BEIRUT

POLY-AMINE BASED TAILORED MADE ORDERED
NANOCASPSULE: PREPARATION, FLUORESCENCE
STUDY AND APPLICATION

by
MAI AHMAD MOUSLMANI

A thesis
submitted in partial fulfillment of the requirements
for the degree of Master of Science
to the Department of Chemistry
of the Faculty of Arts and Sciences
at the American University of Beirut

Beirut, Lebanon
May 2014

AMERICAN UNIVERSITY OF BEIRUT

POLY-AMINE BASED TAILORED MADE ORDERED
NANOCAPSULE: PREPARATION, FLOURECENCE STUDY
AND APPLICATION

by
MAI AHMAD MOUSLMANI

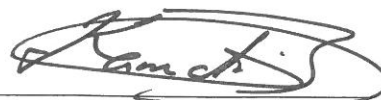
Approved by:

Dr. Digambara Patra, Associate Professor
Chemistry



Advisor

Dr. Kamal Bouhadir, Assocaite Professor
Chemistry



Member of Committee

Dr. Pierre Karam, Assistant Professor
Chemistry



Member of Committee

Date of thesis defense: May 5, 2014

AMERICAN UNIVERSITY OF BEIRUT

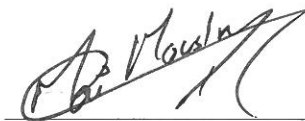
THESIS, DISSERTATION, PROJECT RELEASE FORM

Student Name: Mouslmani Mai Ahmad
Last First Middle

Master's Thesis Master's Project Doctoral Dissertation

I authorize the American University of Beirut to: (a) reproduce hard or electronic copies of my thesis, dissertation, or project; (b) include such copies in the archives and digital repositories of the University; and (c) make freely available such copies to third parties for research or educational purposes.

I authorize the American University of Beirut, **three years after the date of submitting my thesis, dissertation, or project**, to: (a) reproduce hard or electronic copies of it; (b) include such copies in the archives and digital repositories of the University; and (c) make freely available such copies to third parties for research or educational purposes.



Signature

May 16, 2014

Date

ACKNOWLEDGMENTS

Special thanks to my great advisor Dr. Digambara Patra. Thank you for being the wonderful person you are. Thank you for your patience, guidance and kindness throughout these two years. Thank you for giving me all your time especially during the last 3 months, and I know how this is exhausting for you. I didn't have the chance before to express my sincere gratitude, but I know that I have made the best decision by working with you.

I would like to express my sincere appreciation to my thesis committee members Dr. Kamal Bouhadir and Dr. Pierre Karam for their valuable time, suggestions and comments.

I would like to thank my professors who improved my learning experience, throughout the past two years, unique, Dr. Ghauch and Dr. Ghaddar. I am also grateful to the personnel in the Central Research Science Laboratory for their technical help and assistance as well to Mr. Issam Azar and Mrs. Lara Abramian for their help and care.

I would like to thank Dr. Jessica Rosenholm, from Åbo Academi University at Turku, Finland for zeta potential, TGA/DSC and Stimulated emission depletion microscopy (STDE) measurements. Moreover I would like to thank Dr. Markus Peurla, from the University of Turku, Finland for doing some TEM measurements.

Special thanks to Elsy El Khoury and Fatima Sleem for their assistance and support in the lab when I first arrived; and thanks to all the group who worked or still work with Dr Patra's research group Rasha, Zeinab and Mazhar...

Ghinwa and Sahar thank you for your friendship and support whenever I needed, and I really needed it a lot. Thanks to Ghada, Malik, Lubna, Malak and all the graduate students with whom I have shared wonderful moments.

Finally, I would like to thank my wonderful and lovely family, mom, dad my sisters Maha and Nour for their love, care and support. Special thanks for my dearest brother Rakan. I am lucky and blessed to have such family whose believe in me, makes me reach my goals and dreams.

AN ABSTRACT OF THE THESIS

Mai Ahmad Mouslmani for Master of Science
Major: Chemistry

Title: Poly-amine Based Tailored Made Ordered Nanocapsule: Preparation
Fluorescence Study and Application

Various studies have proven the significance of curcumin as an antioxidant, anti-inflammatory, anti-amyloid, anti-HIV, anti-microbial, and anti-tumor agent. Curcumin exists in its enole form and undergoes Excited State Intra-molecular Hydrogen Transfer (ESIHT) during deactivation process. Hence understanding ESIHT of curcumin adds to its medicinal values. At the same time delivery of curcumin has been a major challenge in the drug delivery field due to its poor water solubility and low bioavailability. These two problems can be overcome by applying an approach based on nanotechnology.

Chapters II and III report on curcumin associated poly (allylamine hydrochloride) (PAH) crosslink with dipotassium phosphate and subsequently congregates ~24 nm silica nanoparticles to form hierarchically ordered nanocapsule structures. The capsule sizes are in the range of 100 – 1000 nm depending on concentration of dipotassium phosphate. The fluorescence images confirm that curcumin is present all over the capsules. These nano-structures alter the optical behavior by reversing the excited state intra-molecular hydrogen transfer in curcumin depending on the size of nanocapsules. pH triggers the release of curcumin from the capsule where by a basic environment triggers the maximum release compared to acidic and neutral conditions. The drug release profile of curcumin in nanocapsule follows Higuchi model and depends on the size of nanocapsules. Apart from drug delivery, the biological activity of curcumin within the capsule is important. The researcher studies the 2,2-diphenyl-1-picrylhydrazyl (DPPH) scavenging activity of curcumin by simply measuring the change in DPPH absorbance at 520 nm. Results show that the scavenging activity of the encapsulated curcumin is lower than that of curcumin alone; as well it decreased exponentially with the size of the capsule.

Chapter IV examines the preparation of poly(9-(2-diallylaminoethyl) adenine.HCl-co-sulfur dioxide) (Poly A)/silica nanoparticles based capsules. The dynamic light scattering measurements showed that the capsules are of 700 nm effective hydrodynamic radius and the SEM images reveal that these capsules are spherical in shape. The researcher incorporated curcumin within these capsules as a fluorescent

probe and we tested their sensitivity to different nucleic bases. We found that these capsules are selective for guanine binding.

Chapter V describes how the same method of PAH/CU capsule preparation was used to successfully prepare PAH/ zinc oxide capsules. The SEM images showed that these capsules are spherical with size ranging between 200 and 500 nm. The incorporation of zinc oxide in such capsules changed its luminescence properties; the UV emitting zinc oxide emitted in the visible region. These findings can be used later on for biosensing applications.

CONTENTS

ACKNOWLEDGMENTS	v
ABSTRACT	vi
LIST OF ILLUSTRATIONS	xi
LIST OF TABLES.....	xvii
LIST OF ABBREVIATIONS	xviii
CHAPTER	
I. INTRODUCTION	1
A. Self Assembly.....	1
B. Fluorescence.....	2
1. Principles of Fluorescence.....	3
2. Characteristics of Fluorescence.....	4
a. Stokes' Shift	4
b. Kasha's Rule.....	5
c. Quantum Yield.....	5
d. Fluorescence Lifetime.....	6
e. Fluorescence Quenching.....	6
3. Steady- State and Time-Resolved Fluorescence.....	7
4. Fluorescence Sensing and Nanotechnology.....	8
a. Quantum Dots.....	8
b. Fluorescent Silica Nanoparticles.....	10
c. Gold Nanoparticles.....	10
d. Carbon Nanotubes.....	11
C. Capsules.....	12
1. Capsule synthesis.....	13
a. Hard template routes.....	13
i. Layer by layer assembly.....	13

ii. Direct Chemical Deposition or Adsorption...	15
iii. Sacrificial Template Routes.....	16
b. Soft Template Routes.....	17
i. Emulsion/Phase Separation Procedures.....	17
c. Tandem Self Assembly or Polyamine-salt aggregate....	17
i. Cargo encapsulation.....	19
D. Nanotechnology and Drug Delivery.....	20
1. Nanocapsules and Drug Delivery.....	22
E. Capsules and Sensing Applications.....	23
F. Aims.....	24
II. RELEASE OF CURCUMIN.....	26
A. Introduction.....	26
1. Curcumin and Its Medical Significance.....	26
2. Limitations of Curcumin Delivery and Its Available Delivery Systems.....	27
3. Aims.....	28
B. Materials.....	29
C. Methods.....	29
1. Preparation of Nanocapsules.....	29
2. Morphological Characterization.....	31
3. Spectroscopic Measurements.....	32
4. Other Measurements.....	32
D. Results.....	33
1. Characterization of Nanocapsules.....	33
2. Curcumin Delivery and Its Scavenging Activity.....	43
III. PHOTOPHYSICAL STUDY OF CURCUMIN IN NANO-CAPSULE.....	50
A. Introduction.....	50
1. Excited State Intramolecular Hydrogen Transfer.....	51
2. Photophysical Properties of Curcumin.....	52
3. Objectives.....	52

B. Materials and Methods.....	53
C. Results and Discussion.....	53
IV. SELECTIVE FLUORESCENCE SENSING OF GUANINE AMONG NUCLEOBASES USING NANOCAPSULES.....	64
A. Introduction.....	64
B. Materials and Methods.....	67
1. Materials.....	67
2. Preparation of Poly A Capsule.....	67
3. Morphological Characterization.....	68
4. Spectroscopic Measurements.....	68
C. Results and Discussion.....	68
V. TUNING ZnO NANOPARTICLES BASED ON POLY (ALLYLAMINE HYDROCHLORIDE) MEDIATED NANOCAPSULES FOR VISIBLE EMISSION.....	95
A. Introduction.....	95
B. Materials and Methods.....	96
1. Materials.....	96
2. Preparation of ZnO/ PAH Nanocapsules.....	96
3. Morphological and Spectroscopic Analysis.....	97
C. Results and Discussion.....	97
VI. CONCLUSION.....	107
REFERENCES.....	110

LIST OF ILLUSTRATIONS

Figure	Page
1.1. Jablonski diagram.....	3
1.2. Schematic of Layer-by-Layer (LbL) assembly on planar substrates. (1) Immersion in a positively charged polyelectrolyte solution; (2) rinse; (3) immersion in a negatively charged polyelectrolyte solution; (4) rinse; (5) repeat steps 1–4 until desired number of layers has been deposited; (6) core–shell particles can be the end of the process, or the template is dissolved away to leave a hollow polyelectrolyte capsule.....	15
1.3. Schematic of Layer-by-Layer (LbL) assembly on colloidal substrates. Steps: (1) treat with positively charged electrolyte; (2) centrifugation/rinse for removal of excess polyelectrolyte; (3) treat with negatively charged polyelectrolyte; (4) centrifugation/rinse; (5) repeat steps (1) through (4) to deposit additional layers; (6) template with desired number of layers; (7) polyelectrolyte capsules are formed by removal of colloidal template.....	15
1.4. Schematic of Polymer-Salt Aggregate (PSA) assembly. Steps: (1) polyamine chains are ionically crosslinked with multivalent anionic salt to form polyamine-salt aggregates (PSAs); (2) PSAs act as a template for the shell material deposition in a second mixing step to generate capsules with thick multilayered shells.....	18
2.1. Chemical structures of curcumin tautomers.....	26
2.2. Chemical structure of poly (allylamine hydrochloride) (PAH).....	29
2.3. Illustration of CU interacting with PAH, dipotassium phosphate and SiO ₂ NPs to form NCs.....	31
2.4. (A-B) SEM images of NCs; (A) 10 μm resolution and the inset shows an SEM image of the CU–PAH–dipotassium phosphate mixture before the addition of SiO ₂ NPs; (B) 5 μm resolution.....	33
2.5. Plot of the hydrodynamic radius (R _h) vs. the concentration of dipotassium phosphate where the concentration of the latter ranges between 0.01 and 5 mM. The measurements are done in triplicates.....	34
2.6. (A-B) TEM Images of NCs.....	35
2.7. STED confocal fluorescence image of the nanocapsule. The excitation	

	wavelength was 430 nm and the emission wavelength was 430 nm and the emission was collected using a band filter in the range of 460-600 nm.....	35
2.8.	Plot of [PAH] vs. $(F-F_0)/F_0$. The concentration of curcumin was fixed at 9.0 μ M whereas the concentration of PAH ranged between 0 and 3 mg/ml. F and F_0 are the fluorescence intensities of CU in presence and absence of PAH respectively. The excitation wavelength was 355 nm and the emission wavelength was 440 nm. The measurements were done in duplicates.....	37
2.9.	(a) Apparent zeta potential distribution of curcumin in water, (b) Apparent zeta potential distribution of PAH in water, (c) Apparent zeta potential distribution of PAH and curcumin mixture in water, (d) Apparent zeta potential distribution of PAH and K_2HPO_4 mixture in water, (e) Apparent zeta potential distribution of PAH, curcumin and K_2HPO_4 mixture in water, (f) Apparent zeta potential distribution of nanocapsules.....	37
2.10.	Thermogravimetric analysis of curcumin. TG: Thermogravimetric; DSC: Differential scanning calorimetry; DDSC: Derivative of differential scanning calorimetry.....	40
2.11.	Thermogravimetric analysis of nanocapsule. TG: Thermogravimetric; DSC: Differential scanning calorimetry; DDSC: Derivative of differential scanning calorimetry.....	40
2.12.	Thermogravimetric analysis of different nanocapsules.....	41
2.13.	Raman spectra of curcumin, PAH and nanocapsules.....	42
2.14.	Release of curcumin measured in absorbance scale from NC1 in different pH condition. Data were fitted with Higuchi model [130] for drug release. The measurements were done in duplicates.....	44
2.15.	Release of curcumin measured in absorbance scale from different nanocapsule in pH 5.0. Data were fitted with Higuchi model [130] for drug release. The measurements were done in duplicates.....	45
2.16.	Higuchi dissolution constant (K_H) versus particle size.....	45
2.17.	Chemical structure of 2,2-diphenyl-1-picrylhydrazyl (DPPH).....	47
2.18.	Change in DPPH absorption at 520 nm in the presence of curcumin and nanocapsules of different sizes in de-ionized water at room temperature. The concentration of curcumin and nanocapsules was fixed at 0.5 mg/ml and that of DPPH at 100 μ M. The measurements were done in triplicates.....	48

2.19.	The proposed 2,2-diphenyl-1-picrylhydrazyl (DPPH) scavenging mechanism of curcumin [134].....	48
2.20.	1/ ΔA of DPPH at 520 nm vs. R_h of nanocapsules indicating exponential increase in DDPH scavenging activity of CU.....	49
3.1.	Excited State Intramolecular Hydrogen Transfer (ESIHT) process.....	50
3.2.	UV-Visible absorption spectra of curcumin and nanocapsules of different sizes.....	54
3.3.	Fluorescence excitation spectra at $\lambda_{em} = 520$ nm for CU in buffer and NCs in de-ionized water.....	55
3.4.	Fluorescence emission spectra at $\lambda_{ex} = 427$ nm for CU in buffer and NCs in de-ionized water.....	56
3.5.	Fluorescence emission spectra at $\lambda_{ex} = 450$ nm for CU in buffer and NCs in de-ionized water.....	57
3.6.	Fluorescence emission spectra at $\lambda_{ex} = 355$ nm for CU in buffer and NCs in de-ionized water.....	57
3.7.	Fluorescence emission spectrum of NC at $\lambda_{ex} = 355$ nm along with deconvoluted spectra, the peak at ~ 400 nm is due to scattering.....	58
3.8.	Absorption and excited state deactivation processes of CU in water and NCs.....	59
3.9.	FT-IR spectrum of PAH.....	60
3.10.	FT-IR spectrum of CU.....	60
3.11.	FT-IR spectrum of NC.....	61
3.12.	Plot of N^*/E^* vs. R_h of NCs. The ratio of N^*/E^* is evaluated by measuring fluorescence ratio at 460 nm (normal emission) and 540 nm (ESIHT emission). The measurements were done in triplicates.....	62
3.13.	Fluorescence lifetime decay profiles for CU and NCs at $\lambda_{ex} = 460$ nm and $\lambda_{em} = 560$ nm, IRF is the instrument response function. The data were fitted with biexponential decay with a χ^2 between 1 and 3.....	63
4.1.	Illustration of Poly A interacting with SiO_2 NPs, and CU to form NCs....	68
4.2.	(A) Fluorescence spectra of curcumin in the presence of various nucleobases excited at 425 nm. The concentrations of the curcumin and	

	nucleobases were fixed at 5 μ M and 1 mg/ml respectively; (B) Relative change in fluorescence intensity of curcumin in the presence of nucleobases when the fluorescence intensity of curcumin without nucleobase was normalized to 1. The excitation wavelength was 425 nm and the emission wavelength was 550 nm. The measurements were done in duplicates.....	70
4.3.	The nucleobases used and their corresponding chemical structures.....	71
4.4.	(A) Fluorescence spectra of curcumin with silica NPs in the presence of various nucleobases excited at 425 nm where the concentrations of CU and nucleobases were fixed at 5 μ M and 1mg/ml respectively; (B) Relative change in fluorescence intensity of curcumin with silica NPs in the presence of nucleobases when the fluorescence intensity of curcumin with silica NPs without nucleobase was normalized to 1. The excitation wavelength was 425 nm and the emission wavelength was 495 nm. The measurements were done in duplicates.....	73
4.5.	(A) Fluorescence spectra of aggregates containing silica NPs, curcumin and PAH in the presence of various nucleobases excited at 425 nm where the concentrations of CU, PAH and nucleobases were fixed at 5 μ M, 3 mg/ml and 1mg/ml respectively; (B) Relative change in fluorescence intensity of aggregates containing silica NPs, curcumin and PAH in the presence of nucleobases when the fluorescence intensity of aggregates containing silica NPs, curcumin and PAH without nucleobase was normalized to 1. The excitation wavelength was 425 nm and the emission wavelength was 548 nm. The measurements were done in duplicates.....	75
4.6.	Chemical structure of Poly (9-(2-diallylaminoethyl)adenine.HCl-co-sulfur dioxide) (Poly A).....	77
4.7.	(A) Fluorescence spectra of capsules containing silica NPs, curcumin and Poly adenine (Poly A) in the presence of various nucleobases excited at 425 nm. The concentration of the capsule and nucleobases was fixed at 1mg/ml; (B) Relative change in fluorescence intensity of Poly A capsules in the presence of nucleobases when the fluorescence intensity of Poly A capsules without nucleobase was normalized to 1. The excitation wavelength was 425 nm and the emission wavelength was 543 nm. The measurements were done in triplicates.....	78
4.8.	(A-B-C) SEM images of capsules containing silica NPs, curcumin and Poly adenine (Poly A). (A) 5 μ m resolution whereas (B) 500 nm resolution and (C) 200 nm resolution.....	79
4.9.	FT-IR spectrum of Poly A polymer.....	80

4.10.	FT-IR spectrum of Poly A and curcumin based capsules.....	80
4.11.	Fluorescence lifetime decay profiles for Poly A capsules in the absence and present of different nucleobases at $\lambda_{\text{ex}} = 405 \text{ nm}$ and $\lambda_{\text{em}} = 540 \text{ nm}$. The data was fitted with biexponential decay.....	81
4.12.	FT-IR spectrum of guanine.....	83
4.13.	FT- IR spectrum of guanine and poly A capsules.....	84
4.14.	FT-IR spectrum of adenine.....	84
4.15.	FT-IR spectrum of adenine and poly A capsules.....	85
4.16.	FT-IR spectrum of cytosine.....	85
4.17.	FT-IR spectrum of cytosine and poly A capsules.....	86
4.18.	FT-IR spectrum of uracil.....	86
4.19.	FT-IR spectrum of uracil and poly A capsules.....	87
4.20.	FT-IR spectrum of thymine.....	87
4.21.	FT-IR spectrum of thymine and poly A capsule.....	88
4.22.	(A) Fluorescence spectra of Poly A capsules in various concentration of guanine excited at 425 nm where the concentration of Poly A capsule was fixed at 1mg/ml whereas guanine concentration varied between 0 and 7 mM ; (B) Linear change in fluorescence intensity of Poly A capsules with guanine concentration. The excitation wavelength was 425 nm and the emission wavelength was 526 nm for B. The measurements were done in triplicates.....	91
4.23.	Plot of concentration of $(F-F_0)/F_0$ vs. guanine concentration for estimation of binding constant. The concentration of guanine ranged between 0 and 7 mM and the fluorescence of the capsule was taken at 526 nm. The measurements were done in triplicates.....	92
4.24.	Stability of Poly A capsules compared to curcumin in buffer solution pH 7.5. The curcumin solution contained about 8 % methanol.....	94
5.1.	Illustration of PAH/dipotassium phosphate aggregated interacting with ZnO NPs to form NCs.....	95
5.2.	(A-B-C) SEM images of ZnO congregated capsules. (A) 5 μm resolution; (B) 2 μm resolution; (C) 1 μm resolution.....	99

5.3.	Absorption spectrum of 14 nm ZnO nanoparticles.....	99
5.4.	Fluorescence (or photoluminescence) excitation and emission spectra of 14 nm ZnO nanoparticles in ethanol.....	100
5.5.	Photoluminescence spectra of ZnO capsules at excitation wavelength 280 nm.....	101
5.6.	Photoluminescence spectra of ZnO capsules at excitation wavelength 310 nm.....	102
5.7.	(A) Photoluminescence spectra of ZnO capsules in different pH (phosphate buffer) solution at excitation wavelength 310 nm. (B) Relative change in fluorescence intensity with pH.....	105

LIST OF TABLES

Table		Page
4.1.	Fluorescence lifetime values for Poly A capsules in the absence and presence of different nucleobases at $\lambda_{\text{ex}} = 405 \text{ nm}$ and $\lambda_{\text{em}} = 540 \text{ nm}$. The data was fitted with biexponential decay.....	81
4.2.	Analytical methods for guanine estimation and their linear ranges.....	90

LIST OF ABBREVIATIONS

A	Adenine
CNTs	Carbon nanotubes
CU	Curcumin
CPQ	6,7-dicyano-2,3-di-[4-(2,3,4,5-tetraphenylphenyl)phenyl]quinoxaline
C	Cytosine
DNA	Deoxyribonucleic acid
DLS	Dynamic light scattering
DPPH	2,2-diphenyl-1-picrylhydrazyl
DSC	Differential scanning calorimetry
ESIHT	Excited state intramolecular hydrogen transfer
FISH	Fluorescence in situ hybridization
FRET	Fluorescence Resonance Energy Transfer
FT IR	Fourier transform infrared spectroscopy
G	Guanine
HPLC	High-performance liquid chromatography
HPTS	Hydroxy pyrene trisulfonate
IEP	Isoelectric point
LbL	Layer-by-layer
NC	Nanocapsule
NP	Nanoparticle
PL	Photoluminescence
PAH	Poly (allylamine hydrochloride)

PSAs	Polyamine- salt aggregates
Poly A	Poly(9-(2-diallylaminoethyl)adenine.HCl-co-sulfur dioxide)
QDs	Quantum dots
RNA	Ribonucleic acid
SEM	Scanning electron microscope
SiO ₂ NPs	Silica nanoparticles
TEM	Transmission electron microscope
TGA	Thermogravimetric analysis
T	Thymine
U	Uracil
ZnO	Zinc oxide

CHAPTER I

INTRODUCTION

A. Self Assembly:

Self assembly is a process by which pre-existing distinct components are self-assembled to generate an ordered structure or pattern without any external guidance [1,2]. Self assembly occurs everywhere in nature. Meteorological phenomena such as cloud patterns, astrophysical objects such as solar systems and biological systems like schools of fish and bacterial colonies are examples of natural self assembly [3].

The most extensively studied self assembly process is molecular self assembly. Protein folding is a good example of the latter. Molecular self assembly is usually driven by non covalent interactions including hydrogen bonds, electrostatic interactions and hydrophobic interactions [3]. Interestingly, poly (amino acids) such as poly (L-histidine), poly (L-lysine), and poly (L-arginine) self assemble into hexagonal lamellae [4,5].

As a powerful tool, self-assembly process is being utilized to generate advanced materials out of nanoparticle building blocks where molecular subunits spatially organize into highly defined supramolecular structures [6,7]. Well structured nanoparticles assemblies, like wires, rings, super lattice may be formed on a flat surface [8]. Magneto responsive fluorescent spheres (MFS) are produced by the self assembly of citrate-functionalized magnetic nanoparticles (MNPs) with poly (L-lysine) (PLL) and hydroxy pyrene trisulfonate (HPTS) aggregates [9]. Rotello and co-workers have succeeded to induce the self-assembly of gold nanoparticles into micrometer-sized

spherical aggregates, where polymer chains with complementary hydrogen-bonding pendant groups have been used [7]. Later, Stucky and co-workers mediated nanoparticle (NP) self-assembly to generate hollow microspheres using diblock copolypeptides; by which lysine and cysteine polymer blocks bind to silica and gold NP surfaces, respectively [10]. Poly (L-lysine)-curcumin mediated nanoparticle-assembles microcapsules termed as micro-curcumin are being synthesized [8]. Moreover, self assembly strategies are applied for precise construction of hydrogel materials with desired nano- and micro-structures, for instance, in the presence of salt, β -hairpin peptides self assemble into hydrogel networks [11].

B. Fluorescence:

As a powerful method, now a days fluorescence is being widely used in medical diagnostics, genetic analysis, biotechnology, forensics and other analytical fields. In biophysics and biochemistry, fluorescence spectroscopy, time-resolved fluorescence and fluorescence imaging are considered as primary research tools. Fluorescence is a highly sensitive method where it can work at single molecule scale for localization and measurement of intracellular substances [12].

Typically aromatic molecules are fluorescent. In 1845, Sir Jhon Frederick William Herschel was the first to report the phenomenon of quinine fluorescence in sunlight. Quinine is a widely encountered fluorophore, present in tonic water. The fluorescence of quinine is seen as a faint blue glow at the surface when observed from a right angle to the incident sunlight. Upon the addition of a less polar solvent, the dielectric constant of the solution increases, hence the quinine fluorescence becomes more apparent [13].

In the 1950's, the Department of Defence developed the first spectrophotometer due to their interest in utilizing quinine as an antimalaria drug [14]. In addition to phosphorescence, fluorescence is a type of luminescence: emission of light from a substance at its electronically excited states. Based on the nature of the excited state one of the two phenomena can be reported:

- Phosphorescence (spin forbidden): when the transition is from a triplet excited state to the ground state.
- Fluorescence: when the transition from singlet excited state to the ground state occurs [12].

1. Principles of fluorescence:

In general, the principles of luminescence can be described by the Jablonski's diagram shown in **Figure 1.1** [15].

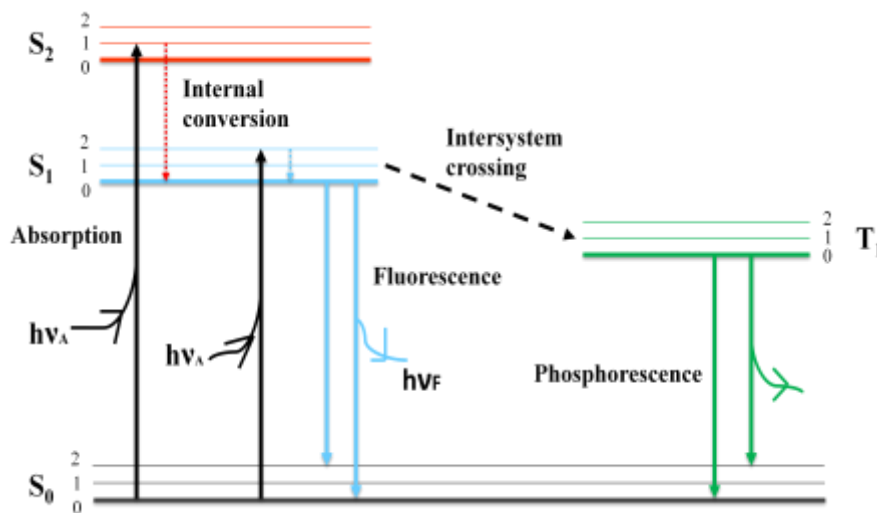


Figure 1.1. Jablonski diagram

Following light absorption, a fluorophore is usually excited to higher vibrational singlet states of S_1 and S_2 . However, molecules in condensed phases rapidly relax to the lowest vibrational level S_1 , in approximately 10^{-12} s, through a radiationless process called internal conversion. After this process is completed, fluorescence emission takes place from a thermally equilibrated singlet state, where the electrons in the ground and the excited state orbitals have opposite spin orientations to the ground state. This phenomenon is very short and occurs approximately in 10 nanoseconds [12]. Intersystem crossing may also occur, where molecules in the S_1 state can undergo a spin conversion to the first triplet state T_1 . The excited electron and the ground state electron have the same spin orientation, hence the transition from the triplet excited state to the ground state is forbidden. However, it can happen and in this case the emission of light is known as phosphorescence.

Phosphorescence is a slow process, where its duration ranges from few milliseconds to seconds. Molecules containing heavy atoms are more likely to be phosphorescent, where intersystem crossing in heavy atoms is much easier than that in lighter atoms [12].

2. Characteristics of fluorescence:

a. Stokes' Shift:

As revealed by Jablonski's diagram, the emission energy is typically less than that of absorption. This phenomenon known as Stokes' shift corresponds to a red shift in the emission spectrum relative to the excitation or absorption spectrum. Internal conversion is one of the common causes of the Stokes' shift. Furthermore, the decay of the fluorophores to higher vibrational levels of S_0 results in further dissipation of

excitation energy. In addition, further Stokes' shift may be due to excited-state reactions, energy transfer, solvent effects, and complex formation. As a result, the interaction between the fluorophore and its environment is expressed by the Stokes' shift [12].

b. Kasha's Rule:

In 1950, Michael Kasha proposed that irrespective of the excitation wavelength, the same emission spectrum is generally observed. Fluorescence is the emission of light from the lowest vibrational states of S_1 to the higher vibrational states of S_0 . Hence, upon excitation the excess of energy absorbed is lost via internal conversion leaving all fluorescent transitions similar [16].

c. Quantum Yields:

The quantum yield of a fluorophore is defined as the ratio of the number of photons emitted over the number of photons absorbed. Substances displaying the brightest emission have the highest quantum yield where it approaches unity. The quantum yield, Q , is given by:

$$Q = \frac{T}{T + k_{nr}}$$

where T is the rate of radiative decay, and k_{nr} is the rate of the non-radiative decay. The intensities of fluorescence are directly proportional to quantum yields. Based on quantum yields one can reveal the position of an intrinsic probe on a macromolecule. For instance, the fluorescence intensity of a weakly fluorescing probe in water is increased when this probe is buried inside a hydrophobic molecule [12].

d. Fluorescence Lifetime

The average time the molecule spends in the excited state prior to return to the ground state is defined as the fluorescence lifetime (τ); it is given by:

$$\tau = \frac{1}{T + k_{nr}}$$

The study of life time is important where it determines the available time for the fluorophore to interact with or diffuse in its environment.

Factors which affect either of the rate constants (T or k_{nr}) can modify the quantum yield and the lifetime. For instance, slow rate of emission or fast rate of internal conversion may render a substance non fluorescent [12].

e. Fluorescence Quenching:

Quenching is referred as the decrease in the fluorescence intensity. Two types of quenching are described: the collisional quenching and the static quenching.

Collisional quenching is due to the deactivation of the excited-state fluorophore upon its contact with other molecule in solution, known as the quencher. Various molecules can act as quenchers including halogens, amines, oxygen and electron-deficient molecules like acrylamide. Static quenching is due to the formation of non fluorescent fluorophore-quencher complexes in the ground state.

Quenching is described by the Stern- Volmer equation:

$$\frac{F_0}{F} = 1 + K_{sv}[Q] = 1 + k_q\tau_0[Q]$$

where F_0 and F are the intensities in the absence and presence of the quencher respectively, K_{sv} is the Stern- Volmer quenching constant, k_q is the biomolecular quenching constant, τ_0 is the unquenched lifetime and $[Q]$ is the quencher concentration. K_{sv} is large when the fluorophore is free in solution and very accessible to the quencher. However, if the latter is away from the fluorophore K_{sv} is low. Fluorescence quenching is important where it is used to determine the position of a probe on a molecule [12].

3. Steady- State and Time- Resolved Fluorescence:

Broadly, there are two types of fluorescence measurements, steady-state and time-resolved. In steady state measurement, the sample is continuously illuminated, and the intensity versus wavelength is recorded. While for the second type of measurement, the sample is exposed to a light pulse, shorter than its decay time and the intensity decay versus time is recorded. It is worth to note that these two measurements are correlated.

For a fluorophore displaying a single decay time (τ), the intensity I is given by

$$I(t) = I_0 e^{-t/\tau}$$

where I_0 is the intensity at $t = 0$ immediately after the pulse.

The steady state intensity I_{ss} and the decay time are related by

$$I_{ss} = \int_0^{\infty} I_0 e^{-t/\tau} dt = I_0 \tau$$

A time-resolved measurement shows two decay times for a probe on a molecule existing in two conformations, while steady-state measurements only reveals average intensities, thus the significance of doing both measurements [12].

4. Fluorescence Sensing and Nanotechnology:

Fluorescence based detection is the most dominant method in the field of biosensing due to its simplicity, the convenience of optical signal transduction, the vast growth achieved in imaging and the availability of organic dyes with diverse spectral properties. However, in fluorescence detection, quantum yields or extinction coefficients of organic dyes and the low dye-to-reporter molecules labelling ratio, makes it difficult to obtain low detection limits [17]. The recent advances in nanotechnology, yielding to the production of submicron-sized materials with unique optical properties, have opened up new perspectives for fluorescence detection. Nanomaterials can be synthesized from organic and inorganic materials. Such materials are of small size scale, less than 100 nm in length along at least one dimension, hence owing a large surface area. Nowadays, nanomaterials are used as detection labels instead of traditional organic dyes due to their superior optical properties including higher photosatability, brighter fluorescence, wider selections of excitation and emission wavelengths, etc [17]. In addition the selection of various probes for higher assay throughput is facilitated by their shape or size-controllable optical properties. These nanostructures are used as solid supports for sensing assays where multiple probe molecules can be attached to each nanostructure leading to simplified design of assay and increased ratio of labelling for higher sensitivity. Nanomaterials applied in the fluorescence based sensing field include quantum dots, silica nanoparticles, gold nanoparticles, carbon dots and carbon nanotubes [17].

a. Quantum Dots (QDs):

In biosensing and imaging fields, quantum dots are considered to be important fluorescence labels [17, 18]. QDs are semiconductor nanocrystals consisting of atoms of elements from groups II to VI (e.g. Zn, Cd, Te, Se) or III – V (e.g. P, As, In) in the Periodic Table [18,19]. Quantum confinement effect is due to their very small size (< 10 nm) resulting in narrow emission bands, wide UV- visible absorption spectra, and size, composition and shape-related optical properties [17,20]. They are excellent labels for high throughput screening due to the high flexibility in excitation wavelength selection with minimal overlap in the emission spectra from multiple QDs.

In comparison with organic dyes, QDs owe similar quantum yields but 10-50 times larger extinction coefficients, and much less rates of photobleaching. The net effect is that QDs have ~ 100-200 times better photostability and 10-20 times brighter fluorescence [21].

QDs are intrinsically fluorescent; hence they serve as reporter molecules for biochemical detection. For instance, Western blot detection kits based on QD can lead to detection limits as low as 20 pg protein per lane [22,23], where as colorimetric or chemiluminescent detection is only able to detect around hundreds of pico grams of protein per lane [24]. Genin et al. developed a smart protein targeting strategy that involves the linkage of QDs to an organic dye of CrAsH. By using this probe Cystine-tagged proteins were traced for more than 150 seconds [25].

Furthermore, QDs can be used in fluorescence in situ hybridization (FISH) offering higher detection limits than organic dyes. For example, the mRNA expression in neurons of a mouse located within the midbrain region was detected by QD FISH at $\times 4$ magnification, whereas it could only be done at $\times 20$ magnification when using Alexa Fluor[26].

QDs are very promising substituent for traditional organic dyes in biochemical labelling. However, their surface properties need to be enhanced for better functionality and aqueous solubility, their stability needs to be improved, their nonspecific binding to biomolecules should be minimized and there *in vivo* toxicity needs to be solved [17].

b. Fluorescent Silica Nanoparticles:

Silica nanoparticles doped with organic dyes have been widely tested as labelling reagent in proteins, pathogens and nucleic acid detection [27,28]. Such type of nanomaterials offer the following advantages in biosensing: (i) silicon is nontoxic and widely abundant; (ii) the nanoparticles can bind easily to biomolecules due to their high surface-to-volume ratio; (iii) the ability to embed a large number of fluorescent dye molecules within each particle increases the dye-to-biomolecule labelling ratio yielding to elevated factors of signal amplification; (iv) In chemical reactions, silica is relatively inert, however its surface can still be modified with well-established chemistries [27,29].

In comparison to quantum dots, fluorescent silica nanoparticles, owe a wider range of size, ranging from a few to hundreds of nanometers; they have better solubility and need less strict size control [27,29]. But, limitations concerning particle aggregation and nonspecific binding on the surface of silica have been reported and needs to be solved [27].

c. Gold Nanoparticles:

Gold (Au) nanoparticles are considered as important FRET-based quenchers, where their Plasmon resonance in the visible region makes them strong scatterers and

absorbers of high extinction coefficient $\sim 10^5 \text{ cm}^{-1}\text{M}^{-1}$ [17]. Gold nanoparticles are gaining more interest in bioassays due to their controllable particle size, and the ability to attach biomolecules containing exposed thiol groups to the surface of gold via gold-sulfur bonds. Furthermore, this gold-sulfur bond facilitates the linkage of other functional groups such as amine and carboxyl groups through sulfur containing ligand [17]. The most known application of Au NPs in FRET-based assays is the labelling of molecular beacons [30].

Bridge molecules can be used to increase the proximity between the fluorophores and Au NPs. For instance, fluorescein molecules form inclusion complexes with β -cyclodextrin (CD) attached to Au NPs; fluorescein was then quenched [17]. This system has been employed for cholesterol detection where fluorescein was freed from the NP through its replacement by cholesterol at the binding site. Here, the system's fluorescence intensity increases with cholesterol concentration [17]. As well, Au NPs are excellent *in vivo* imaging reagents because of their small particle size. For example, Au NP modified with FAM-labelled single-stranded DNA has been employed to image intracellular hydroxyl radicals [31].

d. Carbon Nanotubes:

Another type of unique nanomaterial used in fluorescence-based bioassays is the carbon nanotubes (CNTs). The application of CNTs in sensing is based on its ability to quench organic dyes or QDs [32,33]. In this course, it was shown that multiwall CNTs suppress the photoluminescence (PL) of CdSe QDs via both dynamic and energy transfer quenching mechanisms [33]. In addition, the self-assembly of oligonucleotide-modified QDs and CNTs enable the detection of antigen and DNA down to 0.01 nM

and 0.2 pM levels respectively. Similarly, CNTs can quench organic dyes via an energy transfer mechanism [34]. This concept has been adapted to synthesize a non covalent assembly between ssDNA and CNT for sensing of biomolecule interactions [35].

C. Capsules:

Capsules are tiny sphere-like containers composed of two distinct regions, the core and shell region [36,37]. The core stores and protects the encapsulated material. The shell serves also for encapsulating aims, but its main role is to act as a physical barrier to control the diffusive release of the encapsulated active material [38]. Capsules are classified according to their size into 3 categories, microcapsules, nanocapsules and mesocapsules [39]. Microcapsules are those having diameters greater than 1 μm , nanocapsules are those having diameters less than 100 nm, whereas capsules in 100 nm-1 μm size range are termed as mesocapsules [39].

Liposome or vesicle is one of the earliest capsule structures. It is similar to a living cell without its internal contents, where it is prepared by the self-assembly of phospholipid molecules into bilayered spherical membrane structure [40,41]. In this course, amphiphilic block copolymers that can self-assemble into vesicles have been reported recently [42,43]. These assemblies are known as polymersomes, and owe an increased stability compared to their lipid counter parts. More recently, it has been reported that dendrimersomes, capsular structures, are being formed from the assembly of Janus (two-faced) amphiphilic dendrimers [44]. Dendrimers are of low polydispersity index, hence allowing greater control over the structure and sizes with a structural stability comparable to that of polymersomes [38].

1. Capsule Synthesis:

Capsule synthesis approaches can be widely categorized into two main routes: hard and soft template routes. A more recent route, tandem self assembly, has been developed for capsules synthesis.

a. Hard-Template Routes:

Templating against hard colloids is the most commonly used approach for the synthesis of capsules. Colloidal particles serving as templates include micro- or nano scale polymer, gold, silica and silver *etc.* Typically, to generate core-shell composites a thin coating of the desired material is formed on the template; subsequently the latter can be left or removed to produce filled and hollow spheres respectively [45]. The template removal can be achieved by calcination at elevated temperatures or selective etching in an appropriate solution. For coating the template with a thin shell of the desired material, a wide variety of techniques have been developed [45].

i. Layer by Layer Assembly (LbL):

In 1966, Iler was the first who described the alternate deposition of oppositely charged particles to generate a film of multiple layers [46]. Twenty five years later, Decher and his colleagues adopted this concept for the synthesis of thin films of oppositely charged polymers [47,48]. As a highly versatile method, LbL assembly can be performed on both planar and colloidal substrate of almost any surface chemistry with various polymers and other components, such as, nanoparticles, proteins, DNA, and viruses [49,50,51,52].

This technique involves the immersion of a charged substrate (e.g. negative) into a solution of oppositely charged polymer. The substrate is rinsed and immersed into a negatively charged polyelectrolyte solution once the adsorption of the positively charged polymer reaches equilibrium. This process can be repeated several times to generate multilayered films [53] (see **Figure1.2**).

As well, layer by layer assembly can be performed on colloidal substrates (see **Figure1.3**). The polymer adsorbs on the colloidal substrates in the same manner as on planar surfaces. A cycle of centrifugation and resuspension is the required to remove the polymer solution. Altering the number of deposited layers controls the shell thickness. The formed particles can be in the core-shell state, or the core can be dissolved to get hollow polymeric capsules [53].

LbL assembly technique has been successfully utilized to generate porous capsules of a variety of composite or inorganic materials, such as Plasmon resonance Au [54], photocatalytic TiO₂ [55], ultrathin SnO₂ and MnO₂ [56], magnetic Fe₃O₄ [57] and Mg-Al layered double hydroxide [58].

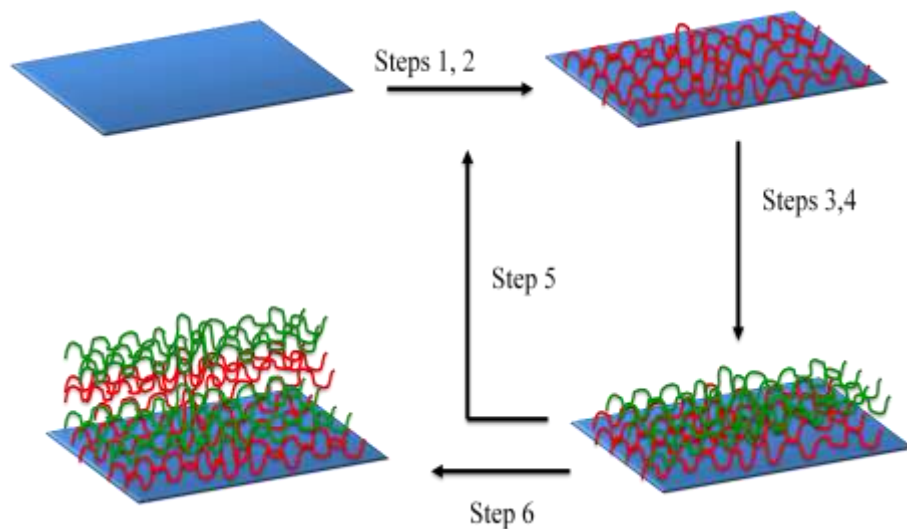


Figure 1.2. Schematic of Layer-by-Layer (LbL) assembly on planar substrates. (1) Immersion in a positively charged polyelectrolyte solution; (2) rinse; (3) immersion in a negatively charged polyelectrolyte solution; (4) rinse; (5) repeat steps 1–4 until desired number of layers has been deposited; (6) core–shell particles can be the end of the process, or the template is dissolved away to leave a hollow polyelectrolyte capsule.

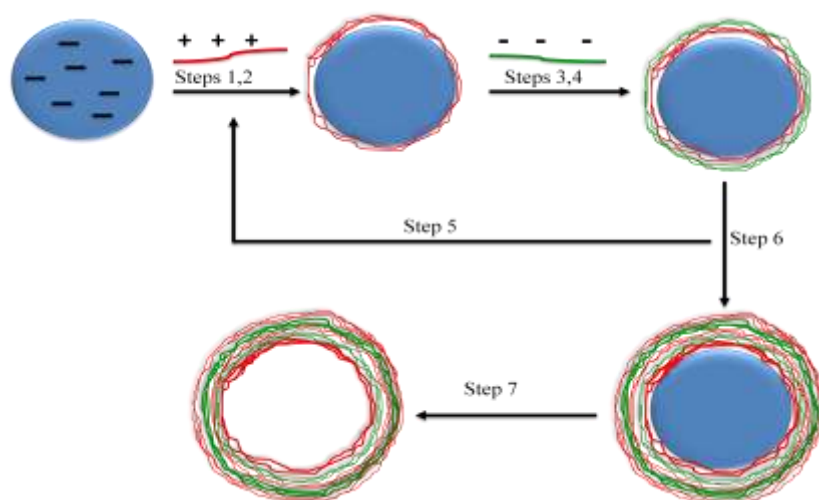


Figure 1.3. Schematic of Layer-by-Layer (LbL) assembly on colloidal substrates. Steps: (1) treat with positively charged electrolyte; (2) centrifugation/rinse for removal of excess polyelectrolyte; (3) treat with negatively charged polyelectrolyte; (4) centrifugation/rinse; (5) repeat steps (1) through (4) to deposit additional layers; (6) template with desired number of layers; (7) polyelectrolyte capsules are formed by removal of colloidal template.

ii. Direct Chemical Deposition or Adsorption:

Although LbL has shown great success in capsule fabrication, it still has some limitations. For instance, the formed capsules are usually of large diameters and the procedure is long and time demanding. To overcome these drawbacks, direct chemical deposition or adsorption method, where special surface modification is not required, has been extensively developed [45]. This technique is widely applied in the preparation of hollow SiO₂ capsules [59,60,61] Hyeon *et al.* [61] adopted this approach for the synthesis of mono-dispersed and discrete core-shell and hollow meso-porous silica nanocapsules where Fe₃O₄ nanocrystal colloid served as a template. Furthermore, this technique is used to generate a variety of capsules with controllable surface morphologies including double shelled SnO₂ [62], hierarchical Pt [63, 64] and nano cup-shaped Fe₂O₃ [65,66].

iii. Sacrificial Template Routes:

The above hard-template routes are considered as simple and easy ways for capsules preparation. But these routes require the use of acid or base medium or high temperature for template removal; hence increasing the cost and risk of large scale-industry. A new synthetic strategy has been developed recently, where micro/nano rods or spheres are first produced and serve as self-sacrificing template for the growth of capsules. The template acts as simple shape-defining molds as well as chemical reagents for the generation of porous capsules [45]. For instance, Zhu and co-workers have synthesized hydroxyapatite (HAp) nanostructured porous hollow ellipsoidal capsules, where these capsules have been formed by a nanoplate network using inorganic CaCO₃ as a template [67].

b. Soft-Template Routes:

Hard-template routes are highly effective and common method for capsule preparation, but the removal of the template usually degrades the integrality and structural robustness of target products. Synthetic approaches based on soft template have been investigated to overcome these limitations. Micelles, liquid crystals, vesicles, reverse micelles, *etc* are organized systems formed via a self-assembling process. Such systems serve as nano-reactors and are used as soft templates for capsule preparation [45].

i. Emulsion/Phase Separation Procedures:

Surfactant molecules, which contain a hydrophilic head and hydrophobic chain, can self-assemble in solution into a wide variety of organized structures, such as micro-emulsions, normal and reverse micelles, lyotropic liquid crystals and vesicles [68]. Such systems have been successfully utilized in capsules templating. For instance, Feldmann and co-workers have produced AlO(OH) hollow capsules through a water-in-oil microemulsion, where the liquid-to-liquid-phase boundary of the micellar system has been applied as a template [69]. Recently, Li and co-researchers have adopted this micellar aggregate templating technique to fabricate hollow meso-porous SiO₂ nanocapsules of tunable size [70].

c. Tandem Self Assembly or Polyamine-salt aggregate 'PSA':

At the present, material chemists widely use the hard and soft-templating synthesis methods for capsule structures preparation. However, drawbacks related to long synthetic steps and high cost, have limited their use in practical applications [71].

To solve these difficulties, a relatively new concept of capsule formation via polyamine-salt aggregate or ‘PSA’ has been developed [6, 72]. This technique is originally termed as ‘tandem self-assembly’ (see **Figure 1.4**)

It involves the combination of a cationic polyamine with a multivalent anionic salt, resulting in the spontaneous generation of ionically crosslinked PSAs [73, 74]. The capsule is formed through further addition of negatively charged shell material on PSAs that serves as the capsule template [75, 76]. For further use, the polyamine-salt template can remain in the capsule’s core; however, after shell formation it can spontaneously disassemble, based on polymer and salt types, leaving a capsule with water filled core. As the polymer part participates in shell formation and is a main shell constituent, the PSA is not strictly a soft or hard template method [38].

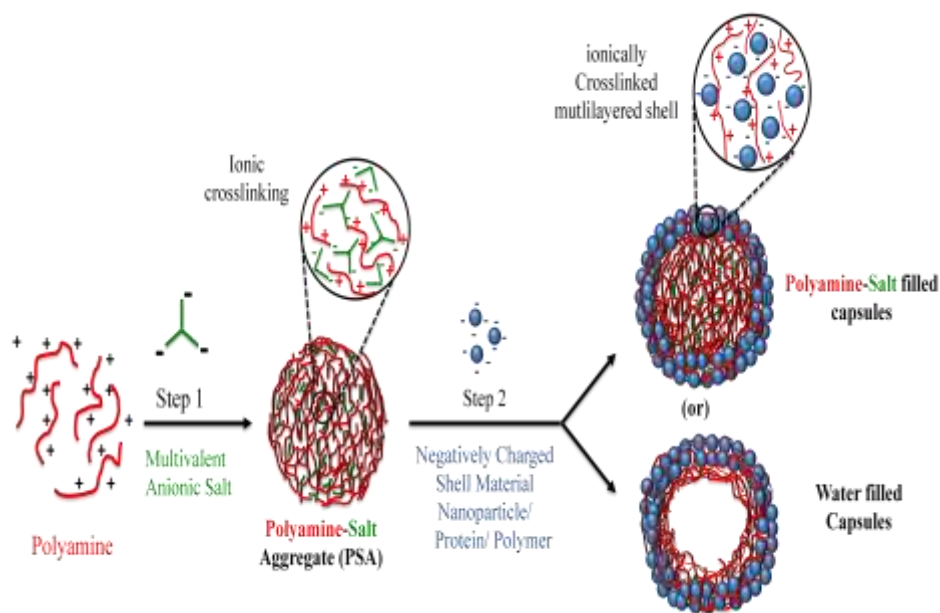


Figure 1.4. Schematic of Polymer-Salt Aggregate (PSA) assembly. Steps: (1) polyamine chains are ionically crosslinked with multivalent anionic salt to form polyamine-salt aggregates (PSAs); (2) PSAs act as a template for the shell material deposition in a second mixing step to generate capsules with thick multilayered shells.

This approach has numerous benefits: (i) the template is formed in situ by the ionic crosslinking of the salt and polyamine; hence a preformed template is not needed [6], (ii) the template is of tunable size, where it can be changed by altering the processing parameters (e.g. aging time [6], polyamine concentration [77], polyamine-salt ratio [6, 73]) to produce capsules of different sizes, (iii) contrary to LbL assembly, there is no need for several centrifugation steps for shell deposition [5], (iv) encapsulation is achieved by adding the cargo prior to the PSAs capping with a shell-forming material [73, 78], (v) the procedure requires mild processing conditions (room temperature and near-neutral pH) and simple mixing [38] and, (vi) the constituents of the capsules including the polyamine and salt as well as the shell forming material can be altered for specific application/cargo [38].

The concept of tandem self-assembly of polymer molecules and charged nanoparticles is broadly applied. For instance, metal oxides nanoparticles, like tin and zinc oxide, can be used to synthesize capsular structures. To generate such capsules, the particle surface must be negatively charged under the conditions of synthesis. Microcapsules formed of citrate-stabilized CdSe and carboxylated polystyrene beads are also being reported. Interestingly, the aggregates of citrate-bridged PAH adsorbed onto a mica surface can yield to dome-like shells. In addition, negatively charged linear polyelectrolytes, such as poly (styrene sulfonic acid) and poly (acrylic acid), can also produce microcapsular structures [2].

i. Cargo Encapsulation:

The encapsulation of a molecular compound is usually achieved by adding it prior to shell material deposition [6, 73, 78]. Similar to the shell materials, the cargo can

be zwitterionic; however, to ensure efficient encapsulation, it needs to have a net negative charge. For small molecules (e.g. dyes, drugs), it is controlled by their pKa's; whereas for larger cargo (e.g. enzymes) it is controlled by their isoelectric point (IEP). Efficient encapsulation is ensured by greater number of net negative groups; hence, highly negative cargo, like siRNA and oligonucleotides, show better encapsulation efficiencies [79]. In addition to electrostatic, hydrogen bonding and hydrophobic effects may have a role in the chemistry of encapsulation; where the effect of the latter is clearly proved in the NIR dye indocyanin green (ICG) encapsulation in PAH phosphate PSA's [77, 79]. Knowing that ICG has only one net negative charge (two negative and one positive), extremely high encapsulation efficiency- up to 26% of the capsule weight- has been reported [77]. This corresponds to the strong hydrophobic interaction of ICG with PAH backbone. Furthermore, encapsulation can occur if the cargo has multiple negative groups. These cargo materials can themselves replace the salts (e.g. phosphate and citrate) to assemble the polyamine. Recently, this has been applied with DOTP⁵⁻, a gadolinium MRI contrast agent [80], whose high encapsulation efficiency is due to its ionic-crosslinking with polyamines (PAH and PLL) [38].

D. Nanotechnology and Drug Delivery:

Nanobiotechnology is an interdisciplinary field that combines biology, chemistry, medicine and engineering. The revolution in this field leads to vast development of drug-delivery systems and devices. Novel formulations and materials are being used for site-specific targeting and controlled release of recombinant proteins, traditional pharmaceuticals, nucleic acids and vaccines [81].

Nano-scale drug-delivery devices are employed to regulate biodistribution to tune the kinetics of release and decrease the toxic side effects of a given drug; hence improving its therapeutic index [82]. More investigations are done to achieve “smart” drug delivery by the generation of delivery systems that include biosensing functionalities with in vivo feedback [83, 84].

The aims of drug delivery are (1) to solve the problems associated with biomolecular therapeutics, including short plasma half-life, potential immunogenicity and low stability, and (2) to increase the drug’s therapeutic activity while minimizing its toxic side effects [85]. Currently, drug-delivery systems are efficient at controlled drug release to generate a high local concentration; but the problem is that release is limited to targeting tissues rather than individual cells [81].

In drug delivery, the nano-meter size range offers a variety of advantages including the ability of drug delivery carriers to pass through cell membranes, reduction of the undesired clearance from the body via spleen or liver and minimization of the drugs absorption by the reticuloendothelial system [85, 86]. As well, smaller particles have higher surface area-to-volume ratios; this elevates the dissolution rate of the particle and helps to overcome their solubility-limited bioavailability [87]. The size variation extremely affects the blood circulation time and bioavailability of a drug carrier [88, 89]; where the most suitable size range for a nanoparticle drug delivery carrier is 10 to 100 nm [90].

Nano-scale drug delivery systems can be manufactured for various applications, including oral, implantable, injectable, inhalable, transdermal and topical drug delivery [81]. Electrostatic binding, physical adsorption, complementary recognition and covalent coupling are techniques used to functionalize nanoparticles

with biomolecules [91]. The linkage of targeting moieties improves receptor-mediated delivery [92]. Furthermore, effective intracellular targeting to specific organelles can be achieved by nanoparticle modification. For example, changing the surface area can control their position in the cell; where cationic particles are found in cytoplasm and within the mitochondria, while anionic particles remain in the lysosomes [93].

For simple drug delivery aims, spherical nanoparticles are the simplest to create, whereas for more complicated applications supra-molecular systems including nanocapsules, nanotubes, dendrimers and nanogels are needed [81].

1. Nanocapsules and Drug-Delivery:

Polymeric and lipid nanocapsules are drug-delivery systems of nano-scale size. These capsules offer efficient targeting and controlled drug release [94, 95]. Their dispersion stability and primary physiological response particularly depend on their outer coating composition. Important factors must be considered during their synthesis including capsule size and thickness, membrane decomposition, radius distribution and surfactant type [94]. To alter their permeability, lipid based nanocapsules can be modified through channel insertion. In addition, antibodies are attached to these capsules to target specific cells or tissues. Lipid based nano-capsules have stable cargo. For instance, Cisplatin nanocapsules show enhanced cytotoxicity against tumour cells in vitro as compared to free drugs [81]. However, the lipid's instability in biological media and sensitivity to external parameters, like osmotic pressure and temperature, limits the lipid nanocapsules' use in drug delivery [81].

Lipid-polymer conjugate nanocapsules have been developed to improve the lipid-based nanocapsule's stability. Such approaches include, the addition of surface-

active polymer creating mixed vascular structures, the coating of the liposome with a polyelectrolyte shell and the polymerization of a two-dimensional network in the hydrophobic core of the membrane [81].

Polyelectrolyte capsules exhibit numerous advantages, such as controlled membrane thickness, release kinetics and surface properties [96]. In response to environmental conditions, like pH and temperature, these capsules can be in both opened and closed states; hence, various materials can be encapsulated and released [97] such as, enzymes, nucleic acids, drugs and dyes [98, 99].

The “vault”, named for its morphology, is a naturally occurring cellular nanoparticle that serves as a biocompatible nanocapsule. The vault is a 13-MDa ribonucleoprotein particle, where hundreds of protein molecules can be sequestered in its internal cavity by the attachment of a vault-targeting peptide to the protein [100]. Interestingly, disulfide cross-linked polymer nanocapsules have been innovated [101]. At physiological pH, disulfide bond provides increased stability to hydrogen bonded multilayer thin films. Moreover, in the presence of thiol-disulfide exchange reagents it makes the system susceptible to disassembly. Consequently, these nanocapsules can be utilized as “biodeconstructible” nano-scale drug-delivery system [97, 102].

E. Capsules and Sensing Applications:

The design of structurally well-defined architectures with stimulus and dynamic responsive properties is one of the main challenges in material chemistry. Interests has been growing in nanomaterials which are responsive to the surrounding environments to transform biochemical and chemical signals into electrical, thermal, mechanical and optical signals, and vice versa [103]. Such materials are important for

sensing applications. Here in, pH sensitive microcapsules structures are being synthesized by the self-assembly of silica NPs with poly (L-lysine) and HPTS (8-hydroxy pyrene-1, 3, 6-trisulfonic acid) aggregates; where the latter is a pH sensitive probe [103]. PAH-phosphate nanocapsules highly loaded with ICG are used as protease-sensitive NIR probes. These polyamine-salt assembly probes owe special and unique features: (1) the NIR dye encapsulation would happen via non-covalent interactions and (2) more efficient quenching is achieved due to homogenous distribution of dye throughout the particle volume [38]. Moreover, hemoglobin gold nanoparticle-assembled capsules (Hb-GNACs) are constructed for biosensing aims. These biosensors have displayed good catalytic performance to hydrogen peroxide (H_2O_2) with detection limit of $0.93 \mu\text{M}$ and a linear range of $1\text{-}140 \mu\text{M}$ [77]. Recently, microcapsules are formed by cross-linking poly (L-lysine) with citrate triggered by silica NPs and acridine orange. These capsules serve as DNA sensors where DNA estimation is in ng ml^{-1} concentration range [104].

F. Aims:

In the present thesis we present, in Chapter II, the preparation method of poly(allyl amine hydrochloride) (PAH) /curcumin (CU) based nanocapsules, including the materials and techniques used. We discuss the effect of dipotassium phosphate on the size of the nanocapsules. We also study their morphology, and propose the location of silica nanoparticles and CU in the capsule. As well we determine the form and percentage by weight of the latter. In addition, we measure the surface charge of the capsule and determine the binding constant of CU and PAH. Besides, we study the release of CU from capsules having different sizes in different environments (acidic,

basic and neutral) for each. We also propose a model for the release profile of curcumin. Finally, we study the 2,2-diphenyl-1-picrylhydrazyl (DDPH) scavenging activity of CU within the capsule and investigate the effect of capsule's size on this activity.

In Chapter III, we focus on the photophysical properties of CU, specifically we highlight the excited state intramolecular hydrogen transfer (ESIHT) phenomena in CU. We study the effect of encapsulation on the latter phenomena; as well we investigate all the possible interactions between the components of the capsule.

In Chapter IV, we explain the synthesis method of Poly Adenine [Poly(9-(2-diallylaminoethyl)adenine.HCl-co-sulfur dioxide)]/ CU based nanocapsules. We determine their morphology and size. Moreover, we study their sensing abilities towards different nucleobases, including guanine, cytosine, adenine, thymine and uracil. We calculate the binding constant of Poly A capsule and guanine. In the last part of this chapter we study the stability of the capsule in neutral conditions (at pH= 7.5).

In Chapter V, we explain the method of preparation of PAH/ zinc oxide (ZnO) nanoparticles based capsule. We determine its morphology and size. We investigate the effect of encapsulation on the luminescence properties of ZnO nanoparticles, and study the effect of pH on its fluorescence.

CHAPTER II

RELEASE OF CURCUMIN

A. Introduction:

1. Curcumin (CU) and Its Medical Significance:

Curcumin, bis (4- hydroxy -3- methoxyphenyl) -1, 6- diene- 3, 5- dione [105], is a natural diphenolic yellow orange pigment extracted from the dried rhizome of turmeric *Curcuma longa*, a perennial herb that is widely cultivated in southeast and south tropical Asia [106]. CU is a β - diketone that tautomerizes between its enol and keto structures (see **Figure 2.1**). The diketo form is favoured in solid phase of CU while enol form in solution [8]. CU is a major component of curry spice, and it is extensively used in traditional Arabic and Indian cooking [105]. For industrial applications, CU is used as a dye for the conservation and colouring of food, as well in cosmetics [107, 108].

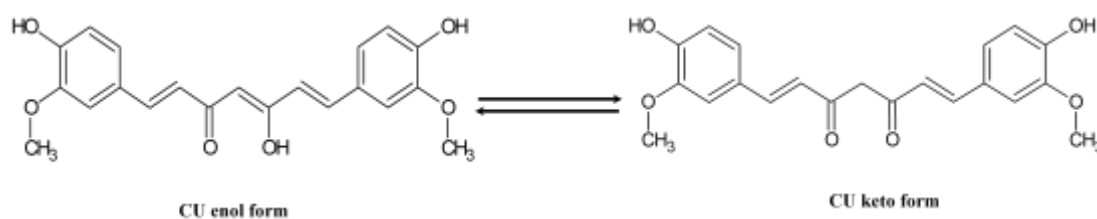


Figure 2.1. Chemical structures of curcumin tautomers.

Concerning its therapeutic efficiency, CU has been applied as a house hold drug since the ancient times [109, 110], where its anti- inflammatory and healing properties are even reported in the sacred books of ayurveda [105].

In the last 20 years, a large number of publications have shown that CU depicts effective therapeutic properties not only as an anti-inflammatory drug [109, 111], but also as a chemo-preventive [112, 113], chemotherapeutic [114, 115], anti-oxidant [112, 116], antiamyloid [117], antiarthritic [118], anti- HIV [8], hepatoprotective [117], antimicrobial [119, 120] and thrombosuppressive [121] agent. In addition, CU is being used in the treatment of cystic fibrosis [122] and Alzheimer disease [123]. Research over the last few decades has proven that CU owes a strong therapeutic potential against numerous types of cancer. CU has been shown to inhibit the proliferation, metastasis and transformation of tumours; where it has been demonstrated that it arrests the cancer cells in various phases of the cell cycle and induces apoptosis (programmed cell death) [106] .

2. Limitations of CU Delivery and its Available Delivery Systems:

Although CU has numerous medicinal benefits with high safety profiles, even at doses as high as 8 g day⁻¹, the administration of CU to patients has a serious practical limitation [8]. Wahlstrom et al. [124] reported that when rats were administered CU at a dose 1 g/Kg, about ¾th of CU was excreted in the feces, whereas negligible amounts of CU were present in the urine. Blood plasma levels and biliary excretions measurements showed that CU is poorly absorbed in the gut; moreover, the CU's quantity that reaches tissues outside the gut is pharmacologically insignificant. Hence, to reach the therapeutic effects of CU in the human body, a person must ingest between 12 to 20 g of CU daily [125].

The low bioavailability and poor water solubility (i.e 0.0004 mg ml⁻¹ at pH 7.3) of CU can be solved by applying nanotechnological delivery approaches [126]. CU has

been encapsulated in bovine serum albumin, chitosan, liposomes [125], polymeric nanoparticles and silica particles [8]. Also it has been complexed with phospholipids and cyclodextrin [127].

The synthesis of curcumin- encapsulated polymeric nanoparticles of N-isopropylacrylamide with N-vinyl-2-pyrrolidone and poly(ethylene glycol) monoacrylate recently has been reported [125]. As well, CU has been encapsulated in poly(L-lysine) based microcapsules termed as Micro-curcumin. The later approach is based on polymer blocks self-assembly on surfaces of nanoparticle. The formed microcapsules are spherical with core/shell structure [8].

3. Aims:

In the present thesis, we aim to encapsulate CU in poly(allylamine hydrochloride) (PAH) (see **Figure 2.2**) based nanocapsules; where CU associated PAH crosslink with dipotassium phosphate and consequently congregates ~ 24 nm SiO₂ nanoparticles to form hierarchically ordered nanocapsule structures of 100-1000nm size depending on the concentration of dipotassium phosphate. We applied these capsules as a vehicle for CU delivery.

The advantages of the present method are: (i) the ease of preparation and purification of the nanocapsules; (ii) unlike earlier delivery systems with silica particles, the formation of template is in situ, hence no need for a preformed template and polymerization/ hydrolysis under acidic condition [8]; (iii) finally, it is fast and doesn't require long hours of preparation steps.

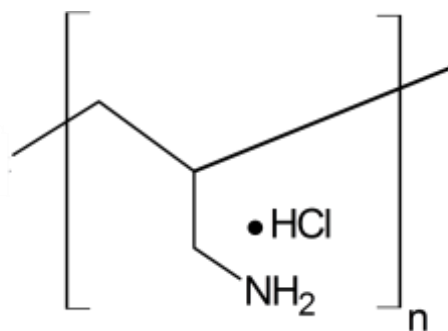


Figure 2.2. Chemical structure of poly (allylamine hydrochloride) (PAH)

B. Materials:

Curcumin was obtained from Acros Organics and directly used without further purification. CU is poorly soluble in water and degrades in aqueous medium, so the stock solution of CU was prepared in 10 % acetone/ de-ionized water. Poly(allylamine hydrochloride) and Silica LUDOX[®] HS-40 Colloidal Silica, 40 wt% suspension in water, were obtained from Sigma- Aldrich; where the silica particle size was ~24 nm (Sigma-Aldrich). PAH stock solution was prepared in de-ionized water of pH 4.4 to ensure the formation of PAH/dipotassium phosphate aggregates. Dipotassium phosphate used was obtained from SOLAR LABORATORIES and its stock solution was prepared in de-ionized water.

C. Methods:

1. Preparation of Nanocapsules (NCs):

Nanocapsules were prepared by mixing 1.3 ml of 3 mg ml⁻¹ poly (allylamine hydrochloride), PAH (pKa=8.6), with 0.5 ml of 1 mg ml⁻¹ of CU. The interaction of CU with PAH was found to be strong due to electrostatic as well as hydrophobic interaction between them; it has been reported that such interactions play a crucial role in the

encapsulation chemistry [6]. Then self-assembly of the mixture solution was achieved by cross-linking the CU-PAH chains with 7.8 ml of 2.5 mM dipotassium phosphate in aqueous media at pH 4.4 and aged for 30 minutes. It is worth to mention that the ionic-crosslinking of polyamines by anionic salts occurs when both have their respective charge, where the latter depends on the pKa values of the salt and polymer [6]. Therefore, a pH of 4.4 maintains the positive and negative charge of PAH (pKa=8.6) and dipotassium phosphate (pKa₁=2.15, pKa₂=6.82 and pKa₃=12.38) respectively. Afterwards, 7.8 ml of 40 wt. % suspension of silica nanoparticles (SiO₂ NPs) at pH ~ 9.8 was added to this aggregated solution. It should be noted that the pH of the colloidal solution increased to 9.5 while adding silica solution. In this course, it has been reported that the capsule shell formation depends on the isoelectric point (IEP) of the nanoparticle (NP) material, where it determines if the NPs will be negatively charged at the pH of the final solution of the polyamine/salt-NP mixture [6]. Before depositing within the shell region, the shell material diffuses through the outer portion of the polyamine/salt aggregate via charge interaction with the positively charged polyamine. Herein, the final pH (9.5) of our capsule mixture insures the diffusion and deposition of silica NPs (IEP~3.5) on the surface of PAH/dipotassium phosphate aggregates. The cloudy solution was kept for 2 hours, and then centrifuged at a speed of 4450 rpm for 20 minutes. The NCs formed were washed 3 times in de-ionized water. Due to their overall net positive charge these aggregates of CU-PAH-dipotassium phosphate could assist the assembly of negatively charged silica nanoparticles, which then shape into hierarchically ordered nanocapsule structures [128] as illustrated in **Figure 2.3**. Similar PAH/silica capsules has been successfully synthesized [6].

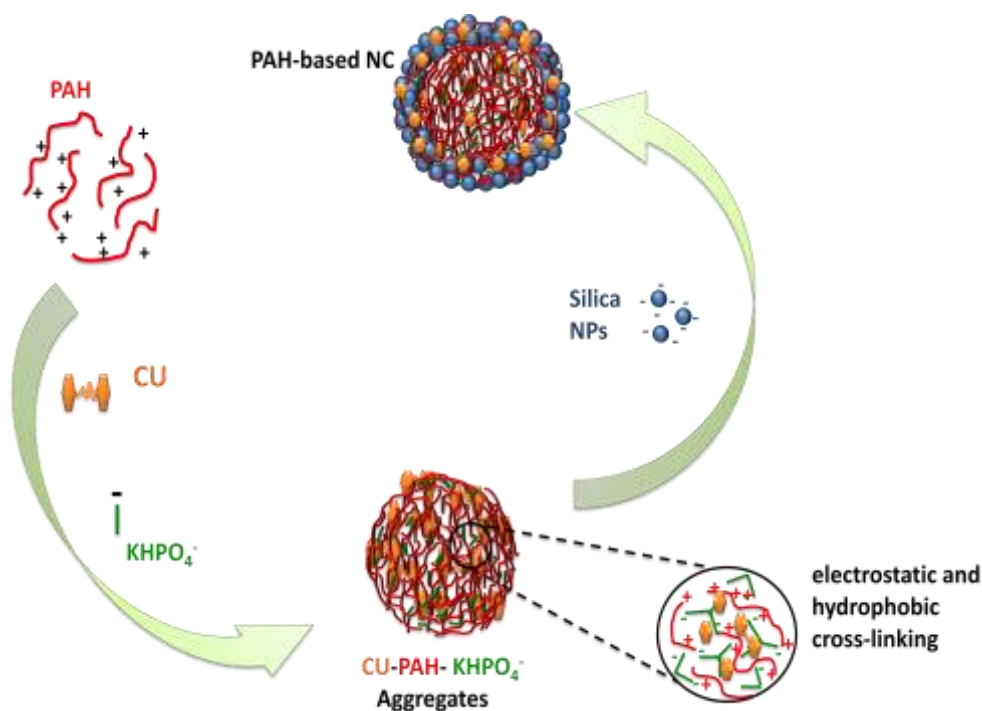


Figure 2.3. Illustration of CU interacting with PAH, dipotassium phosphate and SiO₂ NPs to form NCs.

2. Morphological Characterization:

Scanning electron microscopy (SEM) analysis was done using Tescan, Vega 3 LMU with Oxford Edx detector (Inca XmaW20) SEM, where 3 mg of the NC were dissolved in 5 ml of de-ionized water, and few drops of the nanocapsule suspension were mounted on an aluminium stub, coated with carbon adhesive. After being dried the sample was ready for the SEM analyses. Transmission electron microscopy (TEM) measurement was carried out with a JEOL 2200FS double aberration corrected FEG microscope, operating at 200 kV. TEM samples were prepared by casting a drop of the nanoparticle suspension onto copper grids covered with holey carbon films. The fluorescence image was recorded using a high sensitive STED confocal set up consisted of confocal microscope (Leica TCS SP5 STED, Leica Microsystem), an Argon laser with 430 nm excitation wavelength and APD detector. CU was excited by a wavelength

of 430 nm and emission was collected using a band filter in the range of 460 –600 nm. The particle size distribution was analyzed using DLS (Brookhaven Instruments Corps) technique; with a laser source of 658 nm and a PMT detector (HAMAMATSU, HC120-30). The software used was 90Plus Particle Sizing Software Ver. 5.23 and the dust was set at 40.

2. Spectroscopic Measurements:

The absorption spectra were recorded using a JASCOV-570 UV-VIS-NIR Spectrophotometer at room temperature. The steady-state fluorescence spectra (excitation and emission) were recorded at room temperature using Jobin-Yvon-Horiba Fluorolog III fluorometer and the FluorEssence program where the excitation and emission slits width were 5 nm. The source of excitation was a 100 W Xenon lamp, and the used detector was R-928 operating at a voltage of 950 V. FT-IR-Raman spectrometer (Thermo-Nicolet, Nexus 870) was used to record the Raman spectra in the range of 4000 to 400 cm^{-1} .

3. Other Measurements:

The apparent zeta potential was measured using a Malvern Zetasizer Nano ZS (M3-PALS) using the Non-Invasive Back Scatter technique. The instrument was equipped with a monochromatic red laser operating at 632.8 nm and the data were analyzed with the Malvern Dispersion technology software. Z-average values for three measurements were recorded. The Thermogravimetric Analysis (TGA) and Differential Scanning Calorimetry (DSC) measurements were done using a Netzsch TGA 209 in the

temperature range 0 to 800 °C with an increment of 30 K/ 10 minutes in a N₂ atmosphere.

C. Results:

1. Characterization of NCs:

The SEM images depicted in **Figure 2.4 (A-B)**, show that the NCs are spherical. The SEM image of the CU–PAH–dipotassium phosphate mixture, before silica nanoparticles were added, is shown in the inset of **Figure 2.4 (A)**, which suggests that smaller size spherical aggregates are formed before the silica nanoparticles are added.

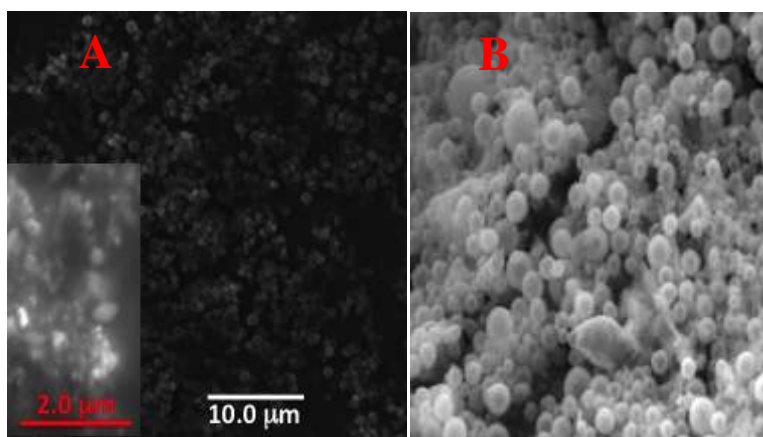


Figure 2.4. (A-B) SEM images of NCs; (A) 10 μm resolution and the inset shows an SEM image of the CU–PAH–dipotassium phosphate mixture before the addition of SiO₂ NPs; (B) 5 μm resolution.

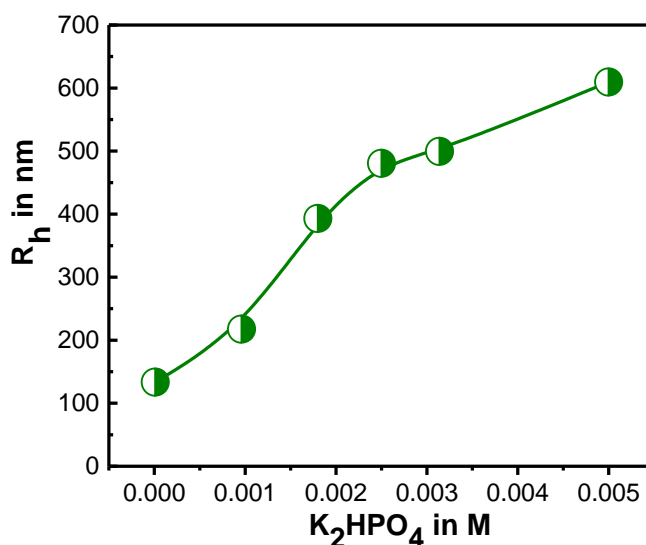


Figure 2.5. Plot of the hydrodynamic radius (R_h) vs. the concentration of dipotassium phosphate where the concentration of the latter ranges between 0.01 and 5 mM. The measurements are done in triplicates.

The particle size distribution of the nanocapsules was analyzed by a dynamic light scattering (DLS) method and was found to have an effective hydrodynamic radius (R_h) of 480 nm for 2.5 mM of dipotassium phosphate. The hydrodynamic diameter size distribution was found to be 0.2–1 μm . Increasing the concentration of dipotassium phosphate to 5 mM increased the R_h value to 610 nm; similarly decreasing the salt concentration to 10 μM produced NCs with an R_h of 133 nm (see **Figure 2.5**). However, the SEM images show that the NCs were found to be much smaller ($R_h = \sim 60$ nm) at the low salt concentration. The high effective hydrodynamic radius is due to the further aggregation of smaller size NCs in solution. The initial size of the core depends on the number of PAH chains that are ionically crosslinked by dipotassium phosphate. This is dependent on the amount of salt added [6]. At low salt concentrations, fewer counterions are displaced still keeping PAH rigid with fewer sites to crosslink with other chains. The increase in the concentration of dipotassium phosphate increases the

negative charges of the salt per positive charge of PAH, which encourages the formation of larger aggregates, thus, increasing the size of the core as well as the hydrodynamic radius of the NC [6]. Such an aggregation was also noticed when NCs were prepared in solution and dried on a carbon adhesive before taking the SEM images.

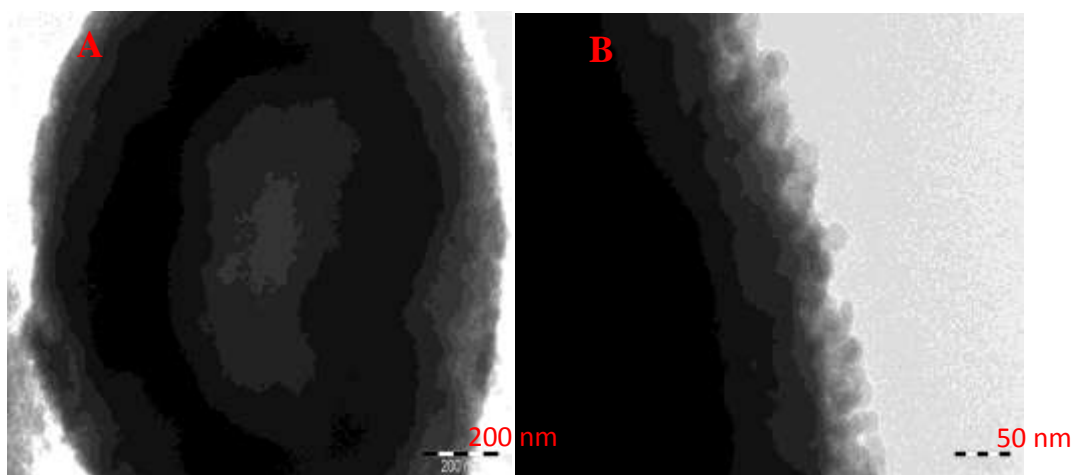


Figure 2.6 (A-B) TEM Images of NCs



Figure 2.7. STED confocal fluorescence image of the nanocapsule. The excitation wavelength was 430 nm and the emission wavelength was 430 nm and the emission was collected using a band filter in the range of 460-600 nm.

The TEM image, **Figure 2.6 A**, of NCs confirms that the silica particles are at the surface and the material at the center is thinner. The thickness of silica was about 100–250 nm (**Figure 2.6 B**). The fluorescence image, **Figure 2.7**, indicates that the fluorescence is coming from all over the capsules suggesting that CU is present all over the capsules.

PAH has a strong binding affinity with curcumin which was confirmed by the high value of their association constant ($K=1.44 \times 10^4 \text{ M}^{-1}$). The latter was found by measuring the fluorescence emission spectra of CU at constant concentration ($3.33 \times 10^{-3} \text{ mg ml}^{-1}$) with various PAH (polymer) concentration from 0 to 3 mg ml^{-1} ; where the excitation wavelength was 350 nm. The association constant was calculated using the following equation [129]:

$$\text{Log} \left[\frac{(F-F_0)}{F_0} \right] = \text{Log}(K) + n \text{Log}[PAH]$$

where K and n are the binding constant and the number of binding sites, respectively. F and F_0 are the fluorescence intensity of curcumin at 450 nm in the presence and absence of PAH. Based on the later equation the plot of [PAH] vs. $(F-F_0)/F_0$ (**Figure 2.8**) demonstrated an excellent linear relationship with linear regression $R^2 = 0.99424$, $n = 0.91$ and $K = 1.44 \times 10^4 \text{ M}^{-1}$.

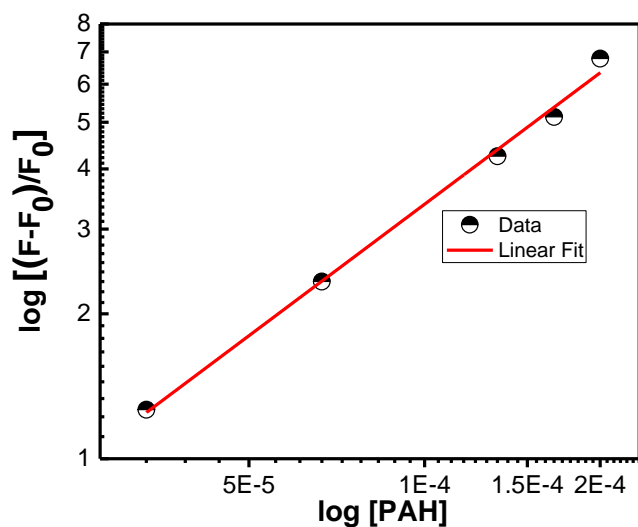


Figure 2.8. Plot of [PAH] vs. $(F-F_0)/F_0$. The concentration of curcumin was fixed at $9.0\mu\text{M}$ whereas the concentration of PAH ranged between 0 and 3 mg/ml. F and F_0 are the fluorescence intensities of CU in presence and absence of PAH respectively. The excitation wavelength was 355 nm and the emission wavelength was 440 nm. The measurements were done in duplicates.

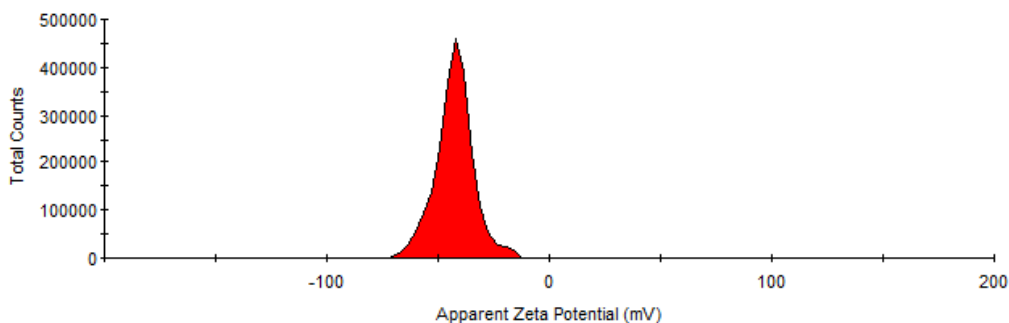


Figure 2.9 a Apparent zeta potential distribution of curcumin in water

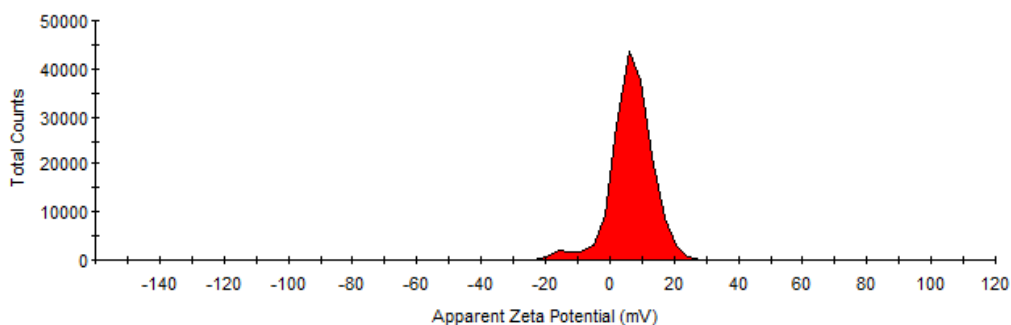


Figure 2.9 b Apparent zeta potential distribution of PAH in water

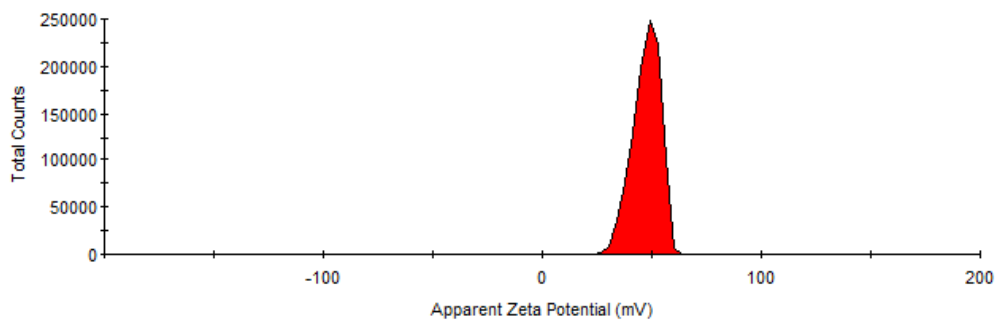


Figure 2.9 c Apparent zeta potential distribution of PAH and curcumin mixture in water

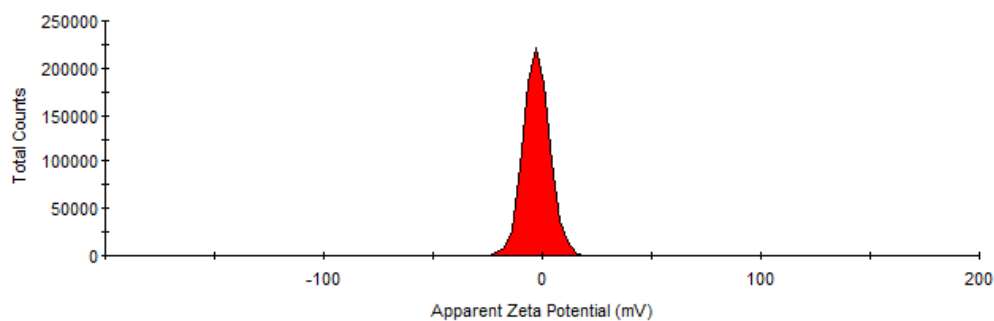


Figure 2.9 d Apparent zeta potential distribution of PAH and K₂HPO₄ mixture in water

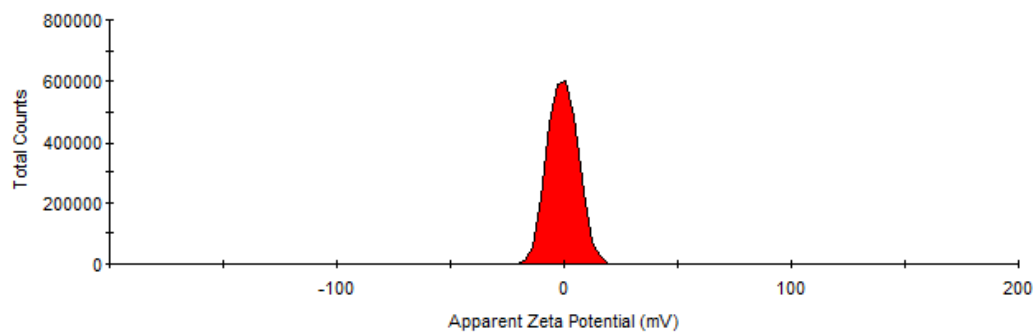


Figure 2.9 e Apparent zeta potential distribution of PAH, curcumin and K₂HPO₄ mixture in water

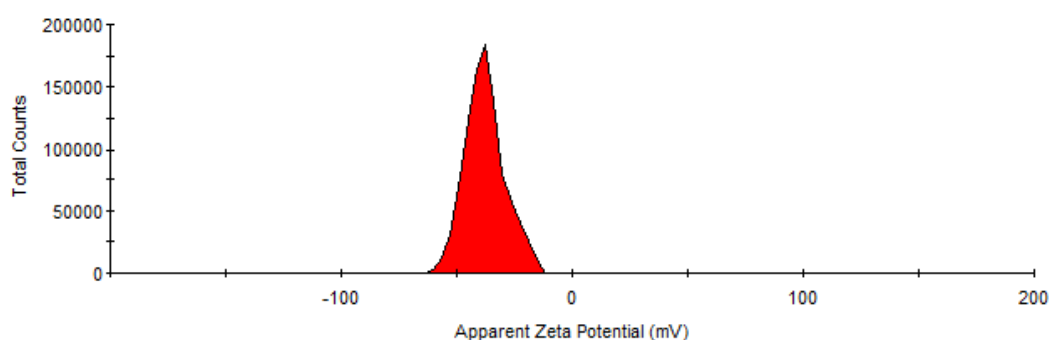


Figure 2.9 f Apparent zeta potential distribution of nanocapsules

The apparent zeta potential give information related to surface charge.

Curcumin is known to be found in enolic form in solution. As depicted in **Figure 2.9a** the zeta potential measurement of curcumin in water showed a value close to -40 mV whereas that of silica NPs used in this study was found to be -37 mV in water. Zeta potential distribution of PAH in water gave a value of $+7$ mV in water as depicted in **Figure 2.9b**. When we measure the zeta potential of PAH and curcumin mixture this value was found to be $+47$ mV (**Figure 2.9c**). This value suggests that interaction of PAH and curcumin is electrostatic and association of curcumin with PAH increases the positive surface charges. This latter increase in surface charge can be explained by the interaction of N^+ of PAH and enol oxygen of curcumin as proved by the FT-IR spectra in chapter 3. On the other hand when PAH was mixed with K_2HPO_4 in the same ratio of experimental condition for synthesizing nanocapsules, this value was close to zero as shown in **Figure 2.9d**. This value did not change appreciably for the mixture of K_2HPO_4 and PAH in the presence of curcumin with a zeta potential value close to 0 mV (**Figure 2.9e**). However, when silica was added and the nanocapsules were formed, the apparent zeta potential value was found to be -38 mV. This means that the surface charge of our synthesized nanocapsules is negative, i.e. similar to silica particles.

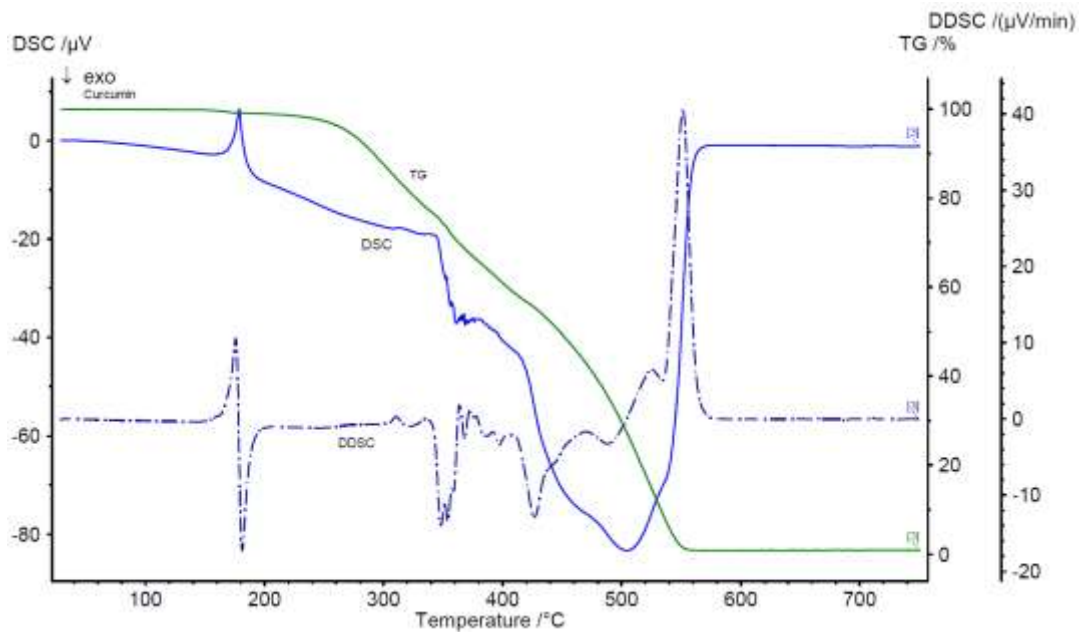


Figure 2.10. Thermogravimetric analysis of curcumin. TG: Thermogravimetric; DSC: Differential scanning calorimetry; DDSC: Derivative of differential scanning calorimetry.

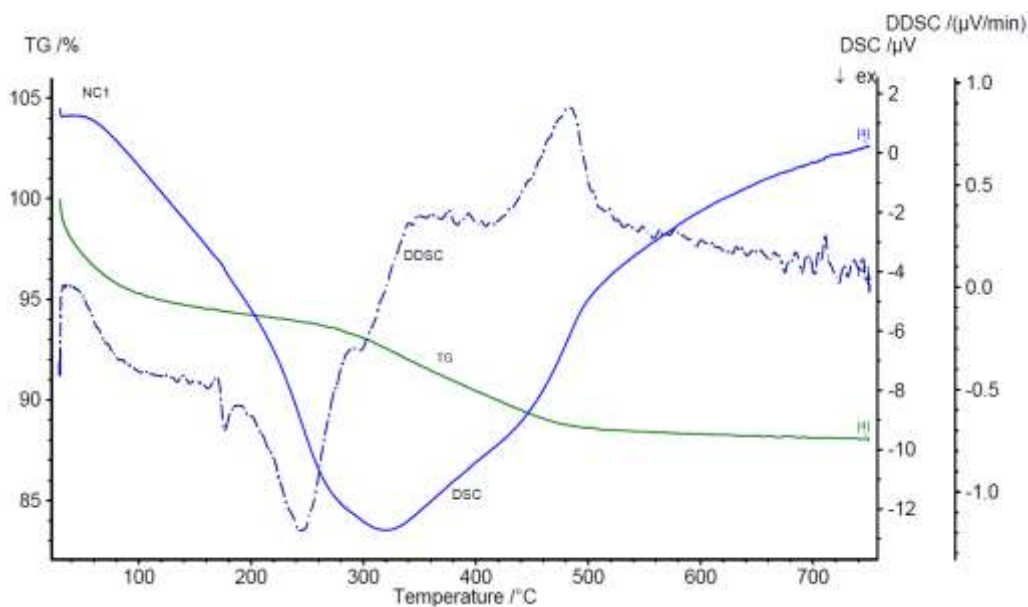


Figure 2.11. Thermogravimetric analysis of nanocapsule. TG: Thermogravimetric; DSC: Differential scanning calorimetry; DDSC: Derivative of differential scanning calorimetry.

TGA data of raw curcumin shown in **Figure 2.10** indicate that the weight-loss occurs around 260 °C and continues till 550 °C. DSC curve shows a major peak at around 500 °C. However, in the case of nanocapsules, the weight-loss starts much

earlier at around 120 °C and continues to 550 °C. The early weight loss is due to presence of PAH in the nanocapsules as depicted in **Figure 2.11**. Similarly, in DSC curve a sharp peak appeared at 300 °C and the peak at 500 °C found in raw curcumin was found as hump.

TGA was further used to estimate percentage of curcumin present in these capsules as shown in **Figure 2.12**. It was found that nanocapsules having the largest size had the highest percentage of curcumin, about 7 %, whereas rest of the capsules had about 4 % during thermal degradation.

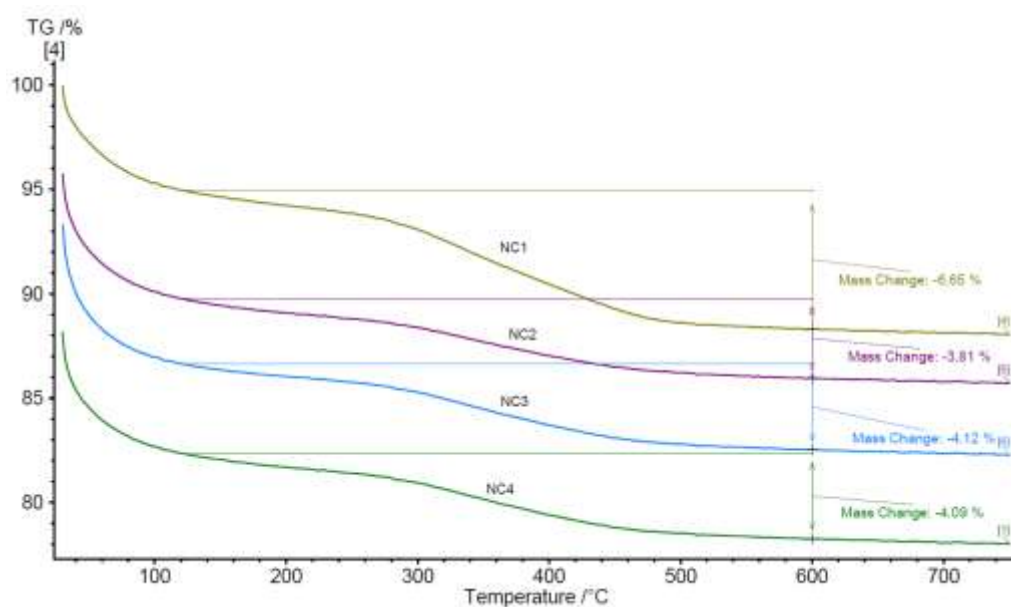


Figure 2.12. Thermogravimetric analysis of different nanocapsules.

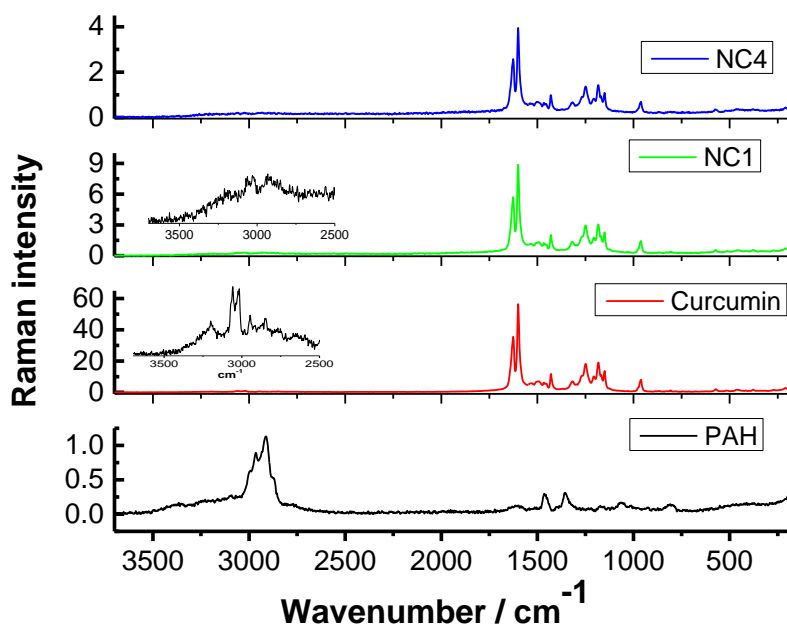


Figure 2.13. Raman spectra of curcumin, PAH and nanocapsules

As shown in **Figure 2.13**, the observed Raman shift of curcumin at around 3200 cm^{-1} might be due to OH band, which is reported to appear at 3545 cm^{-1} in CCl_3 and this band downshifted strongly to 3374 cm^{-1} in acetonitrile [130]. Since aqueous environment heightens the possibilities of hydrogen bonding between curcumin and water (solvent) molecules much more than acetonitrile (solvent), the downshift of OH band is much more expected, thus our observation of 3200 cm^{-1} in Raman spectra for curcumin in water is not surprising. However, we did not find this peak in nanocapsules. The obtained Raman spectra at around 3060 and 3010 cm^{-1} for curcumin are assigned to aromatic $\text{C-H}_{\text{stretching}}$. These peaks were noticed in nanocapsules. PAH gave a strong Raman spectrum at around 2930 cm^{-1} which is assigned to strong aliphatic CH band, this band is also found in the nanocapsules. Absence of peaks in the region of $1650 - 1800\text{ cm}^{-1}$ in Raman spectra of curcumin further suggest that curcumin largely exists in enol form rather than keto form, hence, corroborating earlier findings. The band at 1630

cm^{-1} is due to phenolic OH group. These peaks were predominantly present in the nanocapsules. However, the Raman shift at 1626 cm^{-1} is due to $\nu_{\text{C}=\text{C}}$ and $\nu_{\text{C}=\text{O}}$ of curcumin, which is the same as reported experimental value and close to computed values 1630 cm^{-1} and 1615 cm^{-1} respectively [130]. The band at 1601 cm^{-1} and 1492 cm^{-1} is due to aromatic vibration $\nu_{\text{C}=\text{Cring}}$ of curcumin. The δ_{CH_3} band at 1456 cm^{-1} , $\delta_{\text{PhCCHOH}_{\text{enol}}}$ band at 1314 cm^{-1} and the band at 1247 cm^{-1} are due to $\delta_{\text{COH}_{\text{enol}}}$ of curcumin and are present in nanocapsules' spectra.

2. CU delivery and its scavenging activity:

The release of drug from the NCs is very important for their application as drug delivery vehicles. Delivery of curcumin in different environments was investigated by changing the pH of the solution and CU release from the nanocapsule was estimated by absorption spectrophotometry. The nanocapsules were dissolved in 3 ml of the desired pH solution (5, 7 or 8) and aged for a given interval of time before centrifugation. The samples were centrifuged for 20 minutes at 4450 rpm. The precipitate was left and the solution was collected to measure the absorbance of CU for quantification. It was found that the CU was released from the nanocapsules in acidic (pH=5.0), basic (pH=8.0) and neutral (pH= 7.0) conditions as shown in **Figure 2.14**. However, release of CU was more triggered in basic environment than acidic (~42% relative to basic environment) and neutral (~20% relative to basic environment).

Furthermore, it was found that there is a linear relationship between the amounts of CU released vs. time studied. An equation was proposed by Higuchi [131] where the rate of drug release is related to physical constants based on simple diffusion laws as $R=K_{\text{HT}}^{1/2}$ where R is the amount of drug released, K_{H} is the Higuchi dissolution

constant and t is the time. Many studies have suggested that cancerous cells are acidic; therefore, the release of CU was studied for different nanocapsules in acidic environment. We applied the equation for CU release from different NCs (see **Figure 2.15**) as well as from NC1 in different pH environments (see **Figure 2.14**). Moreover, it was found that the Higuchi dissolution constant (K_H) is related to the particle size where it increases exponentially with the increase in the NCs hydrodynamic radius (R_h) (see **Figure 2.16**).

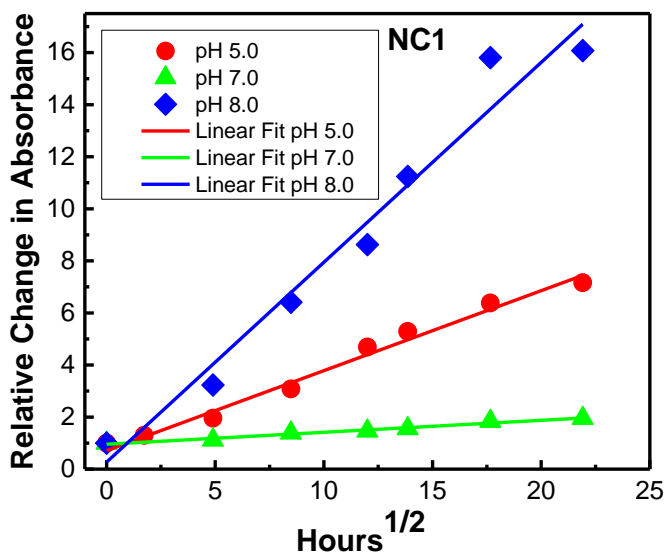


Figure 2.14. Release of curcumin measured in absorbance scale from NC1 in different pH condition. Data were fitted with Higuchi model [130] for drug release. The measurements were done in duplicates.

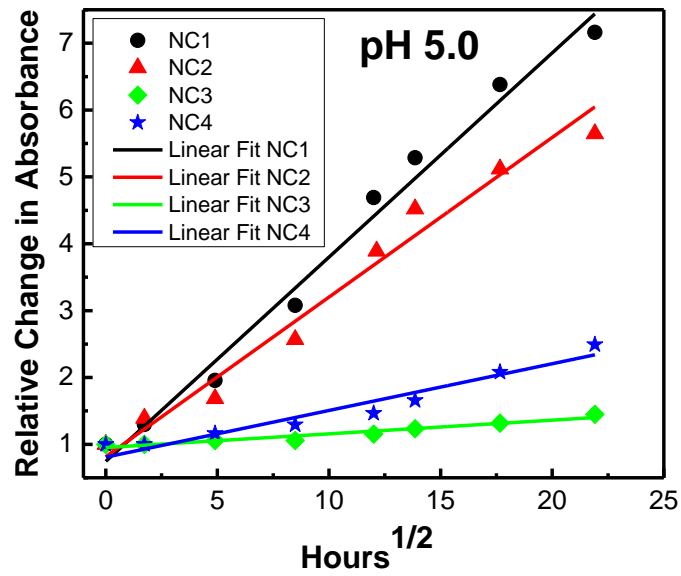


Figure 2.15. : Release of curcumin measured in absorbance scale from different nanocapsule in pH 5.0. Data were fitted with Higuchi model [130] for drug release. The measurements were done in duplicates.

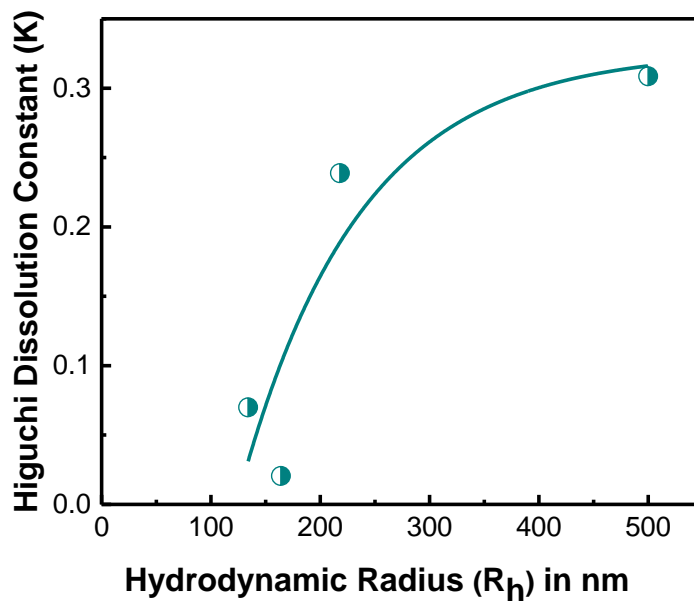


Figure 2.16. Higuchi dissolution constant (K_H) versus particle size

Apart from drug delivery, biological activity of drug molecule within the delivery system has immense importance. The 2,2-diphenyl-1-picrylhydrazyl (DPPH) (see **Figure 2.17**) scavenging activity of curcumin could be simply measured by following the change in absorbance of DPPH at 520 nm and biological activity of curcumin embedded in the nanocapsules can be understood. Therefore, we adopted a similar procedure reported earlier [132] where curcumin samples were mixed with DPPH in the double distilled de-ionized water. The changes of absorption of DPPH at 520 nm were recorded at room temperature. **Figure 2.18** gives the values of absorbance of DPPH at 520 nm in the presence of 0.5 mg/mL curcumin and for different nanocapsules under investigation. The low absorbance change of DPPH in the presence of curcumin suggests a strong scavenging ability of curcumin which is attributed to the donation of H from the β -diketone group of curcumin to DPPH [133]. DPPH radical scavenging mechanism is depicted in **Figure 2.19** [134]. However, the change in absorbance increases 17 fold for the largest nanocapsules under studies compared to same amount of curcumin. This low value is not surprising as curcumin content in these microcapsules (NC1) is about 7 %, therefore, a 15 fold decrease in DPPH scavenging activity is expected as per percentage of availability of curcumin over total weight of the nanocapsules. The further 2 fold decreases could be due to decrease in H-donation ability from the β -diketone group of curcumin to DPPH because of interaction between PAH/silica nanoparticles and curcumin. When the DPPH scavenging activity was compared with other smaller size nanocapsules, the scavenging activity decreased exponentially with the size of the capsules as shown in plot of $1/\Delta A$ vs. R_h in **Figure 2.20**. Although based on weight percentage it was expected to have similar scavenging activity for three other smaller size capsules, which is about 2 fold lower than that of

NC1, the exponential reduction indicates that not only the weight percentage of curcumin in the nanocapsules plays a role, but also the availability of β -diketone group of curcumin for H-donation is important. As the size of the nanocapsules are larger more curcumin per surface area of the nanocapsules are exposed outside for scavenging activity compared to small size nanocapsules where a substantial percentage of curcumin are buried/encapsulated inside the capsules without exposing themselves for scavenging activity.

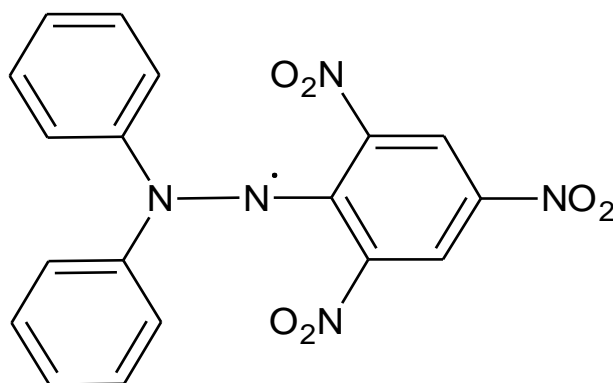


Figure 2.17. Chemical structure of 2,2-diphenyl-1-picrylhydrazyl (DPPH)

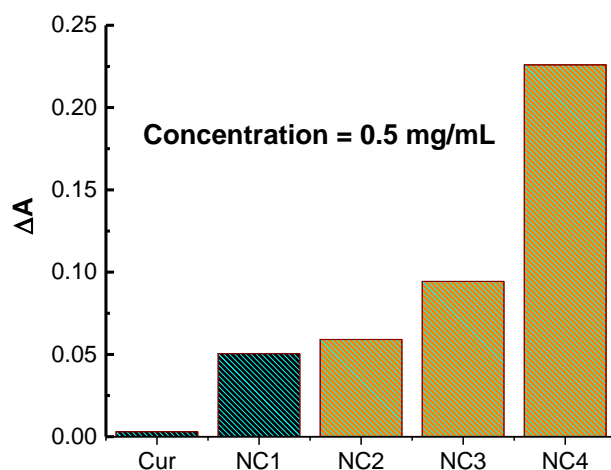


Figure 2.18. Change in DPPH absorption at 520 nm in the presence of curcumin and nanocapsules of different sizes in de-ionized water at room temperature. The concentration of curcumin and nanocapsules was fixed at 0.5 mg/ml and that of DPPH at 100 μ M. The measurements were done in triplicates.

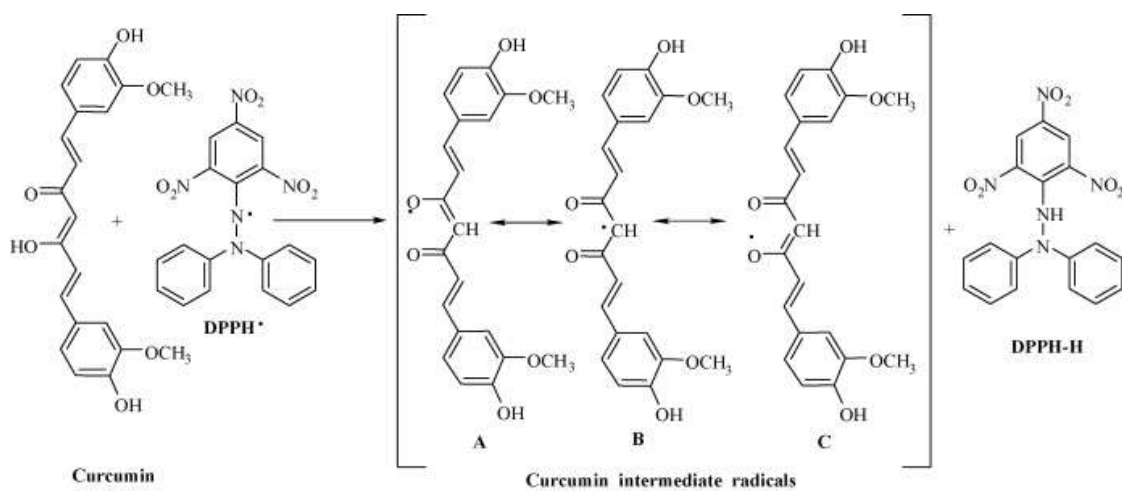


Figure 2.19. The proposed 2,2-diphenyl-1-picrylhydrazyl (DPPH) scavenging mechanism of curcumin [134]

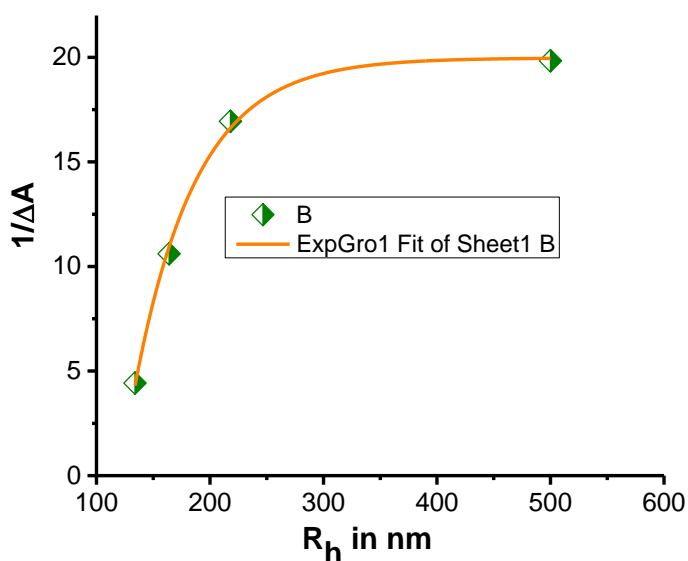


Figure 2.20. $1/\Delta A$ of DPPH at 520 nm vs. R_h of nanocapsules indicating exponential increase in DPPH scavenging activity of CU.

In summary, the interaction of silica nanoparticles with CU/PAH/dipotassium phosphate aggregates to produce spherical nanocapsules of size ranging between 100 and 1000nm. The size of the capsule is controlled by the concentration of dipotassium phosphate where the plot of the hydrodynamic radius with different salt concentrations has showed an excellent linear relationship. Silica nanoparticles are concentrated at the peripheries whereas curcumin is distributed all over the capsule. The high value of the binding constant ($K=1.44 \times 10^4 \text{ M}^{-1}$) for CU and PAH proves the strong interaction between them. The nanocapsules are of negative surface charge. The percentage of CU for the largest NCs is 7% while its 4% for smaller capsules. In the capsule, CU is found in its enol form. The delivery of CU from the NCs is favoured in basic conditions. Moreover, the drug release profile fits Higuchi model. The DPPH scavenging activity of CU is decreased in the capsule. The reduction in the scavenging activity is related to the percentage by weight of CU in the capsule and the availability of the β -diketone group for H-donation.

CHAPTER III

PHOTOPHYSICAL STUDY OF CURCUMIN IN NANO-CAPSULE

A. Introduction:

1. Excited State Intramolecular Hydrogen Transfer (ESIHT):

ESIHT occurs in molecules containing both, a hydrogen donor (-OH, -NH₂) group and a hydrogen acceptor (-N, carbonyl), knowing that in the ground state the two groups are connected via intramolecular hydrogen bonding. When exposed to light, such molecules undergo ESIHT; where the hydrogen covalently bonded to hydroxyl oxygen in the ground state migrates to the carbonyl oxygen in the excited state (see **Figure 3.1**).

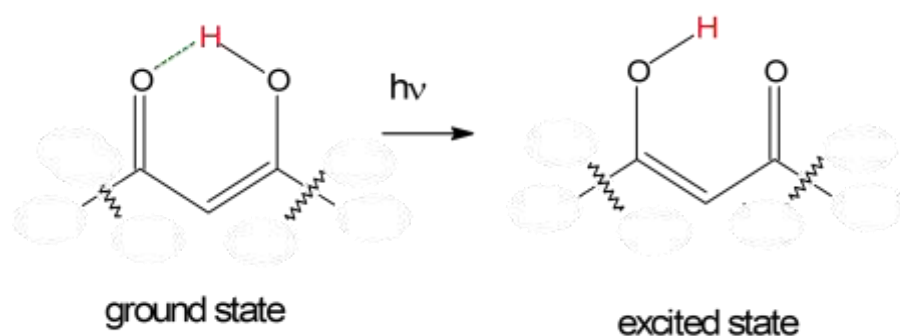


Figure 3.1. Excited State Intramolecular Hydrogen Transfer (ESIHT) process.

In 1955, large Stokes' shifts have been reported in the fluorescence spectra of salicylic acid and its methyl ester; where both compounds possess an intramolecular hydrogen bond between the carbonyl and the phenolic hydroxyl groups. This unusual spectral shift has been attributed to the intramolecular hydrogen transfer in the first

excited singlet state. In 1957, Cohen, Schmidt and Hirschberg have showed that salicylidene anilines photochromic behaviour (reversible colour change) is also a result of excited state proton transfer. In the 1950's, the photochemical stability of 2-hydroxy benzophenone derivatives has been related to intramolecular hydrogen transfer followed by a very fast radiationless deactivation. Following these discoveries, many papers have showed that a wide range of molecules undergo excited state intramolecular proton transfer [135].

Excited state hydrogen transfer has crafted phenomenal inquisitiveness to the understanding of intrinsic mechanisms in the chemical and biological processes [136, 137]. Excited State Intramolecular Hydrogen Transfer (ESIHT) occurs in a unimolecular basis and is used as a model to mimic catalytic reactivity [138]. As well it has been associated with medicinal properties [139]. In material research, fluorescence switching of chromophores has drawn huge interest in order to achieve desirable physicochemical behaviour for imaging and sensing applications [140].

2. Photophysical Properties of Curcumin:

Curcumin (CU) is proven to have anti-oxidant properties. It is considered as a superb H-atom donor; it is even better than thiols [139]. It has been shown that the H-atom transfer plays a significant role in the anti-oxidant action of curcumin [139]. CU is found to exist in its enolic form and undergoes ESIHT during deactivation process [141, 142]. Thus understanding ESIHT of CU adds to its medicinal values.

Although normal (N^*) and ESIHT (E^*) forms can be simultaneously observed for many organic molecules in steady state-spectra, no steady state emission spectrum from the normal form of CU (N^*) in solution or solid has been simultaneously detected, despite

that ESIHT phenomenon in CU has been proved by ultra-fast time-resolved spectra and fluorescence up-conversion data [143, 144], and further supported by theoretical calculations [142, 145].

2. Objectives:

With the objective of revoking ESIHT deactivation process of a model molecule, CU, we apply nanotechnology [128, 146] to synthesize new materials with unique optical properties that can be controlled depending on the size of nanocapsules (NCs). As such, designing of structurally well-defined architectures with stimulus and dynamic responsive properties has been among important trails [147, 148]. CU was identified because of its (i) growing pharmaceutical relevance, (ii) use as popular food spice and, (iii) interesting photophysical properties. Moreover, CU meets our present goal as the emission form (E^*) is only detected and the emission form (N^*) is completely masked in solution in steady state fluorescence spectra.

B. Materials and Methods:

The materials, preparation of the NCs and spectroscopic measurements (including UV-VIS and Steady- State Fluorescence) are the same as mentioned in chapter II. In addition, the chemical structures of CU, PAH and NCs were characterized by FTIR spectroscopy. For this purpose, a Thermo Nicolet 4700 Fourier Transform Infrared Spectrometer equipped with a Class 1 Laser is used. The transmission experiments were performed in the range between 4000 and 400 cm^{-1} using the KBr pellet technique. The fluorescence lifetime measurements were collected using a Jobin-Yvon- Horiba Fluorolog III fluorometer, with pulsed diode laser of (460 nm). Data

Analysis Software was used to analyze the decay data. The peak preset was of 10,000 counts. The used detector was R- 928 operating at a voltage of 950V. The instrumental response function was recorded using colloidal silica.

C. Results and Discussion:

Our study was done on a sample set consisting of four nanocapsules (NC1, NC2, NC3, NC4) of different hydrodynamic radii (500, 217, 164 and 133 nm respectively). The absorption spectra of NCs and CU were found to be similar (see **Figure 3.2**), however, the $S_0 \rightarrow S_2$ transition of CU at ~266 nm was not well resolved in NC. The β - diketone moiety of CU exists entirely in enol form with a trans- geometry in both solid state [149] and solution [150] making the two feruloyl chromophores to interact with each other through a central sp^2 - hybridized carbon atom in common conjugated π - system [151, 152]. The strong π (HOMO) \rightarrow π (LUMO) transition of CU was found to be at 426 nm in buffer solution that masked the weak electronic dipole forbidden $n \rightarrow \pi$ band. This band agrees with the theoretically predicted value for CU in enol form [141, 145].

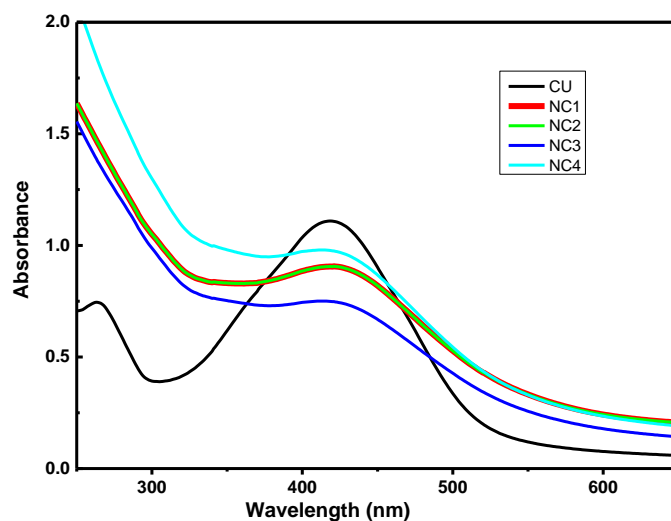


Figure 3.2. UV-Visible absorption spectra of curcumin and nanocapsules of different sizes.

Interestingly, excitation spectrum of CU in buffer solution shows two excitation wavelength bands at ~ 368 nm and ~ 445 nm (**Figure 3.3**) unlike absorption spectrum, which clearly suggests the absorbing and emitting species for CU are different. The first excited state of CU is highly polar due to intramolecular charge transfer from the phenyl ring towards the carbonyl moiety [141, 151, 152] and ESIHT is a major photophysical process in the deactivation of the excited state of CU [141, 153]. The absorption shoulder at ~ 370 nm is due to the weakly allowed π (HOMO-1) \rightarrow π (LUMO) transition and/or virtually forbidden $n \rightarrow \pi$ (LUMO) transition [152]. The emission spectra obtained for CU in water while exciting at 355 nm, 427 nm and 450 nm gave a similar emission spectra with a maximum at ~ 552 nm (for $\lambda_{\text{ex}} = 355$ nm) and maximum at 555 nm (for $\lambda_{\text{ex}} = 427$ and 450 nm) without any emitting band at ~ 450 nm for N^* , thus, the variation in excitation spectrum of CU is due to ESIHT since unusual longer wavelength emission of CU in solution has been found to be due to ESIHT [141, 142].

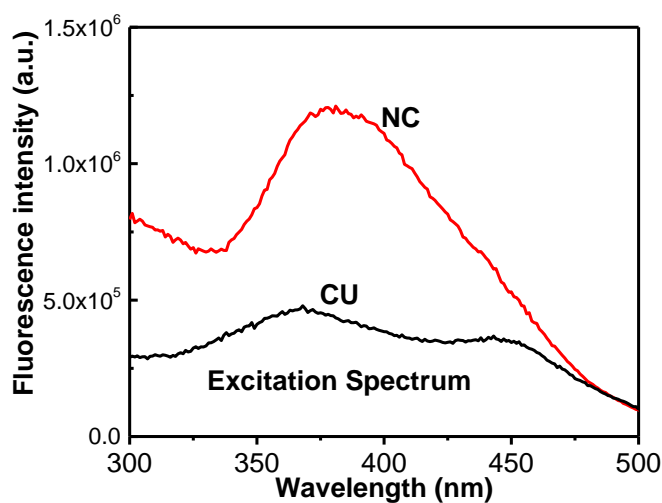


Figure 3.3. Fluorescence excitation spectra at $\lambda_{em} = 520$ nm for CU in buffer and NCs in de-ionized water.

However, the excitation spectrum of NCs showed completely different behaviour compared to CU in water, despite the fact that both CU and NCs have similar strong π (HOMO) \rightarrow π (LUMO) transition absorption (**Figure 3.1**) at 427 nm. In the NCs, the excitation maximum was ~ 50 nm blue shifted compared to strong π (HOMO) \rightarrow π (LUMO) transition absorption band, thus, weakly allowed π (HOMO-1) \rightarrow π (LUMO) transition and virtually forbidden $n \rightarrow \pi$ (LUMO) transition play vital role during fluorescence process in NCs.

The emission spectra for nanocapsules at $\lambda_{ex} = 427$ nm (**Figure 3.4**) and 450 nm (**Figure 3.5**) were similar with a maximum centered at ~ 540 nm, the ~ 15 nm blue shift of emission maximum of NCs compared to CU in water at these excitation wavelengths is due to change in local environment and solvent [141, 155, 156], however, the emission spectrum for NCs obtained at $\lambda_{ex} = 355$ nm (**Figure 3.6**) is largely different with a maximum at ~ 536 nm and an additional new peak at lower wavelength, after deconvolution of this spectrum gave two separate emission spectra centered at ~ 456 nm

and ~ 535 nm respectively (see **Figure 3.7**). A similar observation has been reported for CU in niosomes [157]. The additional peak observed is not due to the change in solvent of NC because of the fact that even at $\lambda_{\text{ex}} = 427$ nm, CU alone gives a much larger blue shift (~ 80 nm) in non-polar solvent environment [155], however, in the present case at $\lambda_{\text{ex}} = 427$ nm the blue shift in emission spectrum was only 15 nm in NC (**Figure 3.4**) instead of ~ 80 nm expected for non-polar solvent environment. Therefore, 15 nm shift (from 550 nm in water to 540 nm in NC) at $\lambda_{\text{ex}} = 355$ nm is due to change in solvent for NC whereas the additional peak at ~ 456 nm is due to other phenomena as explained subsequently.

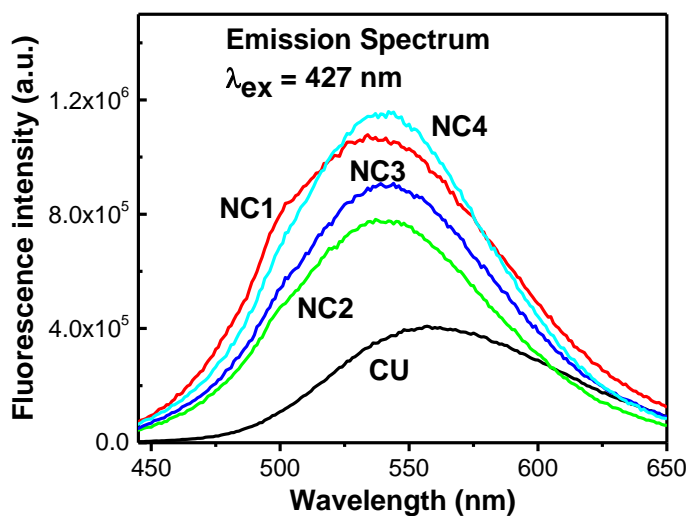


Figure 3.4. Fluorescence emission spectra at $\lambda_{\text{ex}} = 427$ nm for CU in buffer and NCs in de-ionized water.

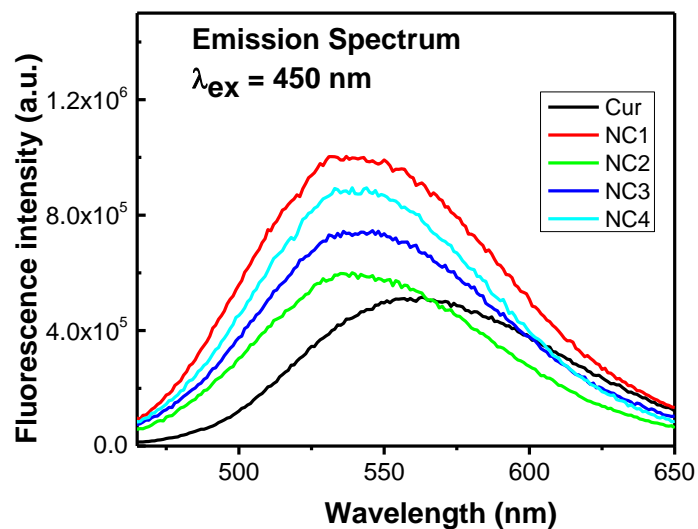


Figure 3.5. Fluorescence emission spectra at $\lambda_{\text{ex}} = 450 \text{ nm}$ for CU in buffer and NCs in de-ionized water.

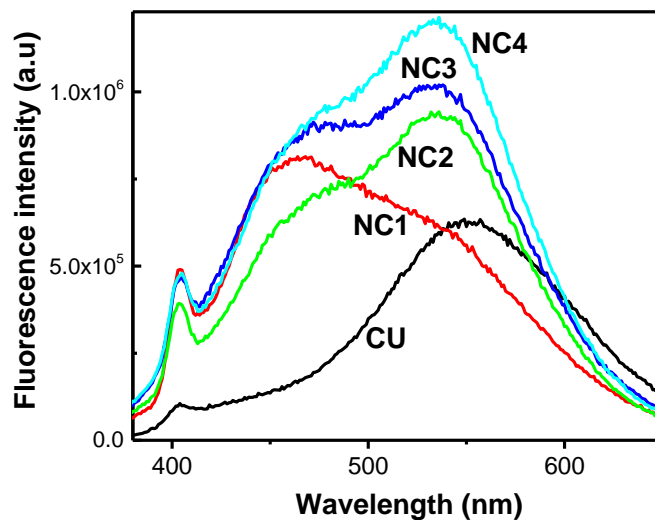


Figure 3.6. Fluorescence emission spectra at $\lambda_{\text{ex}} = 355 \text{ nm}$ for CU in buffer and NCs in de-ionized water.

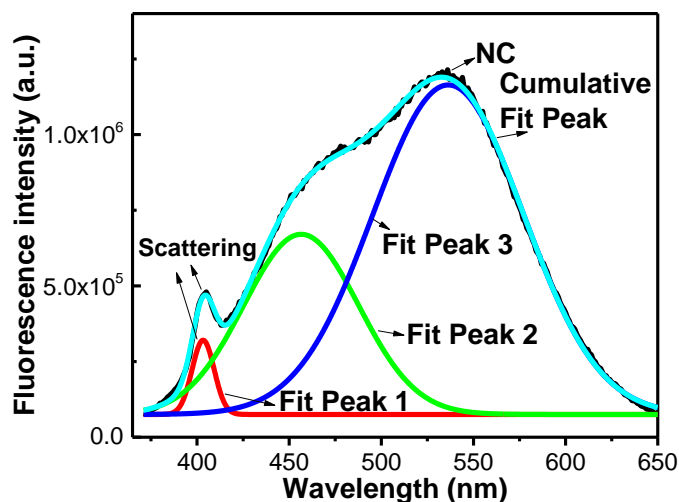


Figure 3.7. Fluorescence emission spectrum of NC at $\lambda_{\text{ex}} = 355$ nm along with deconvoluted spectra, the peak at ~ 400 nm is due to scattering.

In the steady state fluorescence spectrum in water or alcohol the band at ~ 456 nm was never resolved. However, using ultrafast time resolved spectroscopic method the normal emission spectrum (N^*) of CU in methanol at 0 picosecond time scale has been resolved with a maximum at ~ 460 nm whereas the emission spectrum of ESIHT (E^*) form at more than 20 ps is centered at ~ 555 nm that resembles the steady state fluorescence spectrum [143]. It should be noted that there is no remarkable emission band at ~ 465 nm for CU in methanol at $\lambda_{\text{ex}} = 355$ nm [141] indicating that weakly allowed $\pi(\text{HOMO}-1) \rightarrow \pi(\text{LUMO})$ transition and virtually forbidden $n \rightarrow \pi(\text{LUMO})$ transition play insignificant role during steady state fluorescence process of CU in solution. Thus, the observed emission at ~ 456 nm in NCs is because of molecular deactivation without undergoing ESIHT. We further propose that the six membered ring path for ESIHT deactivation process (see **Figure 3.8**) is hindered due to interaction of N^+ of PAH with the O-atoms of enol form of CU.

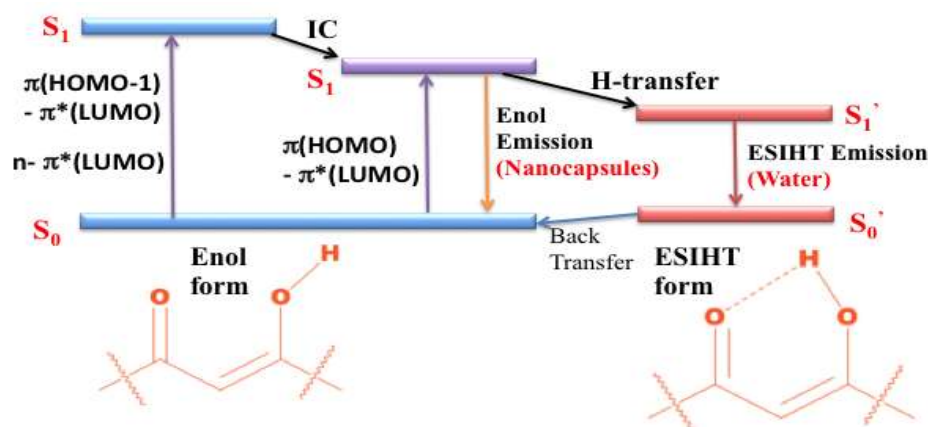


Figure 3.8. Absorption and excited state deactivation processes of CU in water and NCs.

FT-IR spectral data (see **Figures 3.9, 3.10** and **3.11**) further supports our hypothesis. The phenolic O-H vibration of CU was observed at $\sim 3509 \text{ cm}^{-1}$ and 3400 cm^{-1} whereas the peaks found in the range $3392 - 3033 \text{ cm}^{-1}$ in PAH is associated with the N-H stretch. All these prominent peaks in the control samples were not visible in NCs instead of a major peak found at 3448 cm^{-1} . Similarly the peak at 2972 cm^{-1} due to enolic O-H vibration could be detected in CU, but was not clear in NCs. Further, the control peaks at 1627 cm^{-1} and 1603 cm^{-1} for CU are associated with the C=O and C=C vibrations. C=O vibration has another peak at 1510 cm^{-1} . On the other hand for PAH, the peaks at 1608 cm^{-1} and 1457 cm^{-1} are associated with the N-H asymmetric bending and C-H bending. In NCs in these regions only a prominent peak was obtained at 1636 cm^{-1} confirming a strong involvement $-\text{NH}_2$ of PAH and enol form of CU inside the NCs.

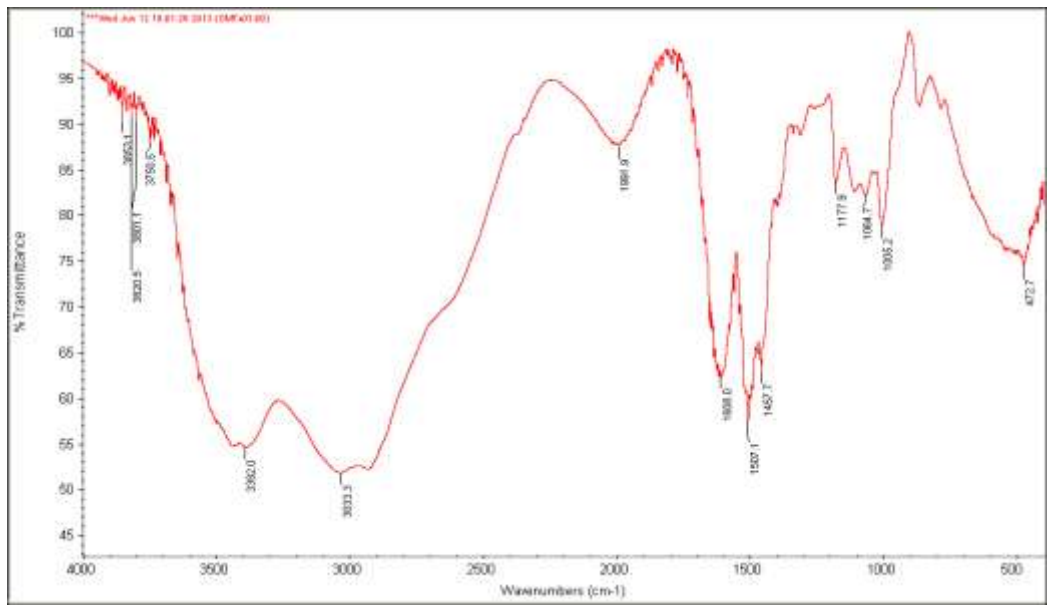


Figure 3.9. FT-IR spectrum of PAH

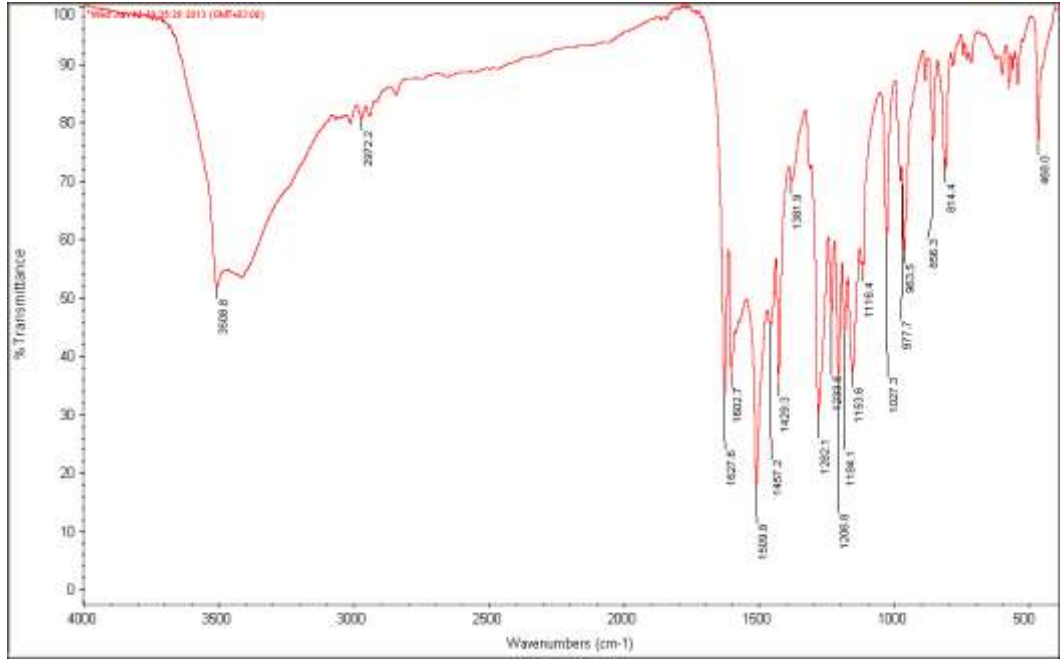


Figure 3.10. FT-IR spectrum of CU

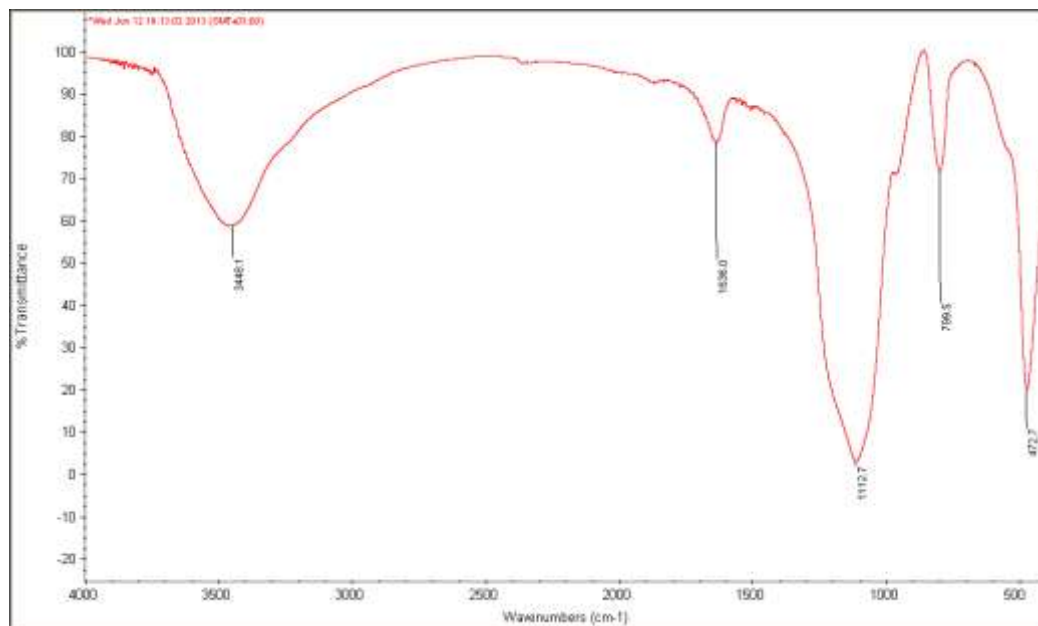


Figure 3.11. FT-IR spectrum of NC

The ratio of N^*/E^* was evaluated by measuring fluorescence ratio at 460 nm (normal emission) and at 540 nm (ESIHT emission). N^*/E^* was found to be 0.25 for CU in water, which increased 3 fold in NCs. Further N^*/E^* enhanced with increase in NCs size as correlated in **Figure 3.12**. The maximum value was found for the NCs having largest size and N^*/E^* could be linearly correlated with the hydrodynamic radius of the NCs.

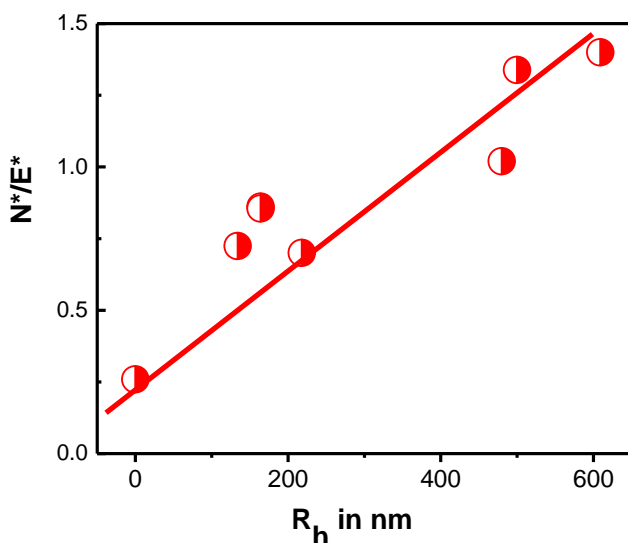


Figure 3.12. Plot of N^*/E^* vs. R_h of NCs. The ratio of N^*/E^* is evaluated by measuring fluorescence ratio at 460 nm (normal emission) and 540 nm (ESIHT emission). The measurements were done in triplicates.

The fluorescence lifetime at $\lambda_{ex}=460$ nm and $\lambda_{em}=560$ nm for CU in buffer could be best fitted with a biexponential decay giving a short component lifetime (τ_1) of ~ 62 ps (99%) and long component lifetime (τ_2) of 3.1 ns (1%). The biexponential decay for NCs in this excitation and emission wavelengths provided $\tau_1 = \sim 242$ ps (80%) and $\tau_2 = 1.90$ ns (20%) when $R_h = 133$ nm. The decay profiles are shown in **Figure 3.13**. Increase in the size of NCs decreased τ_1 to 178 ps (85%) but increased τ_2 to 3.00 ns (15%) when $R_h = 610$ nm. The decrease in τ_2 correlated with the increase in the size of NCs, thus, could be rationalised with decrease in ESIHT process in NC. However, while exciting at 373 nm the biexponential decay of CU in buffer at emission 460 nm (for N^*) gave $\tau_1 = 0.35$ ns (90%) and $\tau_2 = 3.9$ ns (10%) whereas emission at 560 nm (for E^*) gave $\tau_1 = 0.33$ ns (90%) and $\tau_2 = \sim 1.0$ ns (10%). This emission wavelength dependency of CU is not surprising as similar dependency in ethanol is known [158]. At $\lambda_{ex}=373$ nm and $\lambda_{em}=460$ nm, τ_1 value dramatically improved to 0.40 ns in NCs and later on 0.6

ns with increase in R_h of NCs, therefore, the increase in τ_1 could be logically related to emission from N^* .

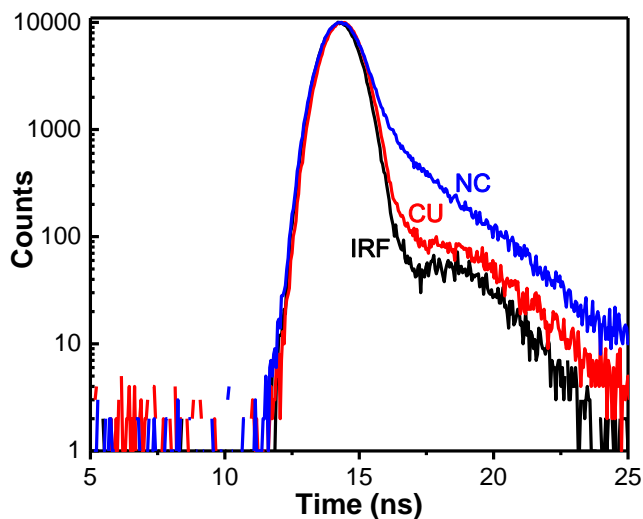


Figure 3.13. Fluorescence lifetime decay profiles for CU and NCs at $\lambda_{ex} = 460$ nm and $\lambda_{em} = 560$ nm, IRF is the instrument response function. The data were fitted with biexponential decay with a χ^2 between 1 and 3.

In summary, PAH-based NCs change the optical behaviour of CU. When exciting at 355 nm a new peak has been seen at 460nm. This peak attributed to the fluorescence of N^* of CU rather than E^* . The FT-IR spectra proved the interaction of N^+ of PAH with the enolic O of CU, thus inhibiting ESIHT process. Furthermore, N^* emission is proved by the increase in τ_1 at $\lambda_{ex}=373$ nm and $\lambda_{em}= 460$ nm.

CHAPTER IV

SELECTIVE FLUORESCENCE SENSING OF GUANINE AMONG NUCLEOBASES USING NANOCAPSULES

A. Introduction:

Nanotechnologies and nanomaterials have been utilized in chemical sensor designing for the recent ten years. Since 2003-2004, this field has witnessed fast development and advancement. The importance of nanomaterials is not only referred to their geometric size. However, a change from macro and micro to nano scale qualitatively changes the physicochemical characteristics (magnetism, optical refraction, electric conductivity, thermal stability and strength, light absorption and emission) and produces new materials of same chemical nature, but having properties and reactivity that are lacking in macro- and microscopic materials. All types of nanoparticles can be incorporated into different inorganic and organic materials; and such nanosensors are applied in both gas and liquid media analysis [159].

During the past years, nucleic acid-based tests have attracted more interest. The vast development of systems with fast, cheap and specific detection of nucleic acids is induced by their numerous applications in various fields including, forensic applications, rapid detection of biological warfare agents, gene analysis and clinical disease and treatment [160]. Accurate diagnosis minimizes the humanitarian and economic costs of infectious diseases; hence enabling efficient disease treatment. In clinical practice, detection of genetic mutations at the molecular level opens up the ability of reliable disease diagnosis prior to the appearance of disease symptoms [161].

Based on the hybridization between a target and its complementary probe, various electrochemical and optical methods have been successfully used [162]. The introduction of nucleic acids' fluorescent labelling method has opened up the ability of utilizing such systems for further research and development.

The recent years have witnessed rapid growth of fluorescent probes as well as wide development of homogenous fluorescence assays, including those based on fluorescence resonance energy transfer (FRET) or quenching mechanisms, for nucleic acid detection [163]. These probes (e.g. molecular beacons) are labelled with both a quencher dye and a fluorescent reporter, where the reporter fluoresces when the two dyes are physically separated after the hybridization [161].

Recently, there have been tremendous demands for utilizing nano materials as biosensing probes. Among such nanostructured materials, nanoparticles have gained more attention [164]. Up to date, nanoparticles consisting of metals (e.g. Au, Pt, Ag and Pd) and inorganic semiconductors (e.g. PbS, TiO₂, Ag₂S...) have been extensively used in DNA biosensing.

In biosensing, DNA detection by nanoparticles is a promising and interesting aspect [165, 166]. To understand more the role of nanoparticles in DNA sensing, the interaction of nanoparticles and nucleobases, that are the most active and major constituents of DNA, is an essential research field [164]. The interaction of gold (Au) nanoparticles and nucleobases have been reported, where experiments showed that adenine (A), guanine (G), cytosine (C) and thymine (T) specifically interact in a sequence based manner with the surfaces of Au [167]. Moreover, the interaction of organic nanoparticles with nucleobases has been investigated; where 6,7-dicyano-2,3-di-[4-(2,3,4,5-tetraphenylphenyl)phenyl]quinoxaline(CPQ) nanoparticles are proved to

be highly sensitive to the various nucleobases. CPQ nanoparticles have shown different fluorescence responses to the four nucleobases in the following order: $G > A > T \geq C$. Each of the nucleobases has remarkably quenched the fluorescence of CPQ nanoparticles where the maximum of the fluorescence intensity of CPQ nanoparticles decreased to 45% of its initial intensity; the concentration of the nucleobases was fixed at 1.6×10^{-4} M [164].

The determination and separation of nucleobases is an important and challenging task due to the significance of these compounds in numerous biological processes. Adenine, cytosine, guanine, thymine and uracil are the building blocks of both RNA and DNA that play an important role in the storage of genetic information and protein biosynthesis [168]. The identification and estimation of individual nucleobases are crucial to understand the sequence of nucleic acids [169]. To do this, a variety of methods are available, including electrochemical detection, capillary electrophoresis followed by UV and high performance liquid chromatography [170]. DNA sequencing has been of great interest for human genomics, forensic sciences, genetic engineering and medicinal applications. Selective estimation of individual nucleobases has tremendous potential application during DNA sequencing [171]. In this course, fluorescence markers are widely used in electrophoresis where a fluorescent marker specific to particular nucleobase may ease the analytical procedure during nucleic acid sequencing [172].

In the present thesis, we have applied the method of self assembly to synthesize Poly(9-(2-diallylaminoethyl)adenine.HCl-co-sulfur dioxide)Poly A/ silica nanoparticles based nanocapsules to which curcumin was incorporated as a fluorescence probe for the detection of nucleobases; in specific guanine. Poly A is a polymer of adenine alone with

a poly amine backbone. The capsules are of various sizes ranging from 200 to 600 nm. The detection mode is based on the change in the fluorescence intensity of curcumin. The advantages of such technique: (i) easy and does not require long hours of capsule preparation, (ii) stable and robust (28% degradation of capsule after 50 hours), (iii) selective for guanine.

B. Materials and Methods:

1. Materials:

Curcumin was obtained from Acros Organics and the stock solution was prepared as mentioned previously in chapter two. Poly A and the nucleobases including, adenine (A), guanine (G), cytosine (C), thymine (T) and uracil (U) were obtained from Sigma- Aldrich and their stock solutions were prepared in de-ionized water. As well, Silica LUDOX[®] HS-40 Colloidal Silica was obtained from Sigma- Aldrich (same as in Chapter II).

2. Preparation of Poly A Capsule:

Encapsulation of curcumin inside the nanocapsules was made using Poly-A as the structure directing agent. In this process 1.3 ml of Poly-A (2mg ml^{-1}) was gently vortex mixed for 20 s with 7.8 ml of negatively charged silica nanoparticles. The obtained cloudy suspension was aged for 2 hours; then it was centrifuged for 20 min at a speed of 4450 rpm. Poly-A/ SiO_2 aggregates were collected. To the latter precipitate 0.5 ml of CU (1mg ml^{-1} prepared in 10% acetone/ de-ionized water solution) and 2.5 ml of de-ionized water were added. The mixture was allowed to age for 30 min, and again centrifuged for 20 min at a speed of 4450 rpm. The precipitate of nanocapsules formed

was washed with de-ionized water for 3 times to remove the excess of CU. The preparation method is depicted in **Figure 4.1**. Finally it was dispersed in 3 ml of de-ionized water for further characterization and investigation.

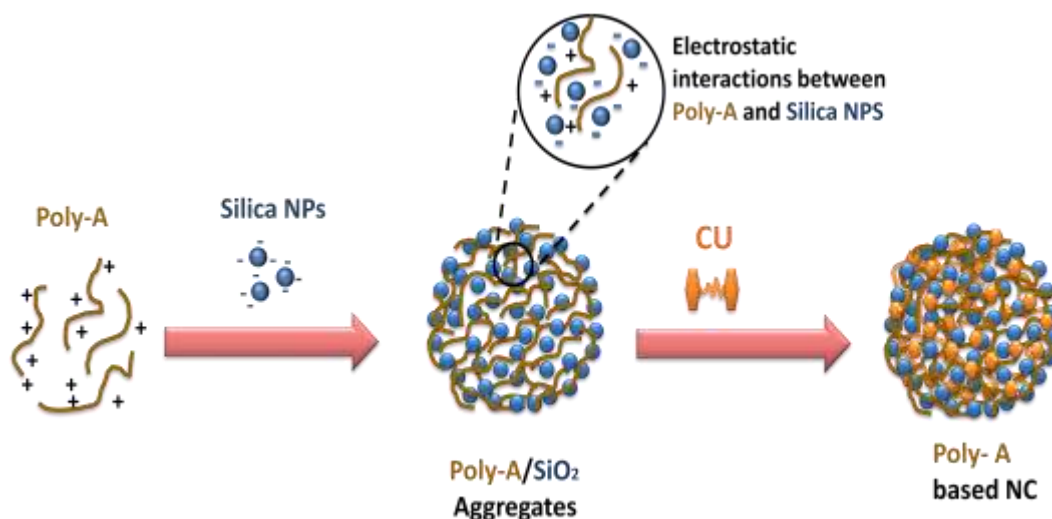


Figure 4.1. Illustration of Poly A interacting with SiO₂ NPs, and CU to form NCs.

3. Morphological Characterization:

The SEM and DLS analysis were done using the same methods given chapter 2.

4. Spectroscopic Measurements:

The steady-state fluorescence spectra (excitation and emission), fluorescence lifetime measurements and FT IR spectra were recorded using the same techniques mentioned in chapter 2.

C. Results and Discussion:

The fluorescence spectra of curcumin in the presence of different nucleobases are shown in **Figure 4.2**. The concentrations of curcumin and nucleobases were fixed at around 5 μ M and 1 mg/mL respectively. There is no appreciable change in the emission maximum of curcumin in the absence or presence of different nucleobases. The relative fluorescence intensity of curcumin in the presence of different nucleobases as shown in **Figure 4.3** has been compared with that of curcumin alone (normalized to unity at emission wavelength 550 nm). As seen in **Figure 4.2B**, there is not much changing in fluorescence intensity except that a slight 4-5 % quenching of intensity for adenine, guanine and thymine whereas 8 to 9 % quenching of fluorescence in the presence of uracil and cytosine. This change is not sufficient to develop an analytical method for selective sensing of nucleobases.

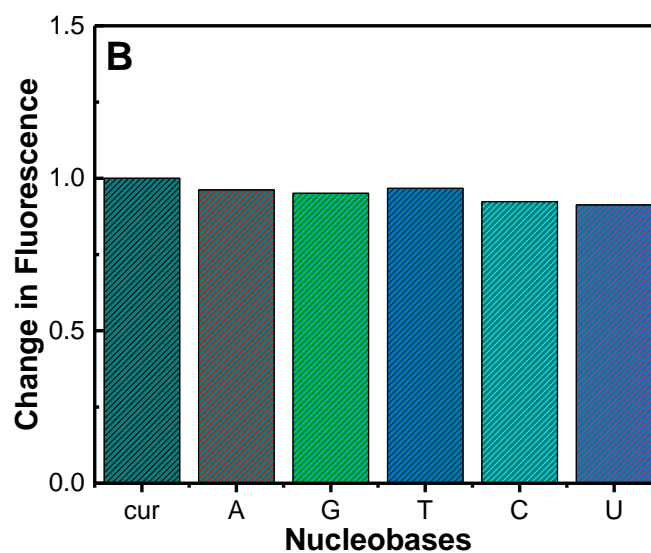
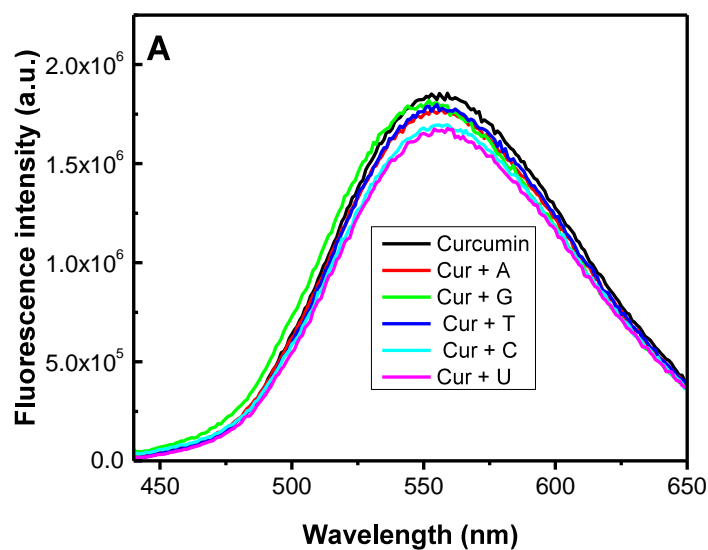


Figure 4.2. (A) Fluorescence spectra of curcumin in the presence of various nucleobases excited at 425 nm. The concentrations of the curcumin and nucleobases were fixed at $5\mu\text{M}$ and 1 mg/ml respectively; (B) Relative change in fluorescence intensity of curcumin in the presence of nucleobases when the fluorescence intensity of curcumin without nucleobase was normalized to 1. The excitation wavelength was 425 nm and the emission wavelength was 550 nm. The measurements were done in duplicates.

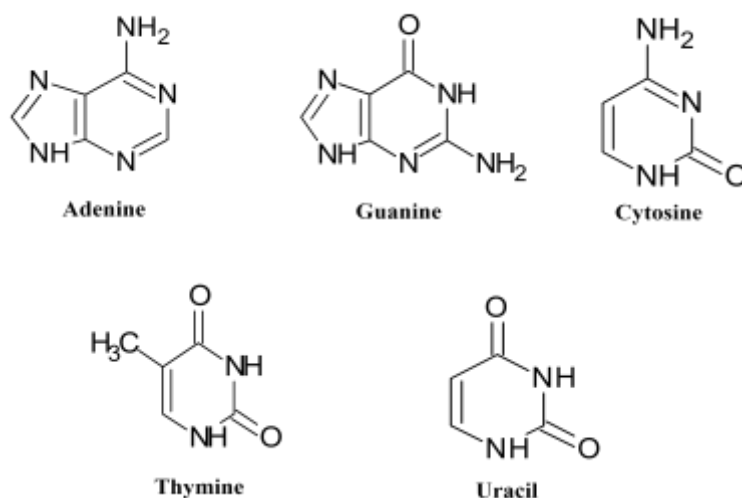


Figure 4.3. The nucleobases used and their corresponding chemical structures.

When curcumin was mixed with silica nanoparticles of about 24 nm size, the fluorescence emission spectrum showed a large blue shift from about 550 nm in water to around 495 nm (**Figure 4.4A**). This large shift might not be due to change in local environment [173], unlike the case observed for curcumin embedded in the phospholipid membranes [174], because the bulk solvent environment of silica particles is still an aqueous medium, therefore, such shift could only be explained based on the strong association of curcumin with silica particles. Interaction of curcumin-silica NPs complex very slightly shifted the maximum towards the lower wavelength range. However, when the fluorescence intensity of curcumin-silica NPs complex was compared in the presence of different bases (fixing the concentration at 1 mg/mL), the fluctuation of fluorescence intensity showed a different behavior unlike the case found for curcumin alone. **Figure 4.4B** depicts that the fluorescence intensity of curcumin-silica NPs complex marginally was quenched in the presence of most of the bases (3 % for uracil, 5 % for thymine, 9 % for adenine and 15 % for cytosine) except guanine for

which a remarkable 20 % enhancement of fluorescence intensity was observed.

Although this trend is different than the one observed earlier for curcumin alone, the change is not significant to get a conclusive selectivity for guanine for fluorescence sensing.

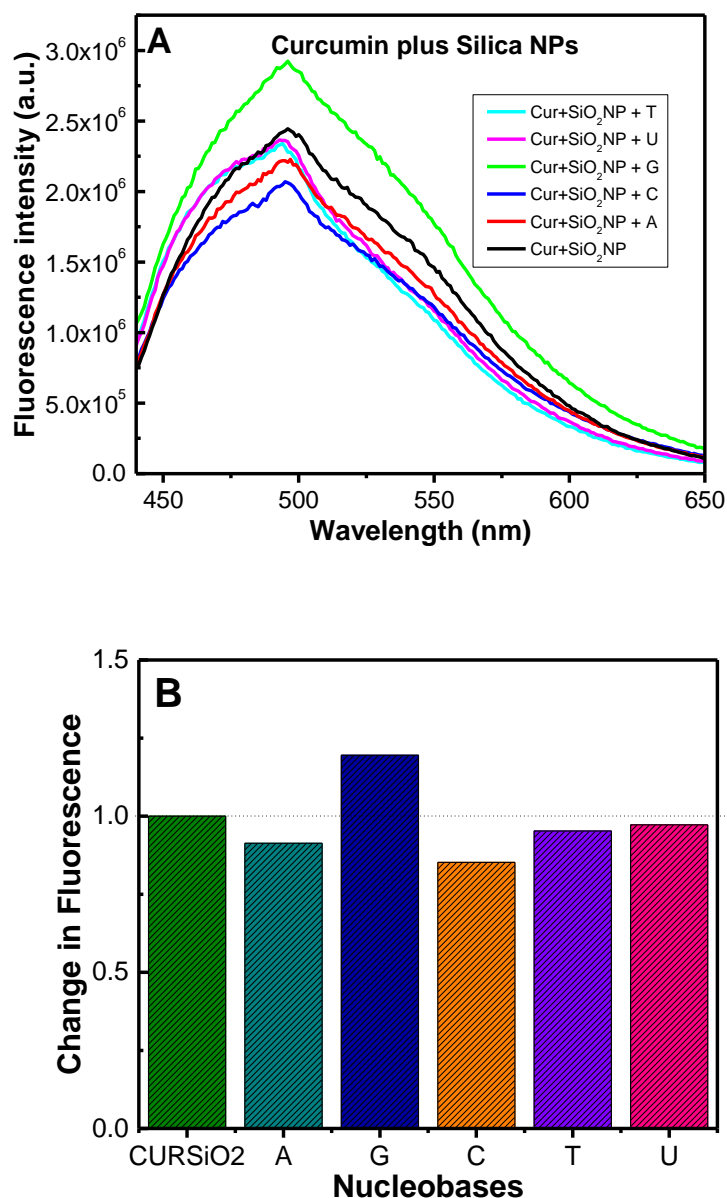


Figure 4.4. (A) Fluorescence spectra of curcumin with silica NPs in the presence of various nucleobases excited at 425 nm where the concentrations of CU and nucleobases were fixed at 5 μ M and 1mg/ml respectively; (B) Relative change in fluorescence intensity of curcumin with silica NPs in the presence of nucleobases when the fluorescence intensity of curcumin with silica NPs without nucleobase was normalized to 1. The excitation wavelength was 425 nm and the emission wavelength was 495 nm. The measurements were done in duplicates.

When we further modified the curcumin-silica NPs complex with poly (allylamine hydrochloride) (PAH), in this case silica nanoparticles were mixed with

PAH and then curcumin was added to form large aggregates. The fluorescence emission spectrum centered at around 547 nm of such PAH aggregates as presented in **Figure 4.5A** were not surprising and similar with a slight red shift compared to the emission spectrum centered at around 540 nm obtained earlier for curcumin based nanocapsule discussed in chapter 3. Note that in earlier case (chapter 3), capsules were prepared using salt (dipotassium hydrogen phosphate); whereas in the present case it is rather a deposition of PAH on the surface of silica nanoparticles. This variation of spectral shift is due to the variation in the local environment of curcumin in these two different preparation modes. Such local environment is expected (as in chapter 3) where silica nanoparticles were put over PAH and curcumin. On contrary, in the present case silica NPs and PAH initially form a complex over which curcumin was deposited, thus, a strong silica-curcumin association is expected in the first case (chapter 3). Interestingly, the addition of base did not change the emission maximum of these aggregates appreciably except for guanine. Herein, when guanine was added a further blue shift of 10 nm was observed, indicating a remarkable interaction between guanine and curcumin-silica-PAH based aggregates. The fluorescence intensity, however, increased marginally 20 – 35 % for most of the bases and the enhancement was even significantly high about 265 % in the presence of guanine (**Figure 4.5B**).

To improve the effectiveness towards selective sensing for guanine further, we tested a synthesized polymer, Poly A, which contains adenine alone with poly amine backbone. The structure is given in **Figure 4.6**. This polymer (Poly A) was used instead of PAH without changing much in experimental conditions. The fluorescence emission spectrum of Poly A based aggregates (**Figure 4.7A**) were similar to PAH based aggregates with a slight shift in maximum due to variation in the local environment of

the polymer, however, the trend in change in emission maximum in the presence of nucleobases were similar to as observed for PAH based aggregates. Nevertheless, the change in selectivity towards guanine for fluorescence assessment was highly remarkable; the fluorescence increase in the presence of most of the bases was nominal 20-40 % while in the presence of guanine the fluorescence enhancement was 500 % (see **Figure 4.7B**).

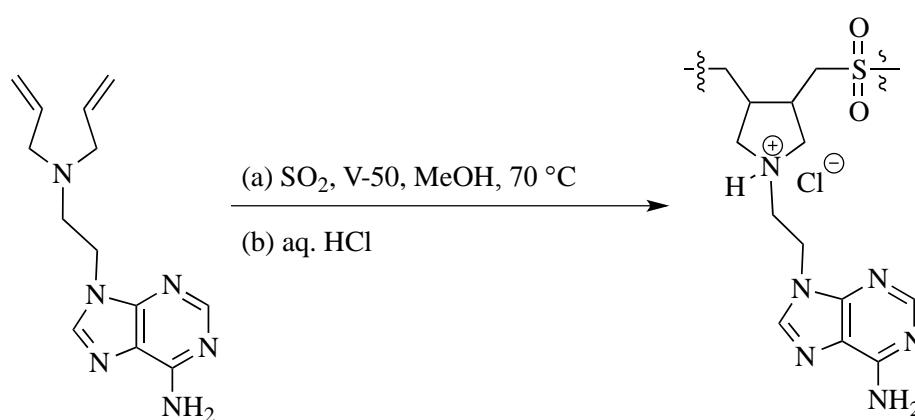


Figure 4.6. Chemical structure of Poly (9-(2-diallylaminoethyl)adenine.HCl-co-sulfur dioxide) (Poly A)

We further characterized these aggregates using SEM and DLS method. The particle size distribution was analyzed by a dynamic light scattering (DLS) technique and was found to have an effective hydrodynamic radius (R_h) of 700 nm. However, the SEM images of Poly A aggregates (**Figure 4.8**) show that the aggregates were found to be of various sizes from 200 to 600 nm, most of them were less than 500 nm. This high effective diameter is due to the further aggregation of smaller size aggregates in solution. These aggregates were found to be spherical. This can be explained by the fact that negative charge of silica nanoparticles encouraging Poly A, having positive charge,

to get adsorbed on its surfaces, which further facilitates the self-assembly of Poly A into spherical capsules. Curcumin does not play a major role during the capsules' formation since when Poly A was mixed with curcumin and then silica nanoparticles were added to the latter mixture, no capsules were observed. It should be noted that during the preparation of Poly A capsules, the unreacted polymer, silica and curcumin were washed out by centrifugation after the formation of the capsules as explained in the experimental section. The self-assembly of poly A polymer is evident from the change in FT IR spectrum. The FT IR spectra of Poly A polymer and Poly A based capsules are shown in **Figures 4.9 and 4.10**, respectively. There is a remarkable difference between the FT IR spectra of the two cases. The prominent peak at around 3422 cm^{-1} of Poly A polymer was not detected for the Poly A capsules.

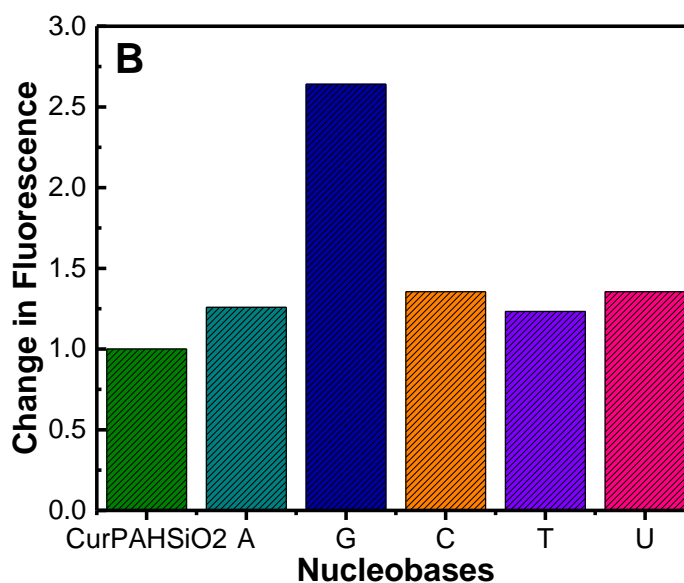
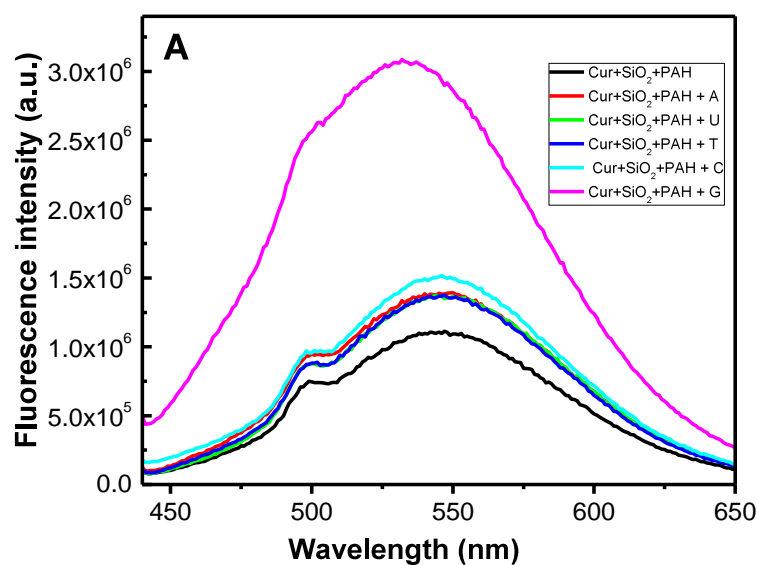


Figure 4.5. (A) Fluorescence spectra of aggregates containing silica NPs, curcumin and PAH in the presence of various nucleobases excited at 425 nm where the concentrations of CU, PAH and nucleobases were fixed at 5 μ M, 3 mg/ml and 1mg/ml respectively; (B) Relative change in fluorescence intensity of aggregates containing silica NPs, curcumin and PAH in the presence of nucleobases when the fluorescence intensity of aggregates containing silica NPs, curcumin and PAH without nucleobase was normalized to 1. The excitation wavelength was 425 nm and the emission wavelength was 548 nm. The measurements were done in duplicates.

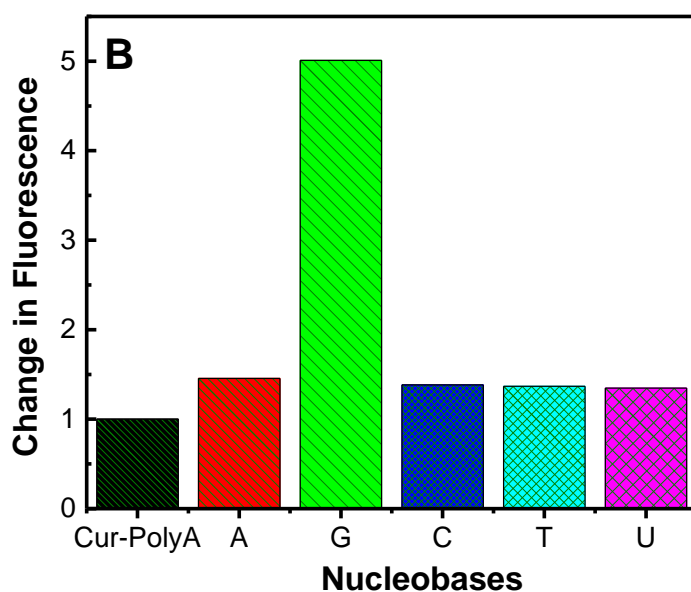
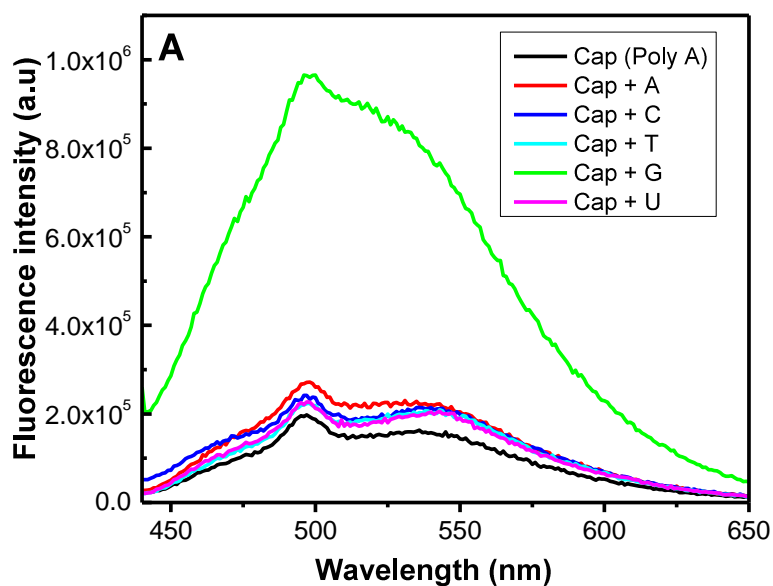


Figure 4.7: (A) Fluorescence spectra of capsules containing silica NPs, curcumin and Poly adenine (Poly A) in the presence of various nucleobases excited at 425 nm. The concentration of the capsule and nucleobases was fixed at 1mg/ml; (B) Relative change in fluorescence intensity of Poly A capsules in the presence of nucleobases when the fluorescence intensity of Poly A capsules without nucleobase was normalized to 1. The excitation wavelength was 425 nm and the emission wavelength was 543 nm. The measurements were done in triplicates.

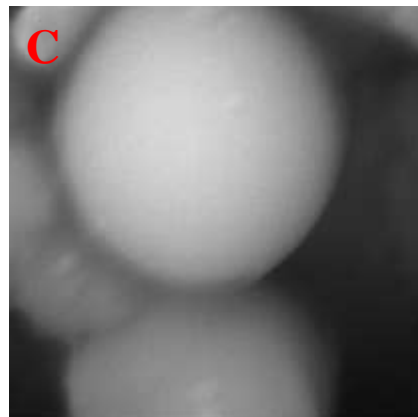
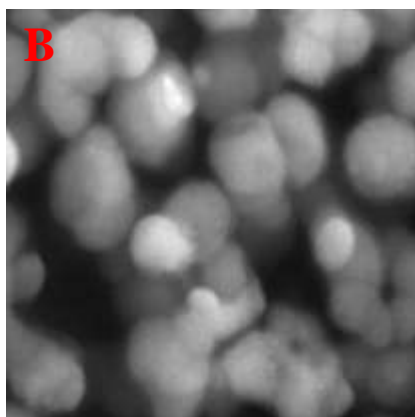
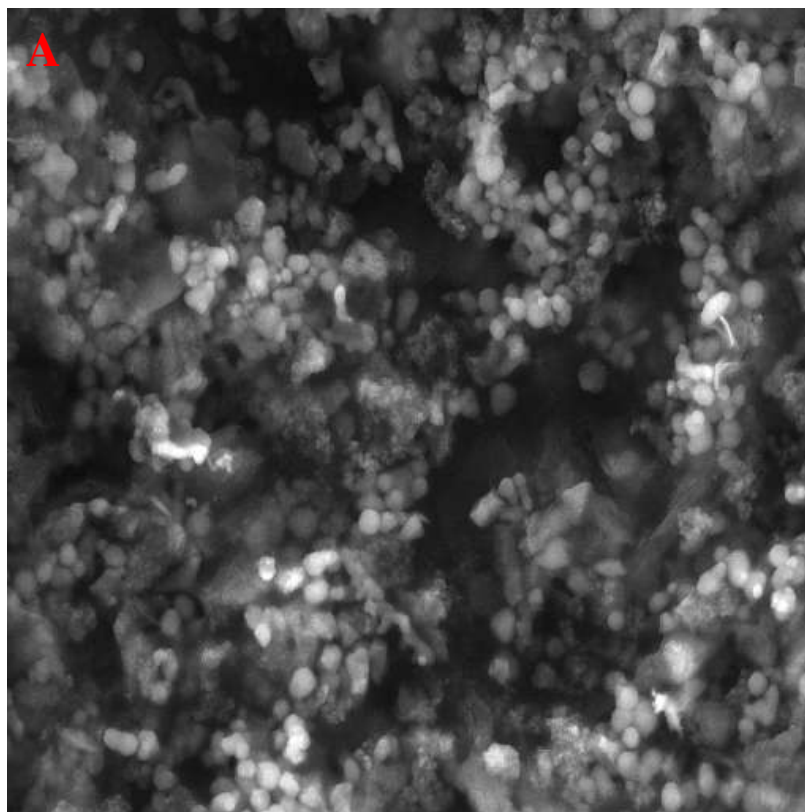


Figure 4.8. (A-B-C) SEM images of capsules containing silica NPs, curcumin and Poly adenine (Poly A). (A) 5 μm resolution whereas (B) 500 nm resolution and (C) 200 nm resolution.

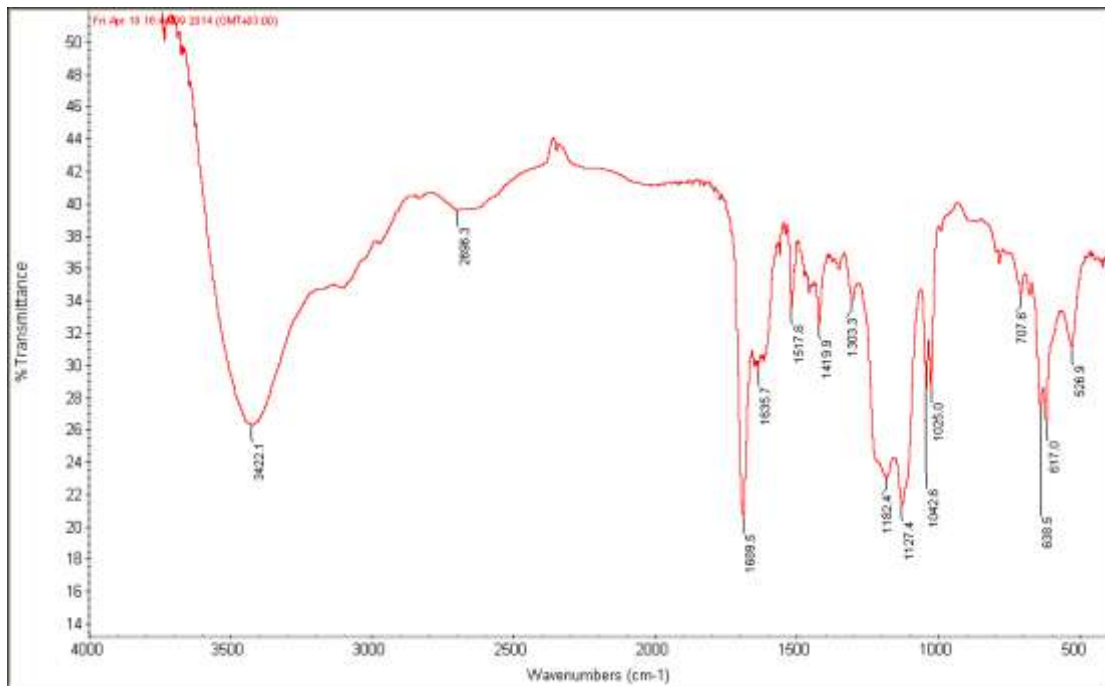


Figure 4.9. FT-IR spectrum of Poly A polymer.

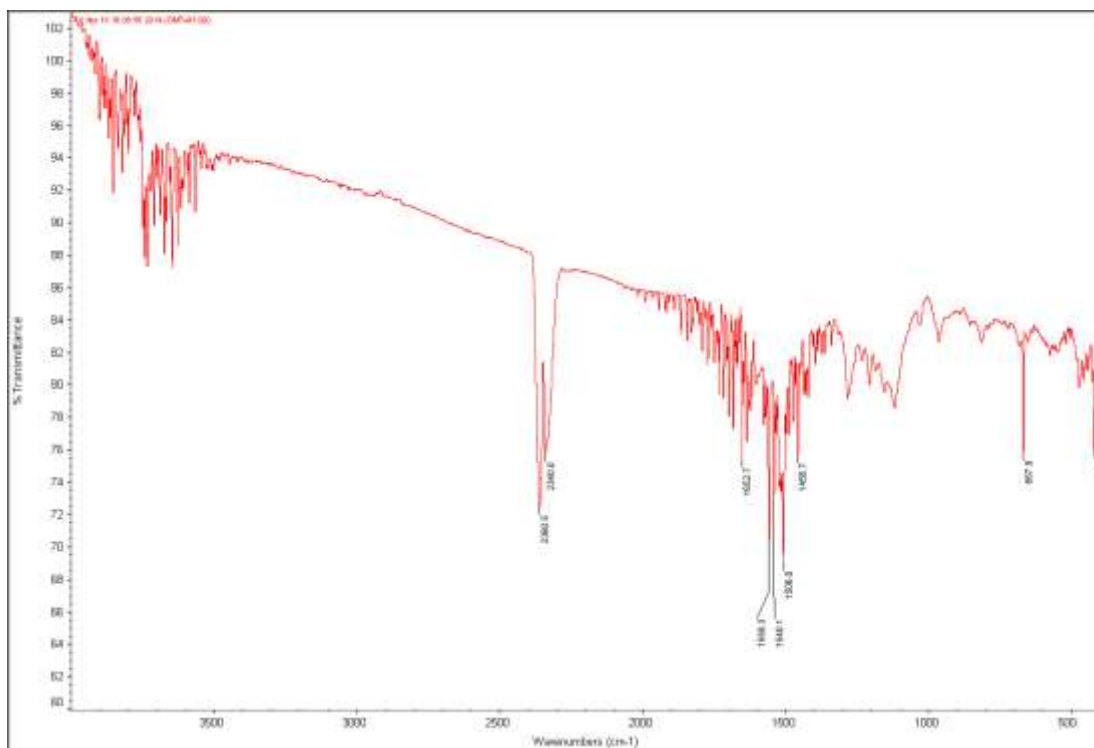


Figure 4.10. FT-IR spectrum of Poly A and curcumin based capsules

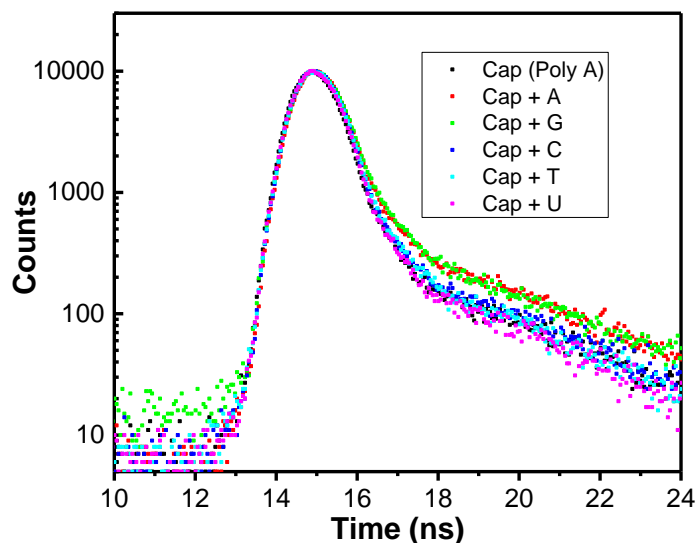


Figure 4.11. Fluorescence lifetime decay profiles for Poly A capsules in the absence and present of different nucleobases at $\lambda_{\text{ex}} = 405$ nm and $\lambda_{\text{em}} = 540$ nm. The data was fitted with biexponential decay.

Table 4.1. Fluorescence lifetime values for Poly A capsules in the absence and presence of different nucleobases at $\lambda_{\text{ex}} = 405$ nm and $\lambda_{\text{em}} = 540$ nm. The data was fitted with biexponential decay.

	Short Lifetime (τ_1) (ps)	Long Lifetime (τ_2) (ns)
Poly A capsule	533 (83%)	4.33 ns (17%)
Cap + C	558 (84%)	4.48 (16%)
Cap + T	569 (85%)	4.22 (15%)
Cap + A	598 (77%)	4.79 (23%)
Cap + U	480 (80%)	3.8 (20%)
Cap + G	643 (81%)	4.73 (19%)

This peak could be due to amino group present in Poly A, and its absence in the capsule could be explained by the expected strong interaction between silica

particles and positive charge of amino group. The strong band around 2360 and 2340 cm^{-1} in the capsules could be due to CO_2 present in the surrounding environment.

The fluorescence lifetime decay profile at $\lambda_{\text{ex}} = 405 \text{ nm}$ and $\lambda_{\text{em}} = 540 \text{ nm}$ for poly A capsule in the absence and presence of nucleobases in water is shown in **Figure 4.11**. The data (see **Table 4.1**) could be best fitted with a biexponential decay giving a short component lifetime (τ_1) of $\sim 533 \text{ ps}$ (83%) and long component lifetime (τ_2) of 4.33 ns (17%). However, in ultrafast femtosecond time-resolved measurement other smaller lifetime components for curcumin have been reported [143, 175], which are not resolved in our present experimental conditions. Nevertheless, the biexponential decay and such values are not surprising where similar lifetime values of curcumin in different solvents have been reported in literature during this time scale [141]. The fluorescence lifetime values of Poly A capsules marginally increased in the presence of cytosine, $\tau_1 = 558 \text{ ps}$ (84 %) and $\tau_2 = 4.48 \text{ ns}$ (16 %), thymine, $\tau_1 = 569 \text{ ps}$ (85 %) and $\tau_2 = 4.22 \text{ ns}$ (15 %), and adenine $\tau_1 = 598 \text{ ps}$ (77 %) and $\tau_2 = 4.79 \text{ ns}$ (23 %). A decrease was observed for uracil, $\tau_1 = 480 \text{ ps}$ (80 %) and $\tau_2 = 3.5 \text{ ns}$ (20 %). Though, the value for long component was found to be 4.73 ns (19%) in the presence of guanine, the short component species increased appreciably in the presence of guanine. These variations of fluorescence lifetime of poly A capsules in the presence of nucleobases could be explained considering two cases: (i) interaction of the capsules with the nucleobases due to hydrophobic and other electrostatic interactions and, (ii) association of the capsules with the nucleobases because of specific base pairings. The improvement in short component as well as long component lifetime of the Poly A capsules in the presence of adenine, cytosine, and guanine could be due to hydrophobic interaction between the nucleobase and Poly A capsules, whereas the decrease in long component lifetime in the

presence of thymine and uracil is caused by specific base pair interaction between adenine group present in Poly A capsule and thymine/uracil. The decrease in short component lifetime in the presence of uracil could also be referred to the same reason whereas the increase in short component lifetime of Poly A capsules in the presence of thymine does not rule out hydrophobic interaction along with specific base pair interaction between thymine and Poly A capsule. To establish this fact we measured the FT-IR spectrum of different nucleobases and compared them with that of mixture of poly A capsules and nucleobases as presented in **Figure 4.12-4.21**.

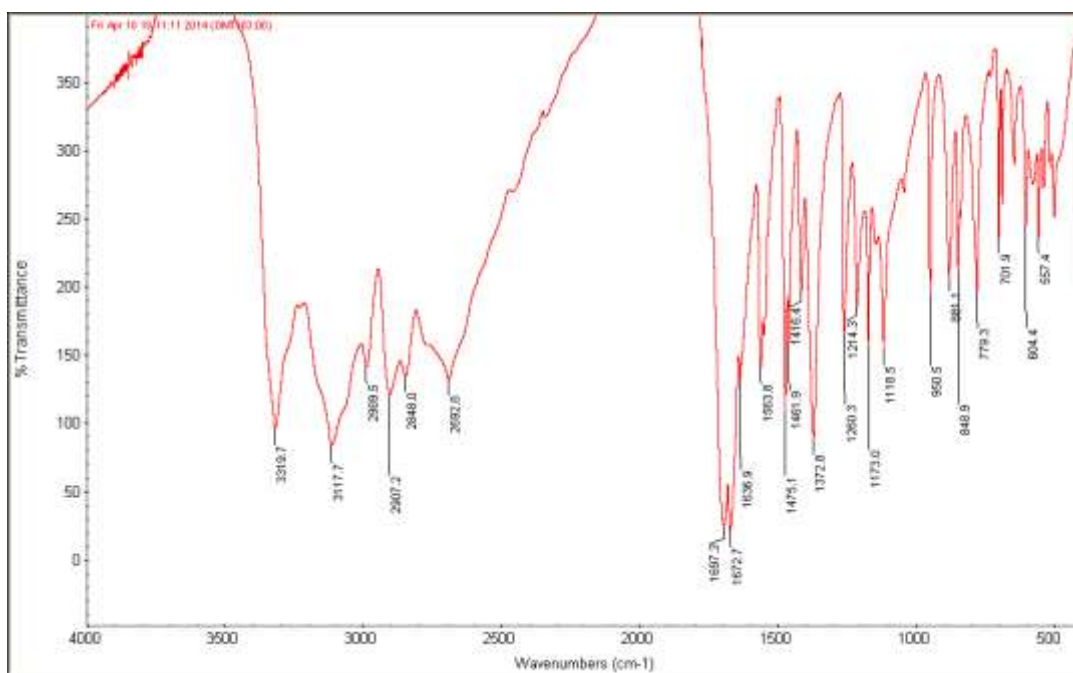


Figure 4.12. FT-IR spectrum of guanine

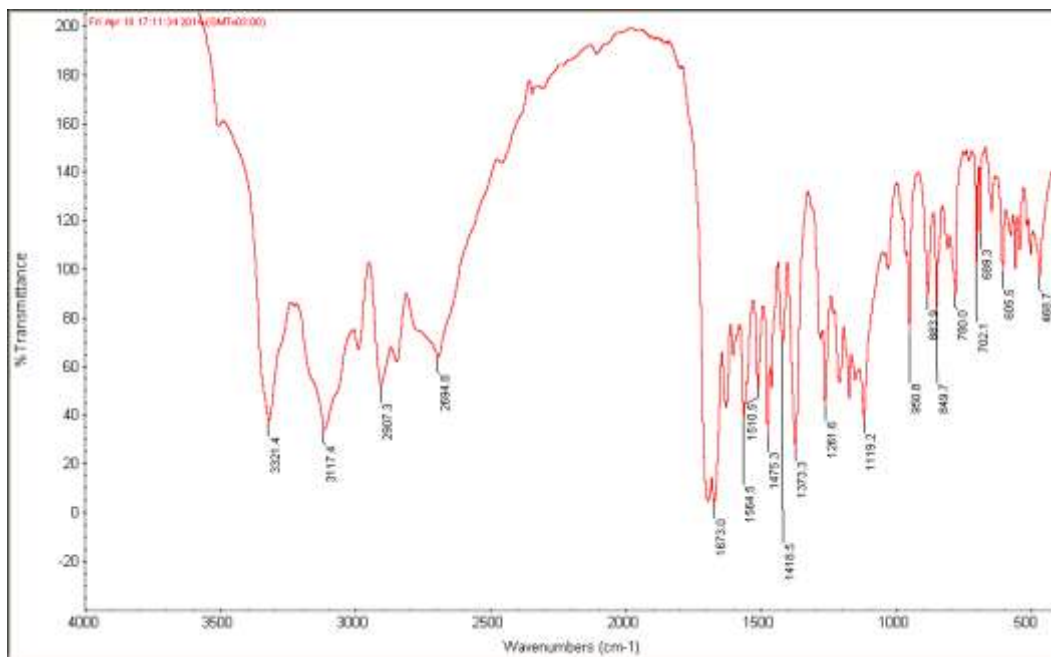


Figure 4.13. FT- IR spectrum of guanine and poly A capsules

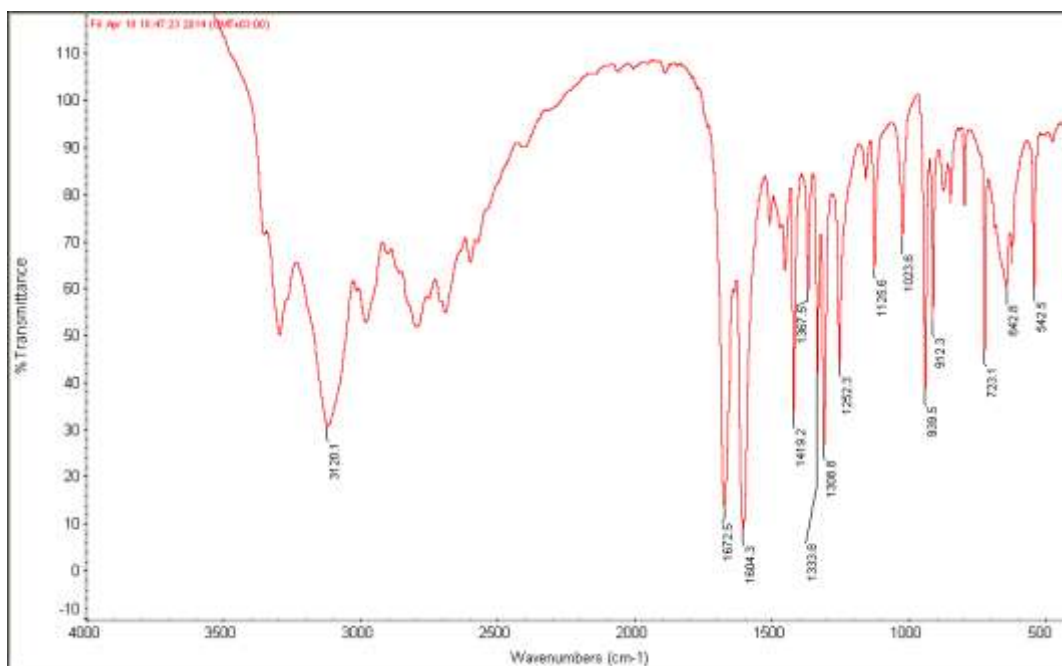


Figure 4.14. FT-IR spectrum of adenine

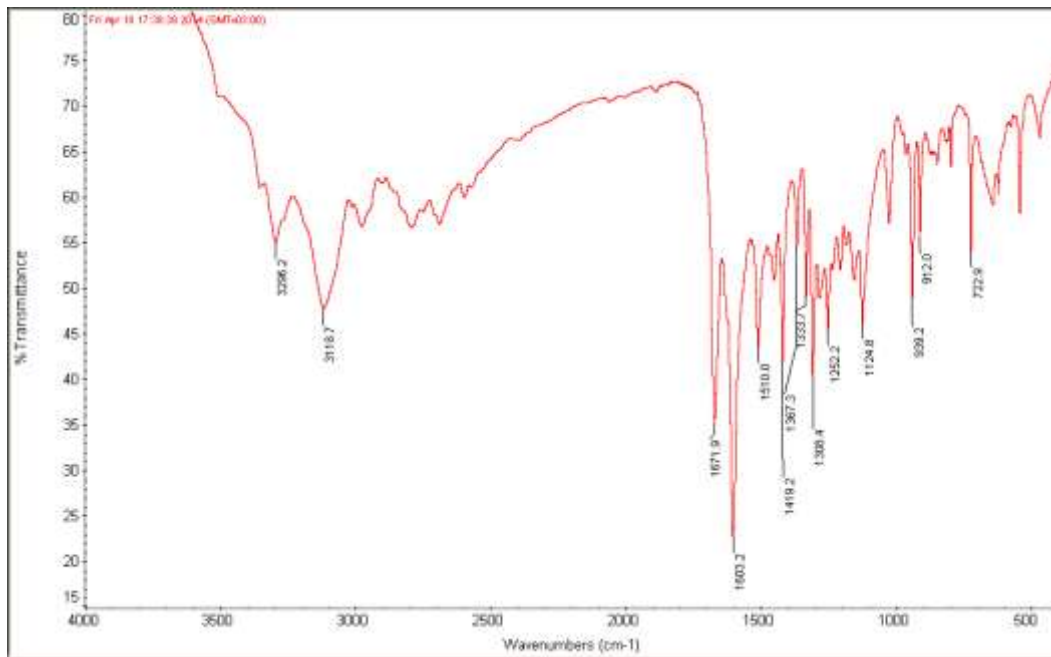


Figure 4.15. FT-IR spectrum of adenine and poly A capsules

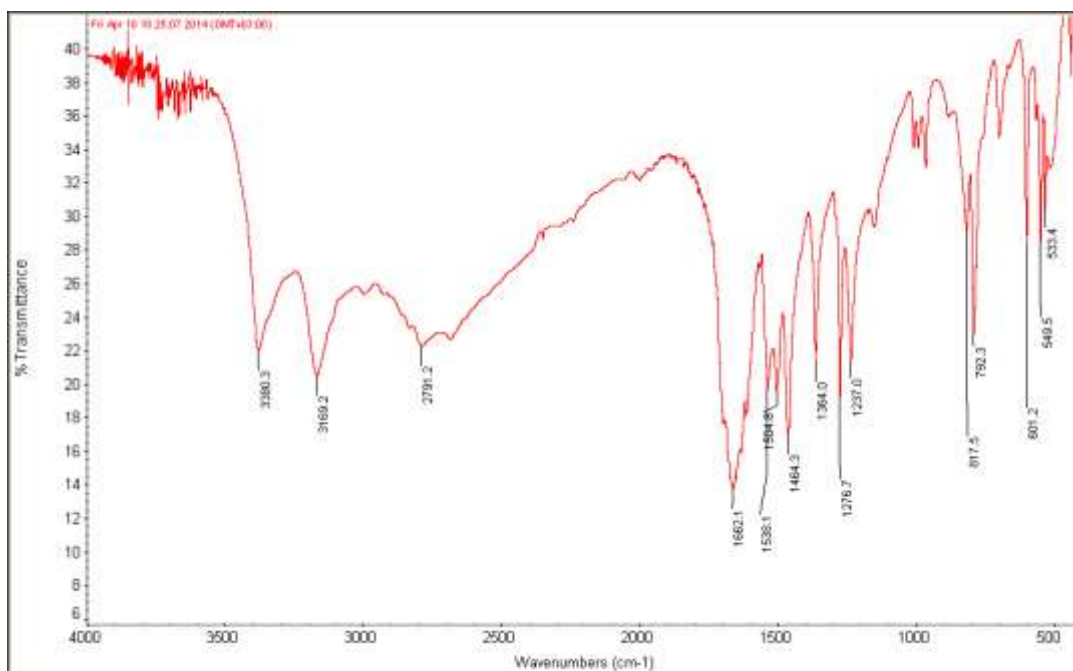


Figure 4.16. FT-IR spectrum of cytosine

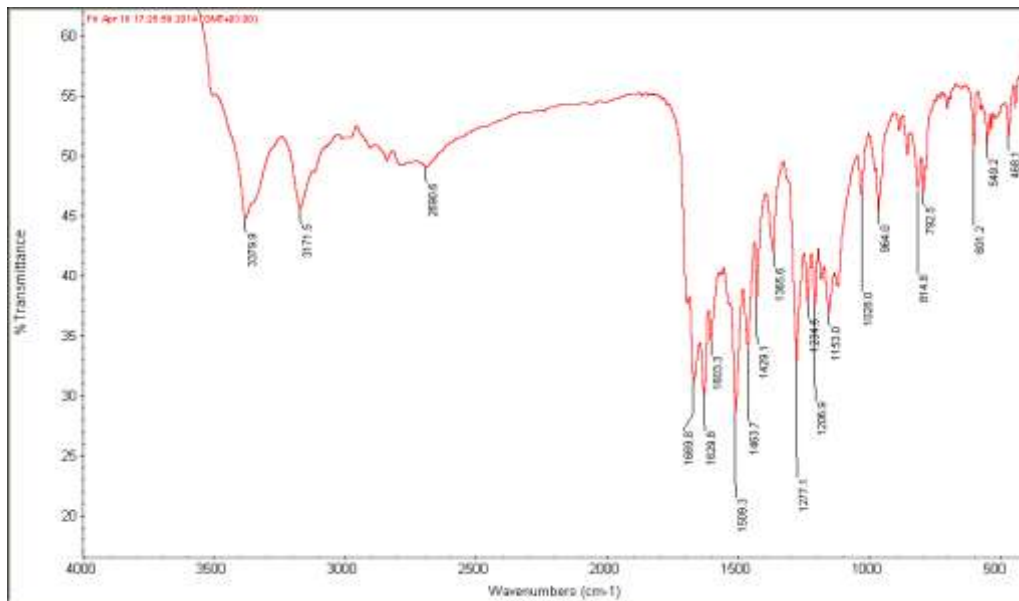


Figure 4.17. FT-IR spectrum of cytosine and poly A capsules

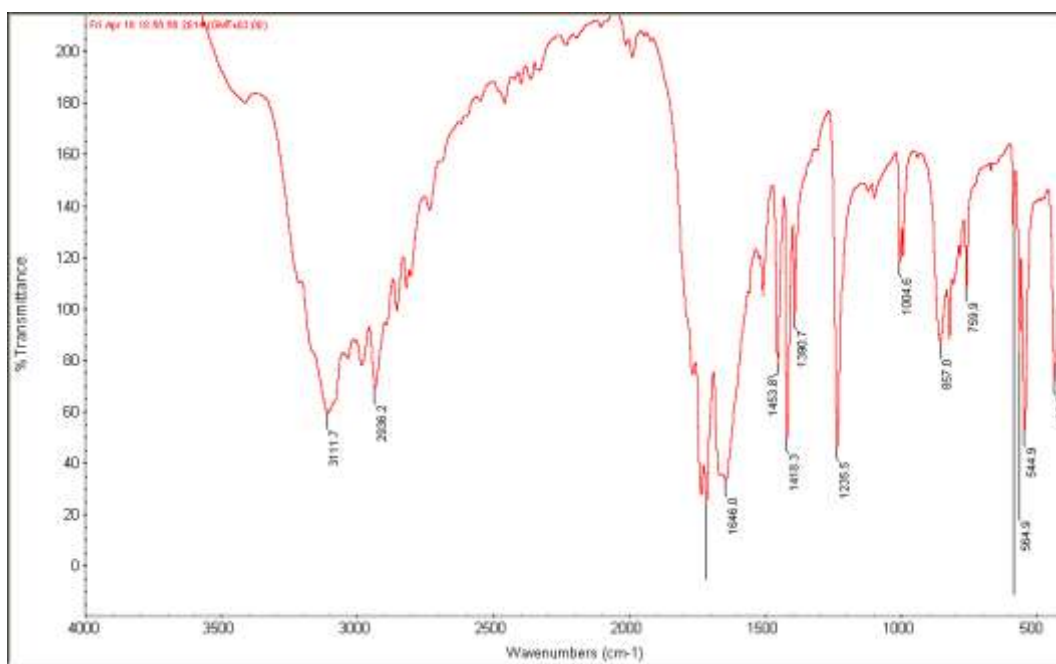


Figure 4.18. FT-IR spectrum of uracil

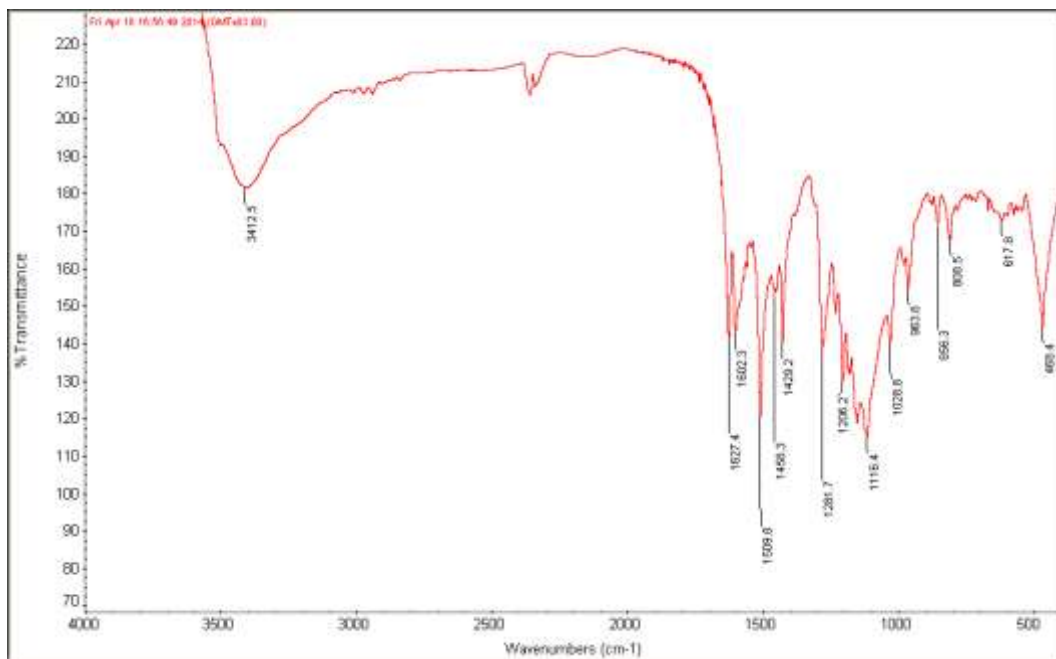


Figure 4.19. FT-IR spectrum of uracil and poly A capsules

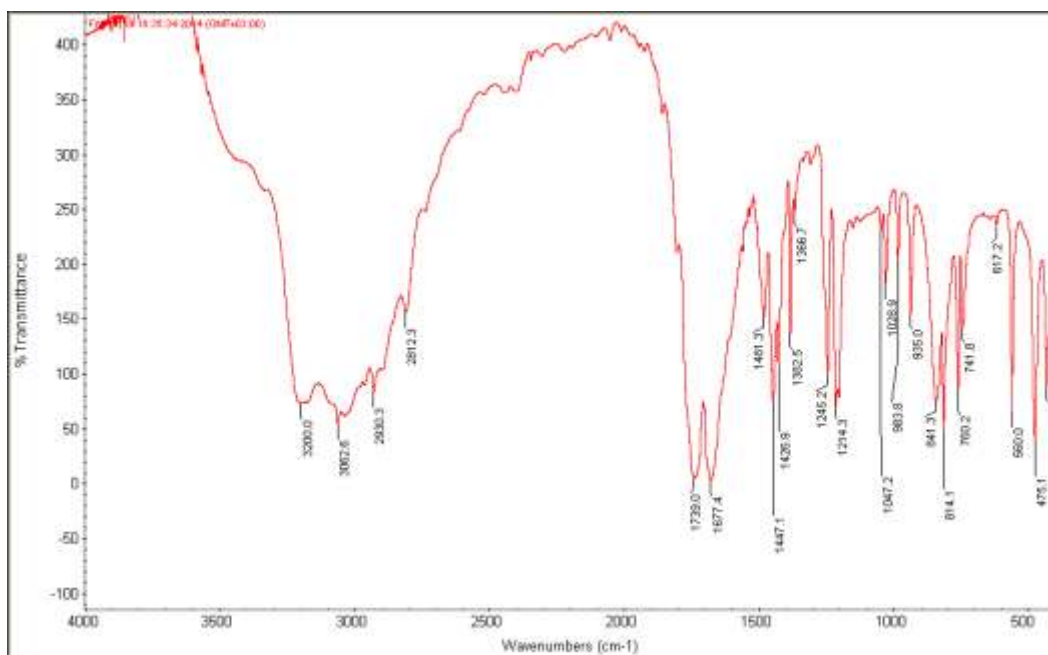


Figure 4.20. FT-IR spectrum of thymine

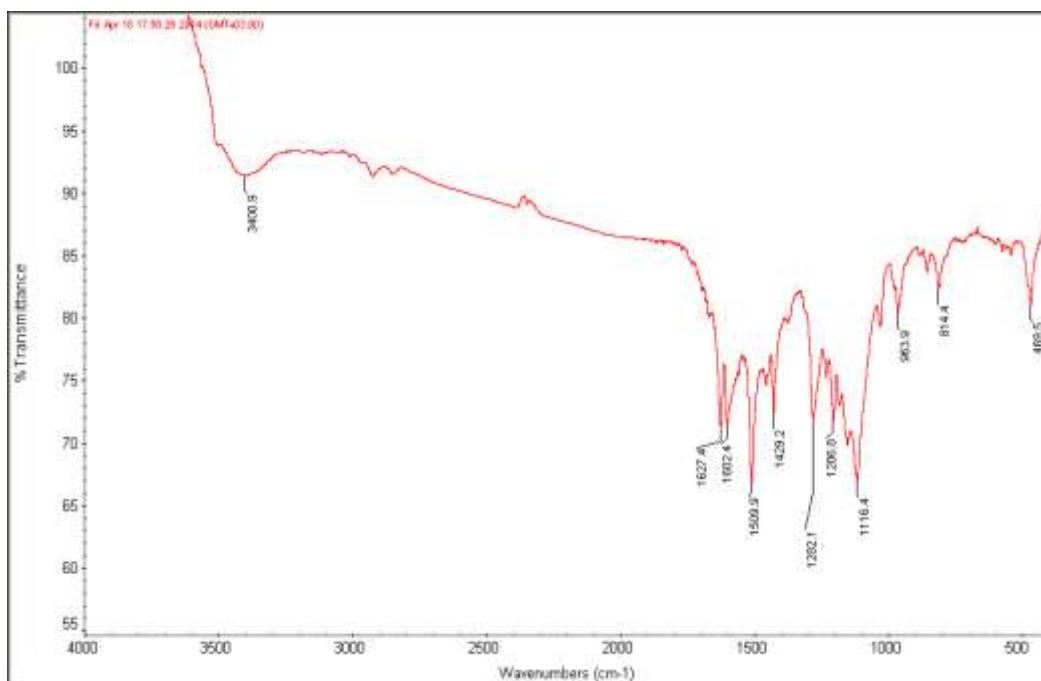


Figure 4.21. FT-IR spectrum of thymine and poly A capsule

As can be seen in FT IR spectra, there is no remarkable difference between the spectra of adenine or cytosine compared to that of Poly A capsules along with adenine or cytosine, especially in the spectral region $3500 - 3100 \text{ cm}^{-1}$ for $-\text{NH}$ stretching. On the other hand Poly A capsules showed a broad prominent peak around 3400 cm^{-1} or 3413 cm^{-1} in the presence of thymine or uracil which were absent in either thymine or uracil. Similarly, the peak at around 3200 cm^{-1} for free thymine and 3111 cm^{-1} for free uracil were absent in poly A capsules mixture with thymine or uracil. This suggests there is a strong base pair interaction of adenine present in Poly A capsule and that of uracil or thymine, which is as expected and validates our hypothesis on change in fluorescence lifetime. However, guanine did not show in specific interaction with Poly A capsules in the FT IR spectrum; and we suspect the interaction is largely due to hydrophobic interaction. This is further supported by the relatively poor solubility of guanine compared to other nucleobases in water.

Realizing the importance of this Poly A based capsules for selective sensing of guanine, the calibration curve for estimation of guanine by Poly A capsules as fluorescence sensing material was tested. The fluorescence spectra of Poly A capsules in the presence of different concentration of guanine is shown in **Figure 4.22A** and the corresponding fluorescence alteration with guanine concentration is plotted in **Figure 4.22B**. As can be seen in the plot, in a wide range of concentration from 0 – 7 mM, the curve showed a linear fit. Most of the available methods for guanine estimation work in lower concentration range as given in **Table 4.2**. *W. Wanget et.al* have reported ,with higher concentration range, a linear dynamic range of 340 -6600 μM using micellar electrokinetic chromatography with indirect laser-induced fluorescence detection method [170].However, the present method showed a wider range than the reported one. The association constant of guanine with poly A capsules was estimated using the following equation [129]:

$$\text{Log} \left[\frac{(F-F_0)}{F_0} \right] = \text{Log}(K) + n \text{Log}[\text{Guanine}]$$

Table 4.2. Analytical methods for guanine estimation and their linear ranges.

Method/reagent	Linear range (μM)	Reference
Chemiluminescence method using phenylglyoxal	0-100	[176]
HPLC with post column fluorescence derivatization using phenylglyoxal reagent	1-25	[177]
Liquid chromatography with fluorometric detection using 3,4-dimethoxyphenylglyoxal (DMPG)	0-0.4	[178]
Electrochemical method based on graphene-ionic liquid-chitosan composite film modified glassy carbon electrode	2.5-150	[179]
Flow injection Chemiluminescence method using hydrogen peroxide	2-600	[180]
Electrochemical approach based on electrodeposition of a nanostructured platinum thin film on a glassy carbon electrode	0.1-500	[181]
Micellar electrokinetic chromatography with indirect laser-induced fluorescence detection	340-6600	[170]
Our method	300-7000	

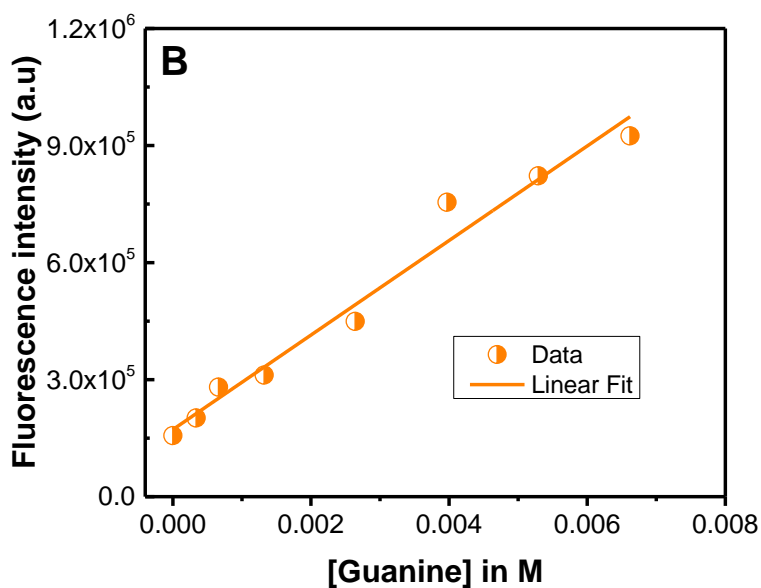
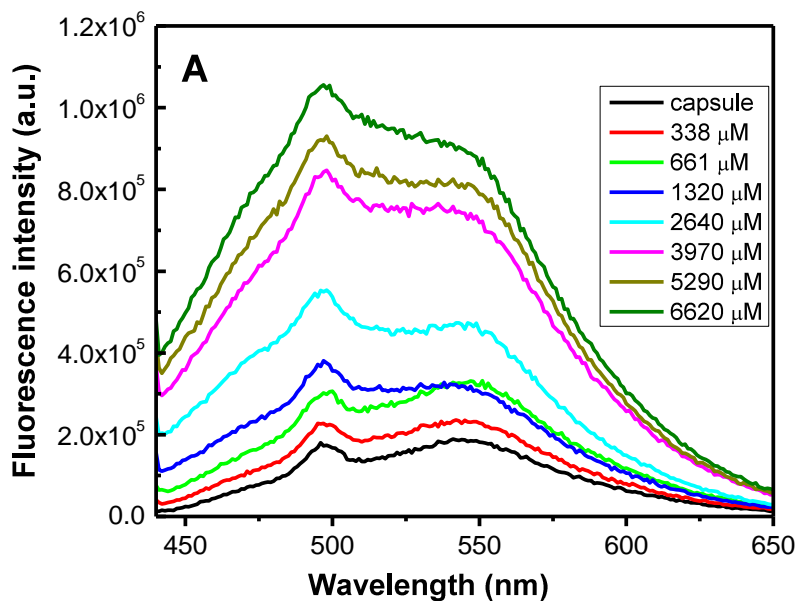


Figure 4.22. (A) Fluorescence spectra of Poly A capsules in various concentration of guanine excited at 425 nm where the concentration of Poly A capsule was fixed at 1mg/ml whereas guanine concentration varied between 0 and 7 mM ; (B) Linear change in fluorescence intensity of Poly A capsules with guanine concentration. The excitation wavelength was 425 nm and the emission wavelength was 526 nm for B. The measurements were done in triplicates.

where K and n are the binding constant and the number of binding sites, respectively. F and F_0 are the fluorescence intensity of Poly A capsules at excitation wavelength 425

nm and emission wavelength 526 nm in the presence and absence of Poly A capsules. The association constant of guanine with Poly A capsules was estimated as $K = 5.50 \times 10^2 \text{ M}^{-1}$ and number of binding sites $n = 0.93$, which is close to 1 as obtained from the graph in **Figure 4.23**. Since poly A capsules are much bigger in size (micrometer range) compared to size of guanine (less than nm), the possibility of more than one guanine molecule binding to Poly A capsule could not be ruled out. It is also important to note that one Poly A capsule has multiple numbers of curcumin units and the present n values might be because of binding between guanine and curcumin.

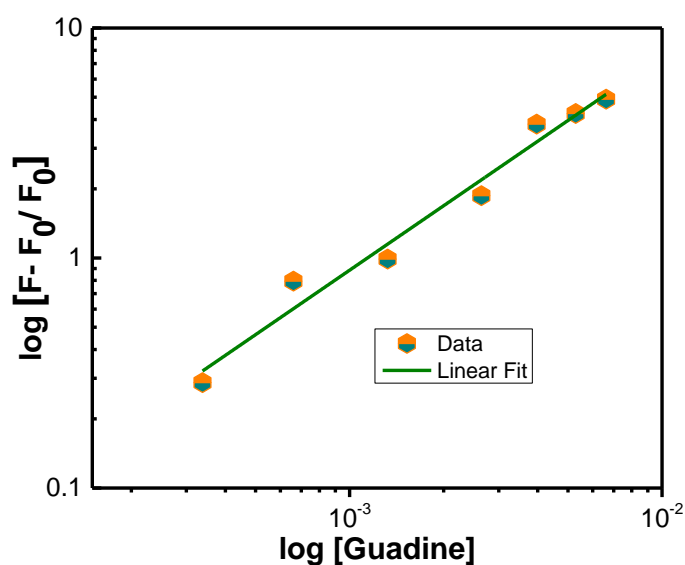


Figure 4.23. Plot of concentration of $(F-F_0)/F_0$ vs. guanine concentration for estimation of binding constant. The concentration of guanine ranged between 0 and 7 mM and the fluorescence of the capsule was taken at 526 nm. The measurements were done in triplicates.

One of the serious concerns about curcumin has been its stability. Studies have shown that the degradation of curcumin in aqueous solution is linked to hydrolysis that occurs rapidly at a pH above neutrality. HPLC data has proven that curcumin degrades to form *trans*-6-(4'-hydroxy-3'-methoxyphenyl)-2,4-dioxo-5-hexanal as the main

product, which further decomposes to vanillin, ferulic acid, and feruloyl methane [182]. . In UV-visible spectral region curcumin exhibited an intense absorption peak around 400 - 425 nm in neutral aqueous environment. In aqueous solution, there are three pK_a values at 8.38, 9.88 and 10.51 corresponding to deprotonation of the three hydroxyl groups of curcumin [183]. It has been established that the contribution of condensation products to the total absorption signal of curcumin are relatively minor, thus, decrease in the visible absorbance over time can be used as a measurement of degradation of curcumin [184]. Therefore, to understand the stability of the present sensing material, the absorbance change of curcumin and Poly A capsule was monitored at 427 nm with time in buffer solution as depicted in **Figure 4.24**. The absorption maximum of curcumin in buffer (7 % methanol) at pH 7.5 decayed relatively quickly in the first 5 hours (30 % degradation) and approximately 62 % of the original value in 50 hours. On the other hand, the degradation of poly A capsules in buffer at pH 7.5 was just 10 % in the first 5 hours. Further with time the degradation was even slower with 28 % degradation after 50 hours which confirmed that degradation of curcumin could be overcome inside the Poly A capsules for better analytical applicability and validates robustness of present method.

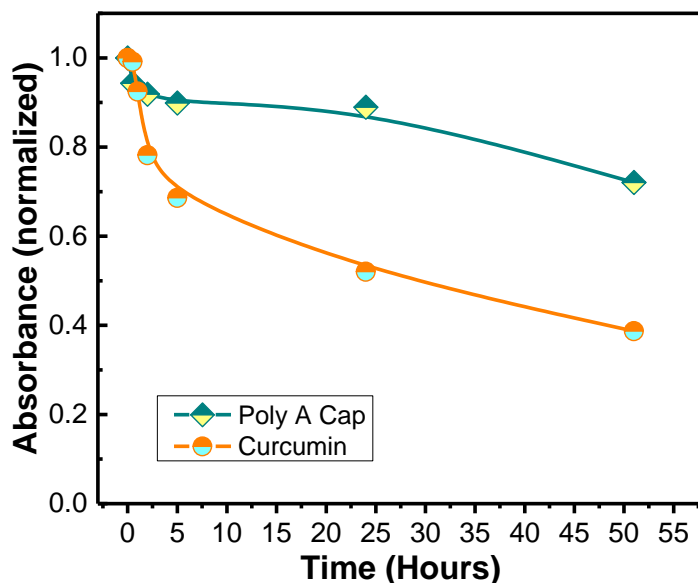


Figure 4.24. Stability of Poly A capsules compared to curcumin in buffer solution pH 7.5. The curcumin solution contained about 8 % methanol.

All in all, the Poly A/silica nanoparticles/CU nanocapsules are synthesized using self assembly approach. The capsules are spherical and their size range is between 200 and 600 nm. These capsules are applied for guanine sensing where in the presence of guanine their fluorescence intensity has been enhanced by 500%. FT-IR spectra along with lifetime measurements suggest that this sensitivity is due to hydrophobic interactions; assisted by the low water solubility of guanine as compared to the other nucleobases. The association constant of Poly A capsule and guanine is $K=5.50 \times 10^2 \text{ M}^{-1}$ and the number of binding constant (n) is equal to 0.93. The present method shows a wider linear dynamic range in higher concentration range as compared to the reported methods. Finally, the degradation study proves that CU stability is improved in Poly A capsule.

CHAPTER V

TUNING ZnO NANOPARTICLES BASED ON POLY (ALLYLAMINE HYDROCHLORIDE) MEDIATED NANOCAPSULES FOR VISIBLE EMISSION

A. Introduction:

Zinc oxide (ZnO) is an important technological material. The large electromechanical coupling, combined with the lack of symmetry center in wurtzite, leads to strong pyroelectric and piezoelectric properties and the consequent application of ZnO in piezoelectric sensors and mechanical actuators. Moreover, ZnO is a semiconductor with a wide band-gap (3.37 eV); so it is suitable for optoelectronic applications of short wavelength [185]. In addition, ZnO crystal has high exciton binding energy (60 meV) that allows efficient excitonic emission at room temperature [186]. Ultraviolet (UV) luminescence at room temperature has been reported in thin films and disordered nanoparticles [185]. ZnO is transparent in the visible region of light [185] and can be doped with transition metals for spintronic applications [187]. Furthermore, ZnO exhibits sensitivity to numerous gas species, mainly carbon monoxide (CO), ethanol (C₂H₅OH), and acetylene (C₂H₂), that makes it adequate for sensing applications [186].

The optical properties of ZnO can be tuned. It has been reported that the dispersion of nickel oxide nanoparticles (NiO NPs) on ZnO surface modifies the optical properties of the latter through a solid state electrochemical reaction at NiO- ZnO interface induced by surface OH groups. This reaction introduced some structural disorder and produced a stress relaxation to the ZnO surface [188]. Such modifications have been translated to changes in the emission spectra of ZnO; where a important in

the visible bands (3 bands centered at 465, 515, 550 nm respectively) has been detected in the presence of NiO NPs. This enhancement has been attributed to the increase in the number of oxygen and zinc vacancies after the addition of NiO NPs [188].

ZnO is environmentally friendly and chemically stable material. As a result, there is a remarkable interest in studying ZnO in the form of single crystals, powders, nanostructures, or thin films [186]. A wide variety of ZnO nanostructures have been reported, including nanowires [189], nanorods and tetrapods [190]. Moreover, core/shell ZnO/SiO₂ nanoparticles have been successfully synthesized; where these structures have showed improved stability and photo-catalytic activity in acidic or alkaline solutions as compared to uncoated ZnO nanoparticles [191].

In the present thesis, PAH based nanocapsules have been prepared to tune the optical properties of 14 nm sized ZnO nanoparticles, specifically for visible emission of ZnO.

B. Materials and Methods:

1. Materials:

Zinc oxide nanoparticles were obtained from PlasmaChem with >99% purity, 14 nm particle size and 30+ 5 m²/g. The stock solution of ZnO was prepared in de-ionized water of pH 9 and of 0.1mg/ml concentration. PAH and K₂HPO₄ were used (same as explained before in chapter 2). Uric acid and ascorbic acid were obtained from Fluka Analytical.

2. Preparation of ZnO/PAH Nanocapsules:

In this process 1.3 ml of PAH (3mg/ml) was gently vortex mixed for 10 s with 7.8 ml of 2.5 mM K_2HPO_4 and aged for 30 min. After wards, 7.8 ml of ZnO nanoparticles (0.1mg/ml) of pH 9 was added to PAH/ K_2HPO_4 aggregates. The pH of ZnO solution was monitored at 9; in such basic conditions ZnO is in the form of $Zn(OH)_3^-$, consequently, this ensures its interaction with the positively charged PAH/ K_2HPO_4 aggregates. The final solution was left to age for 2 hours, then it was centrifuged at a speed of 4450 rpm for 20 min. The capsules were washed for 3 times with de-ionized water and dispersed in 3 ml of de-ionized water for further characterization and investigation.

2. Morphological and Spectroscopic Analysis:

SEM, DLS, FT IR and steady-state fluorescence measurements were done as explained in chapters 2 and 3.

C. Results and Discussion:

ZnO based microcapsules were synthesized by the poly (allylamine hydrochloride) mediated self-assembly method described in chapter 2. In this method, the ionic-cross linking of the PAH chains with multivalent counter anions dipotassium hydrogen phosphate to form spherical polymer aggregates is the key step for the formation of microcapsule structure. However, in this case 14 nm ZnO particles and no curcumin were added. Because of their net positive charge these aggregates afterwards facilitate the assembly of ZnO nanoparticles to form an ordered microcapsule structure in which the shell wall acquires a composite structure consisting of positively charged PAH chains entangled with the ZnO nanoparticles (as shown in **Figure 5.1**). The SEM

images illustrating spherical morphology of the microcapsules with sizes of 200 – 500 nm is shown in **Figure 5.2**. The particle size distribution was analyzed using DLS and it was found that the capsules have an effective hydrodynamic radius of 170 nm.

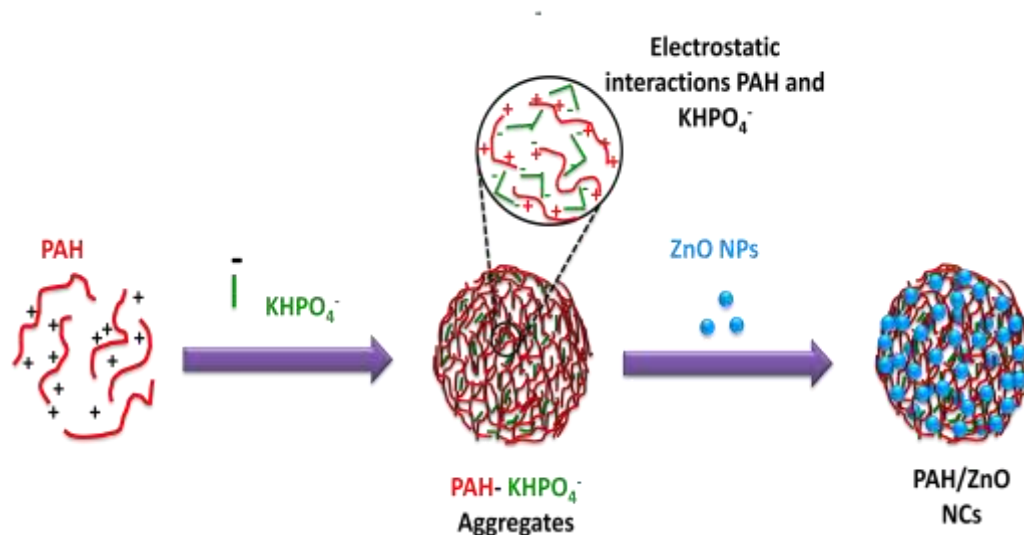


Figure 5.1. Illustration of PAH/dipotassium phosphate aggregated interacting with ZnO NPs to form NCs.

The absorption spectrum of ZnO NPs in this study is shown in **Figure 5.3**. It shows a maximum at around 266 nm and another band at around 330 nm. The photoluminescence spectra of ZnO NPs at excitation wavelength 280 nm and 320 nm are shown in **Figure 5.5**. It is clear that the photoluminescence spectra of ZnO nanoparticles do not change with excitation wavelength, and the emission maximum was observed at around 377 nm and a small band around 360 nm. The emission in 360 - 377 nm could be due to exciton emission of ZnO reported in literature [192] because the ZnO band gap is 3.37 eV at room temperature. Surface state is the main factor which determines ZnO visible luminescence; as ZnO visible emission arises from its defects or vacancies that are located mainly on the nanoparticle surface.

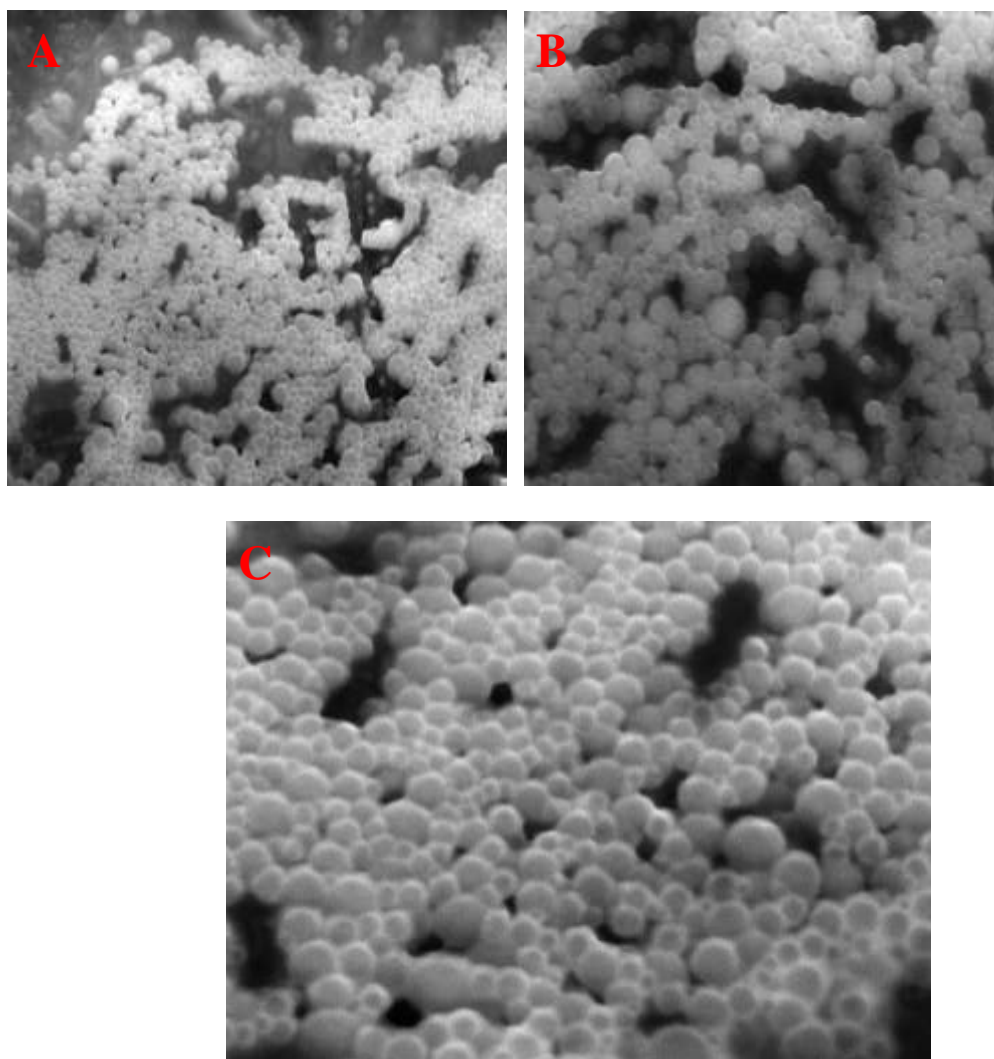


Figure 5.2. (A-B-C) SEM images of ZnO congregated capsules. (A) 5 μm resolution; (B) 2 μm resolution; (C) 1 μm resolution.

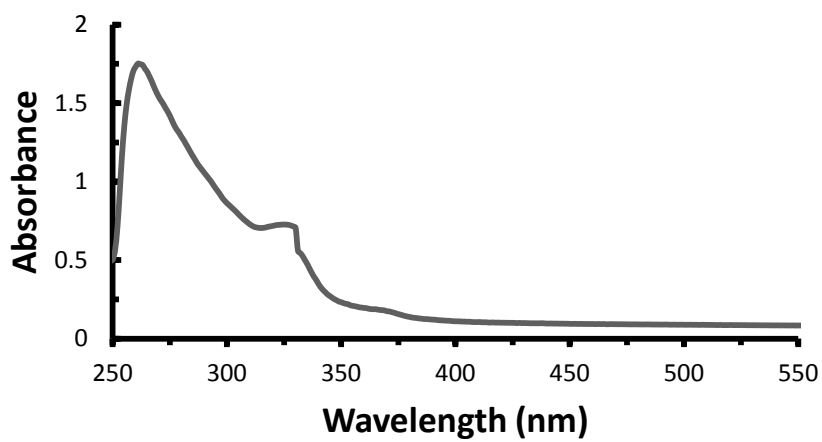


Figure 5.3. Absorption spectrum of 14 nm ZnO nanoparticles

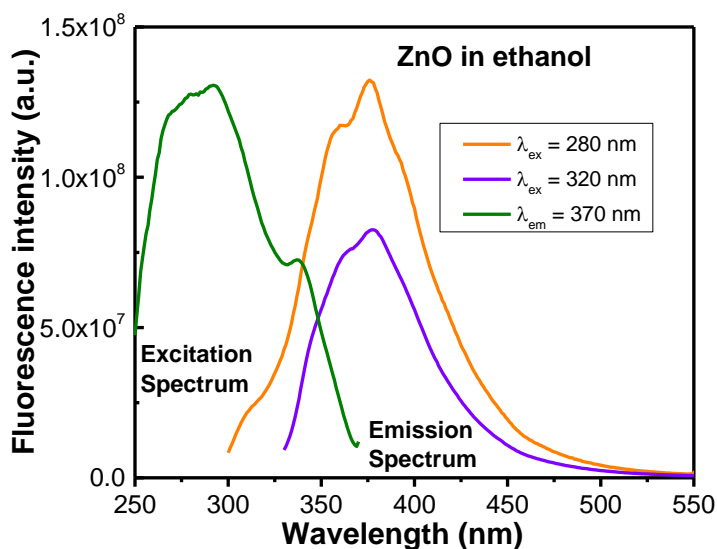


Figure 5.4. Fluorescence (or photoluminescence) excitation and emission spectra of 14 nm ZnO nanoparticles in ethanol.

In the present case, ZnO NPs are highly crystallized, which means there are almost no amorphous phases on the ZnO surfaces, therefore, the photoluminescence is only due to exciton emission. The excitation spectrum of ZnO at emission wavelength 370 nm in solution was found to be similar to absorption spectrum. The normalized fluorescence spectra of ZnO capsules have been compared with ZnO in water and ethanol at excitation wavelength 280 nm (see **Figure 5.5**).

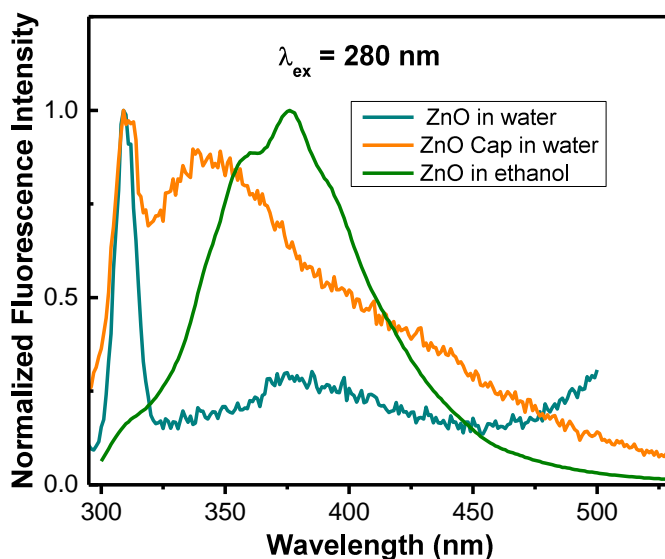


Figure 5.5. Photoluminescence spectra of ZnO capsules at excitation wavelength 280 nm.

It was found that the fluorescence intensity of ZnO in double distilled water was much weaker than in ethanol which is due to poor solubility of ZnO in aqueous environment. A sharp exciton emission of ZnO NPs was observed in ZnO capsules; earlier such increase in exciton emission for ZnO nanostructures has been linked with physical adsorption [193]. It is known that addition of water causes ZnO precipitation and quenches its photoluminescence by destroying luminescence centers [194]. The peak at around 310 nm, which is due to exciton emission band of ZnO, was different from that observed in ethanol. It is known in the literature that surface defects increases the exciton emission, ZnO capsules have higher surface defect compared to ZnO in ethanol. The enhancement in exciton emission has also been linked with increase in crystallinity, and *Chang et al.* have found that polyaniline modification could enhance the UV emission of ZnO nanostructures [195]. Thus, the present capsules control the ZnO crystallization and morphology.

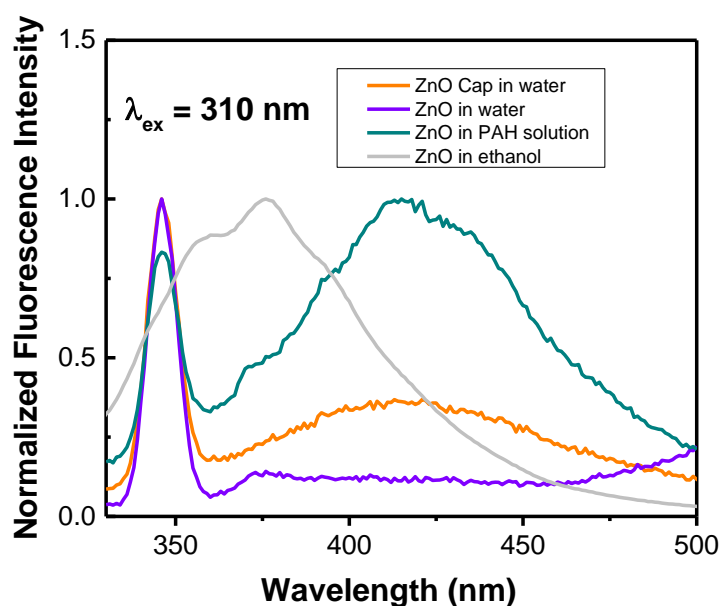


Figure 5.6. Photoluminescence spectra of ZnO capsules at excitation wavelength 310 nm.

Though the main emission maximum at around 377 nm of ZnO NPs did not change both in water and ethanol, a large blue shift of about 37 nm was observed for ZnO capsules. This shift in emission maximum is explained subsequently because the photoluminescence of ZnO in polymer matrix is complex and can be better understood at excitation wavelength 310 nm (at the tail of the band [194]). Interestingly, when we excited at 310 nm, we observed a different emission pattern for ZnO capsules. It should be noted that the emission maximum of ZnO NPs remained the same irrespective of excitation wavelengths (280 nm or 310 nm). On the other hand, the emission maximum shifted to around 420 nm for ZnO capsules as shown in **Figure 5.6**. The excitation wavelength dependence of the photoluminescence shift of ZnO capsules was about 80 nm. This kind of excitation wavelength dependence photoluminescence properties violates Kasha's rule of excitation wavelength independence of the emission spectrum.

Nevertheless, such excitation dependency of emission behaviour of ZnO colloid for different capping agent has been reported. Irimpan *et al.* have shown and explained this phenomenon in terms of existence of a distribution of energetically different molecules in the ground state coupled with a low rate of excited state relaxation process [196]. Such relaxation process includes solvation and energy transfer for excitation dependent photoluminescence behaviour of ZnO capsules. This visible emission is expected for ZnO capsules due to the defects or vacancies that are located mainly on the nanoparticle surfaces during the interaction between PAH and ZnO in the capsules. The red shift in photoluminescence spectra has also been reported for ZnO nanoparticle aggregates [197, 198]. In ZnO capsules, obviously, congregation of ZnO NPs is expected (as explained in the synthesis procedure). But it is also known that ZnO nanoparticle aggregation decreased the photoluminescence intensity along with a red shift in the spectra [197]. To prove that there is a decrease in photoluminescence, the photoluminescence of ZnO capsules was compared with that of ZnO in PAH solution (without making any capsules) and we found that no major change in spectral position was observed. However, the relative photoluminescence intensity of ZnO NPs in the visible region (at 420 nm), as compared to UV exciton emission, has increased in PAH solution. It is expected that PAH will cause defects or vacancies on the nanoparticle surface, so it is normal that ZnO NPs and ZnO capsules could have similar emission maximum as depicted in **Figure 5.5**. However, congregation of ZnO NPs are not expected in PAH solution, thus, the relative photoluminescence quenching in ZnO capsules could be referred to aggregation of ZnO NPs during capsule formation.

pH plays a crucial role in fluorescence applications and alters the fluorescence properties. The influence of pH on emission properties of ZnO capsules as synthesized

was studied in the pH range 5.8 – 8 using phosphate buffer. In this study, we have selected the physiological pH range because we are interested in utilizing such capsules for biological applications later on. The photoluminescence spectra of ZnO capsules in different pH conditions are shown in **Figure 5.7**. There is no appreciable change in spectral position, however, the photoluminescence intensity varied with the pH of the solution. The variation was not systematic; therefore, we chose to work in the double distilled water, close to neutral pH conditions for further studies.

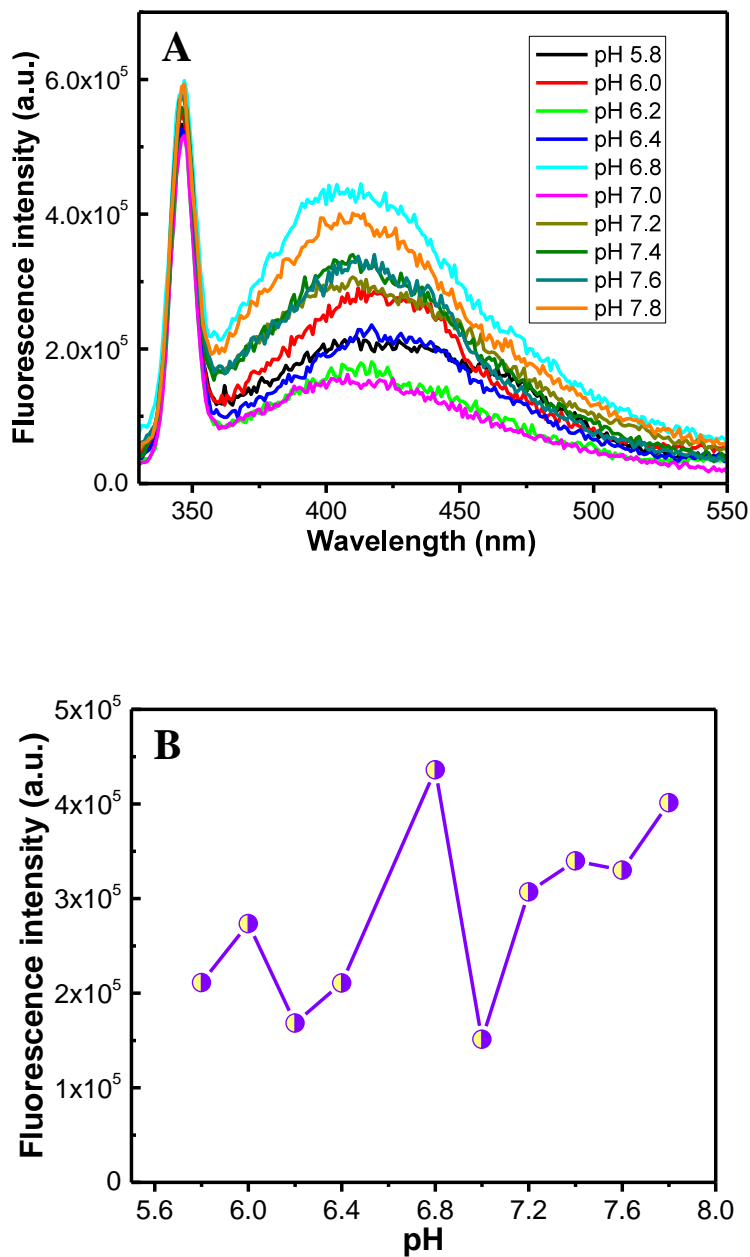


Figure 5.7. (A) Photoluminescence spectra of ZnO capsules in different pH (phosphate buffer) solution at excitation wavelength 310 nm. (B) Relative change in fluorescence intensity with pH.

In summary, PAH/dipotassium phosphate aggregates assemble silica nanoparticles to form spherical NCs. The hydrodynamic radius of the capsules is equal to 170nm. The fluorescence emission of ZnO in the capsule is modified where it emits

in the visible region (peak at 460 nm). The visible emission of ZnO is explained by the modification of its surface.

CHAPTER VI

CONCLUSION

In summary, CU in the presence of PAH and dipotassium phosphate directly assembles silica nanoparticles to form NCs in the size range of 100 to 1000 nm. The size of the NCs could be tailored by varying the salt concentration as the plot of the effective hydrodynamic radius with various salt concentrations has showed an excellent linear fit. CU is distributed all over the capsule whereas silica nanoparticles are more concentrated at the peripheries. CU and PAH have strong interaction with a binding constant $K=1.44 \times 10^4 \text{ M}^{-1}$. The synthesized nanocapsules are of negative surface charge and the NCs of the largest size have the highest percentage of curcumin ~ 7%, while the smaller sized NCs have ~ 4%. CU is in its enol form in the capsule. The delivery of curcumin is found to be favoured in basic environment where maximum release has been recorded as compared to acidic and neutral conditions. In addition, the drug release profile of curcumin follows Higuchi model and depends on the size of the capsule. The DPPH scavenging activity of curcumin decreases when it is encapsulated. As well, the scavenging activity decreases exponentially with the size of the nanocapsules. This reduction in both cases is attributed to the percentage by weight of CU in the capsule as well as to the availability of the β -diketone group of CU for H-donation. The encapsulation of curcumin in such capsules opens up the ability to use such synthesis approach for encapsulating various drug molecules with different formulations and materials. Furthermore, its bioavailability and biocompatibility can be tested for the aid of in vivo drug delivery.

The nanocapsules alter the optical behaviour of CU this is translated as new emission peak at 460 nm when exciting at 355 nm. This peak is due to the fluorescence of normal form of CU rather than ESIHT form. The ESIHT is inhibited due to the interaction of the N⁺ of PAH with the O-atoms of enol form of CU. Revoking the ESIHT process of CU inside the NCs opens up a new emitting deactivation path way that have never been observed in water. Thus, applying nanotechnology optical behaviour could be tuned by tailor made capsules for multiple applications in electronics, sensing and biomedical uses. At the same time ESIHT in such system may help in understanding key fundamental questions of various-H atom transfer path ways of medicinally important and water insoluble drug molecules like CU while using various capsules as drug delivery vehicles.

The self assembly method is applied to synthesize Poly A/ silica nanoparticles/CU nanocapsules. The particles are spherical with various sizes ranging between 200 and 600 nm. These capsules are selective to guanine, where the fluorescence of the capsule is enhanced by 500% when it's present. Life time measurements along with FT IR spectra suggest that the sensitivity of the capsules to guanine is referred to hydrophobic interactions rather than specific base pairing. This is further supported by the relatively low solubility of guanine in water compared to the other nucleobases. The association constant of guanine and Poly A capsule is $K=5.50 \times 10^2 \text{ M}^{-1}$. The degradation study of the capsule proves its stability (28% degradation after 50 hours). Further, we are looking to know more about the composition of our capsule using TGA; as well more studies can be done to test its sensitivity with other nucleosides.

This study opens up a new method, based on steady-state fluorescence, for nucleobases sensing. The importance of such method is its simplicity and robustness. In addition, it is possible to modify various poly-amines with other nucleobases and prepare new capsules formulation for nucleobases and DNA sensing applications.

The interaction of ZnO nanoparticles with PAH/dipotassium phosphate aggregates produces similar spherical nanocapsules of 170 nm effective hydrodynamic radius. ZnO is known to be a UV emitter. However the fluorescence emission of ZnO in the NC is modified where a new peak at 420 nm has been resolved. The visible emission of ZnO is referred to its surface modification, i.e. increase in the number of oxygen and zinc vacancies. To understand more the surface modifications and the crystalline structure of ZnO within the capsule we are looking forward to characterize our sample using X-Ray Diffraction technique. Moreover, to know the position and morphology of ZnO in the capsule we are interested in performing TEM.

This study opens up a new and easy method to modify the optical and surface properties of ZnO and other metal oxides for multiple applications in electronics and sensing fields.

REFERENCES

- [1] J. M. Lehn, Perspectives in Supramolecular Chemistry –From Molecular Recognition Towards Molecular Information Processing and Self-Organization. *Angewandte Chemie-International Edition*, 29 (1990)1304–1319.
- [2] H. Cölfen, S. Mann, Higher-Order Organization by Mesoscale Self-Assembly and Transformation of Hybrid Nanostructures. *Angew. Chem. Int. Ed.*, 42 (2003) 2350–2365.
- [3] C. Gröge, K. Lutz, E. Brunner, Biomolecular Self-Assembly and its Relevance in Silica Biomineralization, *Cell biochemistry and biophysics*, 50 (2008) 23-39.
- [4] F. J. Jr. Padden, H. D. Keith, Crystalline Morphology of Synthetic Peptides, *Journal of Applied Physics*, 36 (1965) 2987–2995.
- [5] F. J. Padden, H. D. Keith, G. Giannoni, Single Crystals of Poly-L-lysine, *Biopolymer*, 7 (1969) 793-804.
- [6] R. K. Rana, V. S. Murthy, J. Yu, M. S. Wong, Nanoparticle Self-Assembly of Hierarchically Ordered Microcapsule Structures, *Advanced Materials*, 17 (2005) 1145-1150.
- [7] A. K. Boal, F. Ilhan, J. E. DeRouchey, T. Thurn-Albrecht, T. P. Russell, V. M. Rotello, Self-assembly of Nanoparticles into Structured Spherical and Network Aggregates, *Nature*, 404 (2000) 746-748.
- [8] D. Patra, F. Sleem, A new method for pH triggered curcumin release by applying poly (l-lysine) mediated nanoparticle-congregation. *Analytica chimica acta*, 795 (2013) 60-68.
- [9] A. J. Amali, P. Saravanan, R. K. Rana, Tailored anisotropic magnetic chain structures hierarchically assembled from magnetoresponsive and fluorescent components, *Angewandte Chemie International Edition*, 50 (2011) 1318-1321.
- [10] M. S. Wong, J. N. Cha, S. K. Choi, T. G. Deming, G. D. Stucky, Assembly of nanoparticles into hollow spheres using block copolypeptides, *Nano Letters*, 2(2002) 583-587.
- [11] B. Ozbas, J. Kretsinger, K. Rajagopal, J. P. Schneider, D. J. Pochan, Salt-triggered peptide folding and consequent self-assembly into hydrogels with tunable modulus, *Macromolecules*, 37(2004) 7331-7337.
- [12] J.R. Lakowicz, Principles of Fluorescence Spectroscopy, third edition ed., Springer, 2006.

- [13] S. Sugden, H. Wilkins, CLXVII.-The parachor and chemical constitution. Part XII. Fused metals and salts, *Journal of the Chemical Society (Resumed)*, (1929) 1291-1298.
- [14] S. Udenfriend, Development of the spectrophotofluorometer and its commercialization, *Protein Science*, 4 (1995) 542-551.
- [15] A. Jablonski, Uber den mechanisms des photolumineszenz von farbstoffphosphoren, *Z Phys*, 94 (1935) 38-46.
- [16] M. Kasha, Characterization of electronic transitions in complex molecules, *Discussions of the Faraday Society*, 9 (1950) 14-19.
- [17] W. Zhong, Nanomaterials in fluorescence-based biosensing. *Analytical and bioanalytical chemistry*, 394(2009) 47-59.
- [18] J. M. Klostranec, W. C. W. Chan, Quantum Dots in Biological and Biomedical Research: Recent Progress and Present Challenges. *Adv. Mater.*, 18 (2006) 1953-1964.
- [19] A. M. Smith, S. Nie, Chemical analysis and cellular imaging with quantum dots, *Analyst*, 129 (2004) 672-677.
- [20] G. Ruan, A. Agrawal, A. M. Smith, X. Gao, & S. Nie, Quantum dots as fluorescent labels for molecular and cellular imaging, In *Reviews in Fluorescence 2006*. Springer US. (2006) 181-193.
- [21] X. Gao, L. Yang, J. A. Petros, F. F. Marshall, J. W. Simons, S. Nie. In vivo molecular and cellular imaging with quantum dots. *Curr. Opin. Biotechnol.* 16 (2005) 63-72.
- [22] R. Bakalova, Z. Zhelev, H. Ohba, Y. Baba, Quantum dot-based western blot technology for ultrasensitive detection of tracer proteins. *Journal of the American Chemical Society*, 127 (2005) 9328-9329.
- [23] R. L. Ornberg, T. F. Harper, H. Liu, Western blot analysis with quantum dot fluorescence technology: a sensitive and quantitative method for multiplexed proteomics, *Nature Methods*, 2(2005) 79-81.
- [24] R. Edgar, M. McKinstry, J. Hwang, et al, High-sensitivity bacterial detection using biotin-tagged phage and quantum-dot nanocomplexes, *Proc. Natl. Acad. Sci. USA*, 103 (2006) 4841-4845.
- [25] E. Genin, O. Carion, B. Mahler, B. Dubertret, N. Arhel, P. Charneau, C. Mioskowski, CrAsH- quantum dot nanohybrids for smart targeting of proteins, *Journal of the American Chemical Society*, 130(2008) 8596-8597.
- [26] P. Chan, T. Yuen, F. Ruf, J. Gonzalez-Maeso, S. C. Sealfon, Method for multiplex cellular detection of mRNAs using quantum dot fluorescent in situ hybridization, *Nucleic acids research*, 33(2005) e161-e161.

- [27] J. E. Smith, L. Wang, W. Tan, Bioconjugated silica-coated nanoparticles for bioseparation and bioanalysis. *Trac Trends in Analytical Chemistry*, 25(2006) 848-855.
- [28] M. Qhobosheane, S. Santra, P. Zhang, W. Tan, Biochemically functionalized silica nanoparticles, *Analyst*, 126 (2001) 1274-1278.
- [29] G. Yao, L. Wang, Y. Wu, J. Smith, J. Xu, W. Zhao, W. Tan, FloDots: luminescent nanoparticles, *Analytical and bioanalytical chemistry*, 385 (2006) 518-524.
- [30] E. K. Sapsford, L. Berti, I. L. Medintz, Materials for Fluorescence Resonance Energy Transfer Analysis: Beyond Traditional Donor–Acceptor Combinations, *Angew. Chem. Int. Ed.*, 45(2006) 4562–4589.
- [31] N. Zhang, Y. Liu, L. Tong, K. Xu, L. Zhuo, B. Tang, A novel assembly of Au NPs– β -CDs–FL for the fluorescent probing of cholesterol and its application in blood serum, *Analyst*, 133(2008) 1176-1181.
- [33] D. Cui, B. Pan, H. Zhang, F. Gao, R. Wu, J. Wang, T. Asahi, Self-assembly of quantum dots and carbon nanotubes for ultrasensitive DNA and antigen detection, *Analytical chemistry*, 80 (2008) 7996-8001.
- [34] B. F. Pan, D. X. Cui, C. S. Ozkan, M. Ozkan, P. Xu, T. Huang, T. F. Liu, H. Chen, Q. Li, R. He, F. Gao, Effects of carbon nanotubes on photo-luminescence properties of quantum dots. *J. Phys. Chem.*, 112 (2008) 939-944.
- [35] R. Yang, Z. Tang, J. Yan, H. Kang, Y. Kim, Z. Zhu, W. Tan, Noncovalent assembly of carbon nanotubes and single-stranded DNA: an effective sensing platform for probing biomolecular interactions, *Analytical Chemistry*, 80 (2008)7408-7413.
- [36] W. Meier, Polymer nanocapsules. *Chemical Society Reviews*, 29 (200) 295-303.
- [37] C. E. Mora-Huertas, H. Fessi, & A. Elaissari, Polymer-based nanocapsules for drug delivery, *International Journal of Pharmaceutics*, 385(2010) 113-142.
- [38] H. G. Bagaria, & M. S. Wong, Polyamine–salt aggregate assembly of capsules as responsive drug delivery vehicles, *Journal of Materials Chemistry*, 21(2011) 9454-9466.
- [39] M. A. Yaseen, J. Yu, B. Anvari, & M. S. Wong, Stability assessment of indocyanine green within dextran-coated mesocapsules by absorbance spectroscopy. *Journal of biomedical optics*, 12(2007) 64031-64031.
- [40] V. P. Torchilin, Recent advances with liposomes as pharmaceutical carriers, *Nature reviews Drug discovery*, 4 (2005) 145-160.
- [41] S. L. Huang, Liposomes in ultrasonic drug and gene delivery. *Advanced drug delivery reviews*, 60(2008) 1167-1176.

- [42] D. E. Discher, & F. Ahmed, Polymersomes, *Annu. Rev. Biomed. Eng.*,8 (2006) 323-341.
- [43] F. Caruso, R. A. Caruso, & H. Möhwald, Nanoengineering of inorganic and hybrid hollow spheres by colloidal templating. *Science*, 282(1998) 1111-1114.
- [44] V. Percec, D. A. Wilson, P. Leowanawat, C. J. Wilson, A. D. Hughes, M. S. Kaucher, & J. Ropponen, Self-assembly of Janus dendrimers into uniform dendrimersomes and other complex architectures, *Science*, 328 (2010) 1009-1014.
- [45] J. Liu, F. Liu, K. Gao, J. Wu, & D. Xue, Recent developments in the chemical synthesis of inorganic porous capsules, *Journal of Materials Chemistry*, 19 (2009) 6073-6084.
- [46] R. K. Iler, Multilayers of colloidal particles. *Journal of Colloid and Interface Science*, 21(1966) 569-594.
- [47]X. Liu, J. Zhang, & D. M. Lynn, Ultrathin multilayered films that promote the release of two DNA constructs with separate and distinct release profiles, *Advanced Materials*, 20 (2008) 4148-4153.
- [48] G. H. J. D. Decher, J. D. Hong, & J. Schmitt, Buildup of ultrathin multilayer films by a self-assembly process: III. Consecutively alternating adsorption of anionic and cationic polyelectrolytes on charged surfaces, *Thin solid films*, 210 (1992) 831-835.
- [49] N. A. Kotov, I. Dekany, & J. H. Fendler, Layer-by-layer self-assembly of polyelectrolyte-semiconductor nanoparticle composite films, *The Journal of Physical Chemistry*, 99 (1995) 13065-13069.
- [50] Y. Lvov, K. Ariga, & T. Kunitake, Layer-by-layer assembly of alternate protein/polyion ultrathin films, *Chemistry letters*, 1994(1994) 2323-2326.
- [51] Y. Lvov, G. Decher, & G. Sukhorukov, Assembly of thin films by means of successive deposition of alternate layers of DNA and poly (allylamine), *Macromolecules*, 26(1993) 5396-5399.
- [52] Y. Lvov, H. Haas, G. Decher, H. Moehwald, A. Mikhailov, B. Mtchedlishvily,... & B. Vainshtein, Successive deposition of alternate layers of polyelectrolytes and a charged virus, *Langmuir*, 10(1994) 4232-4236.
- [53] A. L. Becker, A. P. Johnston, & F. Caruso, Layer-By-Layer-Assembled Capsules and Films for Therapeutic Delivery, *Small*, 6 (2010).
- [54] Z. Liang, A. Susa, & F. Caruso, Gold nanoparticle-based core-shell and hollow spheres and ordered assemblies thereof, *Chemistry of materials*,15 (2003) 3176-3183.

- [55] F. S. X. Y. Caruso, X. Shi, R. A. Caruso, & A. Susa, Hollow titania spheres from layered precursor deposition on sacrificial colloidal core particles, *Advanced Materials*, 13(2001) 740-744.
- [56] C. J. Martinez, B. Hockey, C. B. Montgomery, & S. Semancik, Porous tin oxide nanostructured microspheres for sensor applications, *Langmuir*, 21(2005) 7937-7944.
- [57] F. Caruso, M. Spasova, A. Susa, M. Giersig, & R. A. Caruso, Magnetic nanocomposite particles and hollow spheres constructed by a sequential layering approach, *Chemistry of Materials*, 13(2001), 109-116.
- [58] L. Li, R. Ma, N. Iyi, Y. Ebina, K. Takada, & T. Sasaki, Hollow nanoshell of layered double hydroxide. *Chemical Communications*, 29(2006) 3125-3127.
- [59] W. Eerenstein, N. D. Mathur, & J. F. Scott, Multiferroic and magnetoelectric materials. *Nature*, 442(2006) 759-765.
- [60] P. Wang, D. Chen, & F. Q Tang, Preparation of titania-coated polystyrene particles in mixed solvents by ammonia catalysis, *Langmuir*, 22(2006) 4832-4835.
- [61] Kim, J., Kim, H. S., Lee, N., Kim, T., Kim, H., Yu, T., ... & Hyeon, T. (2008). Multifunctional uniform nanoparticles composed of a magnetite nanocrystal core and a mesoporous silica shell for magnetic resonance and fluorescence imaging and for drug delivery. *Angewandte Chemie International Edition*, 47(44), 8438-8441.
- [62] Z. Z. Yang, Z. W. Niu, Y. F. Lu, Z. B. Hu and C. C. Han, Templated Synthesis of Inorganic Hollow Spheres with a Tunable Cavity Size onto Core-Shell Gel Particle, *Angew. Chem., Int. Ed.*, 42 (2003) 1943.
- [63] F. Swol, Light-driven synthesis of hollow platinum nanospheres, *Chemical Communications*, 22 (2008) 2535-2537.
- [64] R. Yang, H. Li, X. Qiu, & L. Chen, A spontaneous combustion reaction for synthesizing Pt hollow capsules using colloidal carbon spheres as templates, *Chemistry-A European Journal*, 12(2006) 4083-4090.
- [65] D. Jagadeesan, U. Mansoori, P. Mandal, A. Sundaresan and M. Eswaramoorthy, Hollow Spheres to Nanocups: Tuning the Morphology and Magnetic Properties of Single-Crystalline α -Fe₂O₃ Nanostructures. *Angew. Chem., Int. Ed.*, 47 (2008) 7685.
- [66] M. Ohnishi, Y. Kozuka, Q. L. Ye, H. Yoshikawa, K. Awage, R. Matsuno, M. Kobayashi, A. Takahara, T. Yokoyama, S. Bandow and S. Iijima, Phase selective preparations and surface modifications of spherical hollow nanomagnets. *J. Mater. Chem.*, 16 (2006) 3215.
- [67] M. Ma Y., Y. J. Zhu, L. Li, & S. W. Cao, Nanostructured porous hollow ellipsoidal capsules of hydroxyapatite and calcium silicate: preparation and application in drug delivery' *Journal of Materials Chemistry*, 18(2008) 2722-2727.

- [68] J. H. Fendler, Atomic and molecular clusters in membrane mimetic chemistry, *Chemical Reviews*, 87(1987), 877-899.
- [69] D. H. Buchold, & C. Feldmann, Nanoscale γ -AlO (OH) hollow spheres: synthesis and container-type functionality, *Nano letters*, 7(2007) 3489-3492.
- [70] Z. G. Feng, Y. S. Li, D. C. Niu, L. Li, W. R. Zhao, H. R. Chen, L. Li, J. H. Gao, M. L. Ruan and J. L. Shi, A facile route to hollow nanospheres of mesoporous silica with tunable size, *Chem. Commun.*, 2008, 2629.
- [71] H. C. Zeng, Synthetic architecture of interior space for inorganic nanostructures, *Journal of Materials Chemistry*, 16(2006) 649-662.
- [72] G. C. Kini., S. L. Biswal, & M. S. Wong, Non-Layer-by-Layer Assembly and Encapsulation Uses of Nanoparticle-Shelled Hollow Spheres, In *Modern Techniques for Nano-and Microreactors/-reactions*, Springer Berlin Heidelberg, (2010) 89-114
- [73] V. S. Murthy, R. K. Rana, & M. S. Wong, Nanoparticle-assembled capsule synthesis: Formation of colloidal polyamine-salt intermediates, *The Journal of Physical Chemistry B*, 110(2006) 25619-25627.
- [74] G. C. Kini, J. Lai, M. S. Wong, & S. L. Biswal, Microfluidic Formation of Ionically Cross-Linked Polyamine Gels, *Langmuir*, 26(2010) 6650-6656.
- [75] J. Yu, V. S. Murthy, R. K. Rana, & M. S. Wong, Synthesis of nanoparticle-assembled tin oxide/polymer microcapsules, *Chemical communications*, 10(2006) 1097-1099.
- [76] H. G. Bagaria, M. R. Dean, C. A. Nichol, & M. S. Wong, Self-Assembly and Nanotechnology: Real-Time, Hands-On, and Safe Experiments for K-12 Students, *Journal of Chemical Education*, 88(2011) 609-614.
- [77] J. Yu, D. Javier, M. A. Yaseen., N. Nitin, R. Richards-Kortum, B. Anvari, & M. S. Wong, Self-assembly synthesis, tumor cell targeting, and photothermal capabilities of antibody-coated indocyanine green nanocapsules, *Journal of the American Chemical Society*, 132(2010) 1929-1938.
- [78] J. Yu, M. A. Yaseen, B. Anvari, & M. S. Wong, Synthesis of near-infrared-absorbing nanoparticle-assembled capsules, *Chemistry of materials*, 19(2007) 1277-1284.
- [79] N. Zhao, H. G. Bagaria, M. S. Wong, & Y. Zu, A nanocomplex that is both tumor cell-selective and cancer gene-specific for anaplastic large cell lymphoma, *Journal of nanobiotechnology*, 9(2011).
- [80] S. E. Plush, M. Woods, Y. F. Zhou, S. B. Kadali, M. S. Wong, & A. D. Sherry, Nanoassembled capsules as delivery vehicles for large payloads of high relaxivity Gd^{3+} agents, *Journal of the American Chemical Society*, 131(2009) 15918-15923.

- [81] M. Goldberg, R. Langer, & X. Jia, Nanostructured materials for applications in drug delivery and tissue engineering, *Journal of Biomaterials Science, Polymer Edition*, 18(2007) 241-268.
- [82] O. Kayser, A. Lemke, & N. Hernandez-Trejo, The impact of nanobiotechnology on the development of new drug delivery systems, *Current pharmaceutical biotechnology*, 6(2005) 3-5.
- [83] D. G. Anderson, J. A. Burdick, & R. Langer, Smart biomaterials, *Science*, 305(2004), 1923-1924.
- [84] D. A. Lavan, T. McGuire, & R. Langer, Small-scale systems for in vivo drug delivery, *Nature biotechnology*, 21(2003) 1184-1191.
- [85] L. Y. Qiu, & Y. H. Bae, Polymer architecture and drug delivery. *Pharmaceutical research*, 23(2006) 1-30.
- [86] S. Svenson and D. A. Tomalia, Dendrimers in biomedical applications—reflections on the field. *Adv. Drug Deliv. Rev.* **57**, 2106 (2005).
- [87] B. E. Rabinow, Nanosuspensions in drug delivery. *Nature Reviews Drug Discovery*, 3(2004) 785-796.
- [88] O. Ishida, K. Maruyama, K. Sasaki, & M. Iwatsuru, Size-dependent extravasation and interstitial localization of polyethyleneglycol liposomes in solid tumor-bearing mice, *International journal of pharmaceutics*, 190(1999) 49-56.
- [89] G. Kong, R. D. Braun, & M. W Dewhirst. Hyperthermia enables tumor-specific nanoparticle delivery: effect of particle size, *Cancer research*, 60(2000) 4440-4445.
- [90] K. I. Ogawara, M. Yoshida, K. Furumoto, Y. Takakura, M. Hashida, K. Higaki, & T. Kimura, Uptake by hepatocytes and biliary excretion of intravenously administered polystyrene microspheres in rats, *Journal of drug targeting*, 7(1999) 213-221.
- [91] E. Katz, & I. Willner, Integrated nanoparticle–biomolecule hybrid systems: synthesis, properties, and applications, *Angewandte Chemie International Edition*, 43(2004), 6042-6108.
- [92] T. M. Allen, Ligand-targeted therapeutics in anticancer therapy, *Nature Reviews Cancer*, 2(2002) 750-763.
- [93] J. Panyam, & V. Labhasetwar, Biodegradable nanoparticles for drug and gene delivery to cells and tissue, *Advanced drug delivery reviews*, 55(2003) 329-347.
- [94] C. Mayer, Nanocapsules as drug delivery systems. *Int. J. Artif. Organs* **28**, 1163 (2005).

- [95] K. N. Burger, R. W. Staffhorst, H. C. de Vrijlder, M. J. Velinova, P. H. Bomans, P. M. Frederik, & B. de Kruijff, Nanocapsules: lipid-coated aggregates of cisplatin with high cytotoxicity, *Nature medicine*, 8(2002) 81-84.
- [96] H. Ai, J. J. Pink, X. Shuai, D. A. Boothman, & J. Gao, Interactions between self-assembled polyelectrolyte shells and tumor cells, *Journal of Biomedical Materials Research Part A*, 73(2005) 303-312.
- [97] S. A. Sukhishvili, & S. Granick, Layered, erasable polymer multilayers formed by hydrogen-bonded sequential self-assembly. *Macromolecules*, 35(2002) 301-310.
- [98] L. Dähne, S. Loporatti, E. Donath, & H. Möhwald, Fabrication of micro reaction cages with tailored properties. *Journal of the American Chemical Society*, 123(2001) 5431-5436.
- [99] O. P. Tiourina, A. A. Antipov, G. B Sukhorukov., N. I Larionova., Y. Lvov, & H. Möhwald, Entrapment of α -Chymotrypsin into Hollow Polyelectrolyte Microcapsules. *Macromolecular Bioscience*, 1(2001) 209-214.
- [100] V. A. Kickhoefer, Y. Garcia, Y. Mikiyas, E. Johansson, J. C. Zhou, S. Raval-Fernandes, ... & L. H. Rome, Engineering of vault nanocapsules with enzymatic and fluorescent properties, *Proceedings of the National Academy of Sciences of the United States of America*, 102(2005) 4348-4352.
- [101] D. T. Haynie, N. Palath, Y. Liu, B. Li, & N. Pargaonkar, Biomimetic nanostructured materials: inherent reversible stabilization of polypeptide microcapsules, *Langmuir*, 21(2005) 1136-1138.
- [102] A. N. Zelikin, J. F. Quinn, & F. Caruso, Disulfide cross-linked polymer capsules: en route to biodeconstructible systems, *Biomacromolecules*, 7(2006) 27-30.
- [103] A. JoseáAmali, & R. KumaráRana, Poly (L-Lysine)–pyranine-3 coacervate mediated nanoparticle-assembly: fabrication of dynamic pH-responsive containers. *Chemical Communications*, 48(2012) 856-858.
- [104] D. Patra, & F. Sleem, Acridine orange and silica nanoparticles facilitated novel robust fluorescent hollow microcapsules toward DNA bio-sensor, *Colloids and Surfaces A: Physicochemical and Engineering Aspects*, 443 (2014) 320-325.
- [105] L. Nardo, A. Andreoni, M. Bondani, M. Másson, & H. Hjorth Tønnesen, Studies on curcumin and curcuminoids. XXXIV. Photophysical properties of a symmetrical, non-substituted curcumin analogue, *Journal of Photochemistry and Photobiology B: Biology*, 97(2009) 77-86.
- [106] S. Shishodia, M. M. Chaturvedi, & B. B. Aggarwal, Role of curcumin in cancer therapy, *Current problems in cancer*, 31(2007) 243-305.
- [107] K. Balasubramanian, Molecular orbital basis for yellow curry spice curcumin's prevention of Alzheimer's disease, *J. Agric. Food Chem.* 54 (2006) 3512–3520.

- [108] C.F. Chignell, P. Bilski, K.J. Reszka, A.G. Motton, R.H. Sik, T.A. Dahl, Spectral and photochemical properties of curcumin, *Photochem. Photobiol.* 59 (1994) 295–302.
- [109] R.N. Chopra, I.C. Chopra, K.L. Honada, L.D. Kapur, *Indigenous Drugs of India*, second ed., Duhr, Calcutta, 1958.
- [110] A. Krishnamoorthy, *The Wealth of India: A Dictionary of Indian Raw Materials and Industrial Products*, CSIR, New Delhi, 2 (1950) 402.
- [111] J.T. Mague, W.L. Alworth, F.L. Payton, Curcumin and derivatives, *Acta Cryst. C* 60 (2004) 608–610.
- [112] A. Khafif, S.P. Schantz, T.C. Chou, D. Edelstein, P.G. Sacks, Quantification of chemopreventive synergism between (-)-epigallocatechin-3-gallate and curcumin in normal, premalignant and malignant human oral epithelial cells, *Carcinogenesis* 19 (1998) 419–424.
- [113] M.T. Huang, R.C. Smart, C.Q. Wong, A.H. Conney, Inhibitory effect of curcumin chlorogenic acid, caffeic acid, and ferulic acid, on tumor promotion in mouse skin by 12-O-tetradecanoylphorbol-13-acetate, *Cancer Res.*, 48 (1988) 5941–5946.
- [114] J. Woo, Y. Kim, Y. Choi, D. Kim, K. Lee, J.H. Bae, D.S. Chang, Y.J. Jeong, Y.H. Lee, J. Park, T.K. Kwon, Molecular mechanisms of curcumin-induced cyclotoxicity: induction of apoptosis through generation of reactive oxygen species, downregulation of Bcl-XL and IAP, the release of cytochrome c and inhibition of Akt, *Carcinogenesis* 24 (2003) 1199–1208.
- [115] M.J. Van Erk, E. Teuling, Y.C.M. Staal, S. Huybers, P.J. van Bladeren, J.M.M.J.G. Aarts, B. van Ommen, Time- and dose-dependent effects of curcumin on gene expression in human colon cancer cells, *J. Carcinogen.* 3 (2004) 1–17.
- [116] R.C. Srimal, B.N. Dhawan, Pharmacology of di-ferulyl methane (curcumin), a non-steroidal anti-inflammatory agent, *J. Pharm. Pharmacol.* 25 (1973) 447–452.
- [117] Y. Kiso, Y. Suzuki, N. Watanabe, Y. Oshima, & H. Hikino, Antihepatotoxic principles of *Curcuma longa* rhizomes, *Planta med.*, 49 (1983) 185-187.
- [118] S.D. Deodhar, R. Sethi, R.C. Srimal. Preliminary study on antirheumatic activity of curcumin (diferuloyl methane). *Indian J. Med. Res.*, 71 (1980) 632–634
- [119] R. De, P. Kundu, S. Swarnakar, T. Ramamurthy, A. Chowdhury, G.B. Nair, A.K. Mukhopadhyay. Antimicrobial activity of curcumin against *Helicobacter pylori* isolates from India and during infections in mice. *Antimicrob. Agents Chemother.*, 53 (2009)1592–1597.
- [120] Y. Wang, Z. Lu, H. Wu, F. Lv. Study on the antibiotic activity of microcapsule curcumin against foodborne pathogens. *Int. J. Food Microbiol.*, 136 (2009) 71–74

- [121] R. Srivastava, M. Dikshit, R.C. Srimal, B.N. Dhawan. Antithrombotic effect of curcumin. *Thromb. Res.*, 40 (1985) 413–417.
- [122] F. Yang, G.P. Lim, A.N. Begum, O.J. Ubeda, M.R. Simmons, S.S. Ambegaokar, P. Chen, R. Kayed, C.G. Glabe, S.A. Frautschy, G.M. Cole, Curcumin inhibits formation of amyloid β oligomers and fibrils binds, plaques, and reduces amyloid in vivo, *J. Biol. Chem.* 280 (2004) 5892–5901.
- [123] M.E. Egan, M. Pearson, S.A. Weiner, V. Rajendarn, D. Rubin, J. Glochner-Pagel, S. Canney, K. Du, G.L. Lukacs, M.F. Caplan, Curcumin, a major constituent of turmeric corrects, cystic fibrosis defects, *Science* 304 (2004) 600–602.
- [124] B. Wahlstrom, G. Blenow, A study on the fate of curcumin in rat. *Pharmacol. Toxicol.*, 43(1978) 86–92.
- [125] R. K. Basniwal, H. S. Buttar, V. K. Jain, & N. Jain, Curcumin nanoparticles: preparation, characterization, and antimicrobial study. *Journal of agriculture and food chemistry*, 59(2011) 2056-2061.
- [126] P. Anand, H. B. Nair, B. Sung, A. B. Kunnumakkara, V. R. Yadav, R. R. Tekmal, B. B. Aggarwal, Design of curcumin-loaded PLGA nanoparticles formulation with enhanced cellular uptake, and increased bioactivity in vitro and superior bioavailability in vivo. *Biochem. Pharmacol.*, 79 (2010) 330–338.
- [127] K. Maiti, K. Mukherjee, A. Gantait, B. P. Saha, P. K. Mukherjee, Curcumin-phospholipid complex: Preparation, therapeutic evaluation and pharmacokinetic study in rats. *Int. J. Pharm.* 330 (2007) 155–163.
- [128] D. Patra, A. J. Amali, & R. K. Rana, Preparation and photophysics of HPTS-based nanoparticle-assembled microcapsules, *Journal of Materials Chemistry*, 19 (2009) 4017-4021.
- [129] K. A. Connors, Binding Constants. The measurements of molecular complex stability. Wiley, New York, (1987).
- [130] T. M. Kolev, E. A. Velcheva, B. A. Stamboliyska, M. Spitteller, DFT and experimental studies of the structure and vibrational spectra of curcumin, *Int. J. Quant. Chem.* 102 (2005) 1069-1079.
- [131] T. Higuchi, Mechanism of sustained action medication: theoretical analysis of rate of release of solid drugs dispersed in solid matrices, *J. Pharm. Sci.* 52 (1963) 1145-1148.
- [132] B. Ozcelik, J. H. Lee, D. B. Min, Effects of Light, Oxygen, and pH on the Absorbance of 2,2-Diphenyl-1-picrylhydrazyl, *J. Food Sci.* 68 (2003) 487–490.

- [133] S. V. Jovanovic, S. Steenken, C. W. Boone, M. G. Simic, H-Atom Transfer Is A Preferred Antioxidant Mechanism of Curcumin, *J. Am. Chem. Soc.* 121 (1999) 9677–9681.
- [134] T. Ak, & İ. Gülçin, Antioxidant and radical scavenging properties of curcumin. *Chemico-biological interactions*, 174 (2008) 27-37.
- [135] J. N. Pitts, G. S. Hammond, K. Gollnick, *Advances in Photochemistry*, New York: J. Wiley & sons, 10(1977).
- [136] T. Elsäasser and H. J. Bakker, *Ultrafast hydrogen bonding dynamics and proton transfer processes in the condensed phase*, Kluwer Academic Publishers, Dordrecht, Boston, 2002.
- [137] U. Pischel, D. Patra, A. L. Koner and W. M. Nau, Investigation of polar and stereoelectronic effects on pure excited-state hydrogen atom abstractions from phenols and alkylbenzenes, *Photochem. Photobiol.*, 82(2006), 310.
- [138] A. P. Demchenko, K.-C. Tang and P.-T. Chou, Excited-state proton coupled charge transfer modulated by molecular structure and media polarization, *Chem. Soc. Rev.*, 42(2013) 1379.
- [139] S. V. Jovanovic, S. Steenken, C. W. Boone and M. G. Simic, H-Atom Transfer Is A Preferred Antioxidant Mechanism of Curcumin, *J. Am. Chem. Soc.*, 121(1999) 9677.
- [140] C. Yun, J. You, J. Kim, J. Huh and E. Kim, Photochromic fluorescence switching from diarylethenes and its applications, *J. Photochem. Photobiol., C*, 10 (2009) 111.
- [141] S. M. Khopde, K. I. Priyadarsini, D. K. Palit and T. Mukherjee, Effect of solvent on the excited-state photophysical properties of curcumin, *Photochem. Photobiol.*, 72(2000) 625-631.
- [142] L. Shen and H.-F. Ji, *Spectrochim. Acta, Part A*, 67(2007) 619.
- [143] R. Adhikari, P. Mukeerjee, T. W. Kee and J. W. Petrich, Excited-State Intramolecular Hydrogen Atom Transfer and Solvation Dynamics of the Medicinal Pigment Curcumin, *J. Phys. Chem. B*, 113 (2009) 5255.
- [144] T. W. Kee, R. Adhikary, P. J. Carlson, P. Mukherjee and J. W. Petrich, Femtosecond Fluorescence Upconversion Investigations on the Excited-State Photophysics of Curcumin, *Aust. J. Chem.*, 64 (2011) 23.
- [145] L. Kong, K. I. Priyadarsini and H.-Y. Zhang, A theoretical investigation on intramolecular hydrogen-atom transfer in curcumin, *J. Mol. Struct.*, 684 (2004) 11.
- [146] D. Patra, R. Aridi and K. Bouhadir, Fluorometric Sensing of DNA Using Curcumin Encapsulated in Nanoparticle-Assembled Microcapsules Prepared from

Poly(Diallylammonium Chloride-Co-Sulfur Dioxide), *Microchimica Acta* 180, no. 1-2 (2013) 59-64.

[147] J. N. Anker, W. P. Hall, O. Lyandres, N. C. Shah, J. Zhao and R. P. Van Duyne, Biosensing with plasmonic nanosensors *Nat. Mater.*, **7** (2008) 442.

[148] K. S. Soppimath, D. C W. Tan and Y. Y. Yang., pH-Triggered Thermally Responsive Polymer Core–Shell Nanoparticles for Drug Delivery, *Advanced Materials* 17, 3 (2005) 318-323.

[149] H. H. Tonnesen, J. Karlsen and A. Mostad, Detection of bacterial DNA in lymph nodes of Crohn's disease patients using high throughput sequencing. *Acta Chem. Scand., Ser. B*, **36** (1982) 475.

[150] M. M. Yallapu, M. Jaggi and S. C. Chauhan, Curcumin nanoformulations: a future nanomedicine for cancer, *Drug Discovery Today*, **17** (2012) 71.

[151] P. H. Bong, Spectral and photophysical behaviors of curcumin and curcuminoids, *BULLETIN-KOREAN CHEMICAL SOCIETY*, **21**(2000) 81-86.

[152] F. Zsila, Z. Bikádi and M. Simonyi, Molecular basis of the Cotton effects induced by the binding of curcumin to human serum albumin, *Tetrahedron: Asymmetry*, **14** (2003) 2433.

[153] I. Presiado, Y. Erez, R. Gepshtein, N. Koifman and D. Huppert, Pressure effect on the excited-state proton transfer from curcumin to monols, *J. Photochem. Photobiol., A*, **247** (2012) 42.

[154] V. Galasso, B. Kovač, A. Modelli, M. F. Ottaviani and F. Pichierri, Spectroscopic and Theoretical Study of the Electronic Structure of Curcumin and Related Fragment Molecules, *J. Phys. Chem. A*, **112** (2008) 2331.

[156] D. Patra, C. Barakat, Synchronous fluorescence spectroscopic study of solvatochromic curcumin dye, *Spectrochimica Acta Part A: Molecular and Biomolecular Spectroscopy*, **79** (2011) 1034-1041.

[156] D. Patra, C. Barakat and R. M. Tafech, Study on effect of lipophilic curcumin on sub-domain IIA site of human serum albumin during unfolded and refolded states: A synchronous fluorescence spectroscopic study, *Colloids Surf., B*, **94** (2012), 354.

[157] B. N. PrashantháKumar, Exploring the fluorescence switching phenomenon of curcumin encapsulated niosomes: in vitro real time monitoring of curcumin release to cancer cells. *RSC Advances*, **3**(2013) 2553-2557.

[158] Y. Erez, I. Presiado, R. Gepshtein and D. Huppert, Temperature Dependence of the Fluorescence Properties of Curcumin, *J. Phys. Chem. A*, **115** (2011) 10962- 10971.

- [159] S. N. Shtykov, & T. Y. Rusanova, Nanomaterials and nanotechnologies in chemical and biochemical sensors: capabilities and applications. *Russian Journal of General Chemistry*, 78(2008) 2521-2531.
- [160] D. Gresham, D.M. Ruderfer, S.C. Pratt, J. Schacherer, M.J. Dunham, D. Botstein, and L. Kruglyak, Genome-wide detection of polymorphisms at nucleotide resolution with a single DNA microarray. *Science*, 311(2006) 1932-1936.
- [161] L. Wang, Y. Zhang, J. Tian, H. Li, & X. Sun, Conjugation polymer nanobelts: a novel fluorescent sensing platform for nucleic acid detection, *Nucleic acids research*, 39(2011) e37-e37.
- [162] A. Sassolas, B.D. Leca-Bouvier, and L.J. Blum, DNA biosensors and microarrays. *Chem. Rev.*, 108 (2008) 109-139.
- [163] V.V. Didenko, (ed.), *Fluorescent Energy Transfer Nucleic Acid Probes: designs and Protocols*. Human Press, Totowa, NJ. (2006)
- [164] X. Xu, S. Chen, L. Li, G. Yu, & Y. Liu, Photophysical properties of polyphenylphenyl compounds in aqueous solutions and application of their nanoparticles for nucleobase sensing, *Journal of Materials Chemistry*, 18(2008) 2555-2561.
- [165] D. J. Maxwell, J. R. Taylor, & S. Nie, Self-assembled nanoparticle probes for recognition and detection of biomolecules, *Journal of the American Chemical Society*, 124 (2002) 9606-9612.
- [166] J. A. Hansen, R. Mukhopadhyay, J. Ø. Hansen, & K. V. Gothelf, Femtomolar electrochemical detection of DNA targets using metal sulfide nanoparticles, *Journal of the American Chemical Society*, 128 (2006) 3860-3861.
- [167] P. Sharma, H. Singh, S. Sharma, & H. Singh, Binding of gold nanoclusters with size-expanded DNA bases: a computational study of structural and electronic properties, *Journal of Chemical Theory and Computation*, 3 (2007) 2301-2311.
- [168] W. H. Brown, *Introduction to Organic and Biochemistry*, fourth ed., Brooks/Cole Publication, Monterey, 1987, 418.
- [169] R. G. Blazej, W. Goodwin, S. A. Heath, F. Hillenkamp *et.al.*, *Analytical Techniques in DNA Sequencing*, CRC Taylor and Francis, edited by B. K. Nunnally, 2005.
- [170] W. Wang, L. Zhou, S. Wang, Z. Luo, & Z. Hu, Rapid and simple determination of adenine and guanine in DNA extract by micellar electrokinetic chromatography with indirect laser-induced fluorescence detection. *Talanta*, 74(2008)1050-1055.

- [171] P. Adams, J. J. Austin, I. Braslavsky *et.al.*, , New High Throughput Technologies for DNA Sequencing and Genomics, ELSEVIER, first ed. edited by K. R. Mitchelson, 2007.
- [172] L. Mahmodian, M. R. Mohamadi, N. Kaj, M. Tokshi, Y. Baba, Handbook of Capillary and Microchip Electrophoresis and Associated Microtechniques, CRC Taylor and Francis group, 3rd ed. edited by J. P. Landers, 2008.
- [173] D. Patra, C. Barakat, Synchronous fluorescence spectroscopic study of solvatochromic curcumin dye, *Spectrochimica Acta Part A*, 79(2011) 1034 – 1041.
- [174] D. Patra, E. El Khoury, D. Ahmadieh, S. Darwish, R. M. Tafach, Effect of curcumin on liposome: Curcumin as a molecular probe for monitoring interaction of ionic liquids with 1,2-dipalmitoyl-sn-glycero-3-phosphocholine liposome, *Photochemistry and Photobiology*, 88(2012) 317 – 327.
- [175] R. Adhikary, P. J. Carlson, T. W. Kee, & J. W. Petrich, Excited-state intramolecular hydrogen atom transfer of curcumin in surfactant micelles, *The Journal of Physical Chemistry B*, 114 (2010) 2997-3004.
- [176] M. Kai, Y. Ohkura, S. Yonekura, & M. Iwasaki, Chemiluminescence determination of guanine and its nucleosides and nucleotides using phenylglyoxal. *Analytica chimica acta*, 287(1994) 75-81.
- [177] S. Yonekura, M. Iwasaki, M. Kai, & Y. Ohkura, Determination of guanine and its nucleosides and nucleotides in human erythrocytes by high-performance liquid chromatography with postcolumn fluorescence derivatization using phenylglyoxal reagent. *Journal of Chromatography B: Biomedical Sciences and Applications*, 654(1994) 19-24.
- [178] Y. Ohba, M. Kai, H. Nohta, & Y. Ohkura, Alkoxyphenylglyoxals as fluorogenic reagents selective for guanine and its nucleosides and nucleotides in liquid chromatography. *Analytica chimica acta*, 287(1994) 215-221.
- [179] X. Niu, W. Yang, J. Ren, H. Guo, S. Long, J. Chen, & J. Gao, Electrochemical behaviors and simultaneous determination of guanine and adenine based on graphene-ionic liquid-chitosan composite film modified glassy carbon electrode. *Electrochimica Acta*, 80 (2012) 346-353.
- [180] Y. Mei, L. Ran, H. Dongyan, & G. Yuying, A novel flow-injection chemiluminescence system for the determination of guanine. *Luminescence*, 20(2005) 307-310.
- [181] S. Chatterjee, & A. Chen, Facile electrochemical approach for the effective detection of guanine. *Electrochemistry Communications*, 20 (2012) 29-32.

- [182] Y. J. Wang, M. H. Pan, A. L. Cheng, L. I. Lin, Y. S. Ho, C. Y. Hsieh, & J. K. Lin, Stability of curcumin in buffer solutions and characterization of its degradation products. *Journal of pharmaceutical and biomedical analysis*, 15 (1997) 1867-1876.
- [183] M. Bernabé-Pineda, M. T. Ramírez-Silva, M. Romero-Romo, E. González-Vergara, & A. Rojas-Hernández, Determination of acidity constants of curcumin in aqueous solution and apparent rate constant of its decomposition. *Spectrochimica Acta Part A: Molecular and Biomolecular Spectroscopy*, 60 (2004) 1091-1097.
- [184] M. H. Leung, H. Colangelo, & T. W. Kee, Encapsulation of curcumin in cationic micelles suppresses alkaline hydrolysis. *Langmuir*, 24(2008) 5672-5675.
- [185] Z. L. Wang, Zinc oxide nanostructures: growth, properties and applications. *Journal of Physics: Condensed Matter*, 16 (2004) R829.
- [186] A. B. Djurišić, & Y. H. Leung, Optical properties of ZnO nanostructures. *Small*, 2 (2006) 944-961.
- [187] B. Schwenzer, J. R. Gomm, & D. E. Morse, Substrate-induced growth of nanostructured zinc oxide films at room temperature using concepts of biomimetic catalysis. *Langmuir*, 22(2006) 9829-9831.
- [188] F. Rubio-Marcos, C. V. Manzano, J. J. Reinoso, I. Lorite, J. J. Romero, J. F. Fernández, & M. S. Martín-González, Modification of optical properties in ZnO particles by surface deposition and anchoring of NiO nanoparticles. *Journal of Alloys and Compounds*, 509 (2011) 2891-2896.
- [189] M. H. Huang, S. Mao, H. Feick, H. Yan, Y. Wu, H. Kind,... & P. Yang, Room-temperature ultraviolet nanowire nanolasers. *Science*, 292(2001) 1897-1899.
- [190] W. D. Yu, X. M. Li, & X. D. Gao, Self-catalytic synthesis and photoluminescence of ZnO nanostructures on ZnO nanocrystal substrates. *Applied physics letters*, 84 (2004) 2658-2660.
- [191] J. Zhai, X. Tao, Y. Pu, X. F. Zeng, & J. F. Chen, Core/shell structured ZnO/SiO₂ nanoparticles: Preparation, characterization and photocatalytic property. *Applied Surface Science*, 257 (2010) 393-397.
- [192] H. M. Xiong, Photoluminescent ZnO nanoparticles modified by polymers. *Journal of Materials Chemistry*, 20(2010) 4251-4262.
- [193] S. F. Wei, J. S. Lian, & Q. Jiang, Controlling growth of ZnO rods by polyvinylpyrrolidone (PVP) and their optical properties. *Applied Surface Science*, 255(2009) 6978-6984.
- [194] E. A. Meulenkaamp, Size dependence of the dissolution of ZnO nanoparticles. *The Journal of Physical Chemistry B*, 102(1998) 7764-7769.

- [195] M. Chang, X. L. Cao, H. Zeng, & L. Zhang, Enhancement of the ultraviolet emission of ZnO nanostructures by polyaniline modification. *Chemical Physics Letters*, 446(2007), 370-373.
- [196] L. Irimpan, B. Krishnan, A. Deepthy, V. P. N. Nampoore, & P. Radhakrishnan, Excitation wavelength dependent fluorescence behaviour of nano colloids of ZnO. *Journal of Physics D: Applied Physics*, 40(2007) 5670.
- [197] H. M. Xiong, Z. D. Wang, D. P. Xie, L. Cheng, & Y. Y. Xia, Stable polymer electrolytes based on polyether-grafted ZnO nanoparticles for all-solid-state lithium batteries. *Journal of Materials Chemistry*, 16(2006) 1345-1349.
- [198] M. L. Singla, M. M. Shafeeq & M. Kumar, Optical characterization of ZnO nanoparticles capped with various surfactants. *Journal of Luminescence*, 129(2009), 434-438.

